Anthropogenic Emissions and the Future of Our Atmosphere:

I. Cyclohexanol Chemistry and Aerosol Formation in an Environmental Chamber

II. K_2CO_3-Based Sorbent Development and Testing in a Packed Bed Reactor for CO_2 Capture

Thesis by
Hannah Kate Szentkuti

In Partial Fulfillment of the Requirements
for the Degree of
Doctor of Philosophy

California Institute of Technology

Pasadena, California

2025

Defended December 17th, 2024

Hannah Kate Szentkuti
ORCID: 0009-0000-2232-6333

ACKNOWLEDGEMENTS

Like many PhD students, I've spent a long time thinking about this section of my dissertation. I could not have made it here without the support of countless people from many different stages and aspects of my life. To begin, I want to thank the dozens of educators that instilled in me a passion for science and learning in general. I was fortunate to attend Ocean Shore School—"the alternative school"—a K–8 in the Bay Area known for its exceptional level of parent involvement. This community support made possible many unique experiences, including Ability Awareness Day, Beach Day, Outdoor Ed, and Ocean's Week. These events encouraged students to connect deeply with the environment, animals, and—true to the school's name—Earth's oceans. Thank you to the many teachers who made this possible including Mrs. Shiela Gamble-dorn, Mrs. Virginia Szczepaniak, Mrs. Steva Steele, Mrs. Jan Keaney, Mrs. Fran Quartini, Mrs. Patty McNally, Mrs. Katy Stearns and Mrs. Sandy Mills. At Oceana High School, my love for science was further cultivated by three exceptional educators: Mr. Ryan Reidy, Mr. Paul Orth, and Mr. Jay Gould. Each of them brought kindness and enthusiasm into the classroom. I am especially grateful to Mr. Gould, who was one of the first people to encourage me to seriously pursue a career in science.

I also want to acknowledge the importance of quality public education, something that is under attack as I write. All children, regardless of economic status, deserve passionate educators. Please, support the teachers and protect public education.

I was incredibly fortunate to attend Mills College -also in the bay area- where I got to be a part of another unique educational experience. Mills, which has since become a part of Northeastern University, was at the time one of the last women's colleges in the United States. In my experience, learning science in a non-male setting gave me the opportunity to take up more space, ask more questions, be bolder, and receive more support. At Mills I learned to ask questions, accept the discomfort that comes with confusion and learning, to support other scientists, and most importantly that science is not done in a vacuum. Thank you to the faculty who helped shape my scientific identity: Drs. Elisabeth Wade, Beth Kochly, Felisa Wolfe-Simon, Jared Young, Lynn Delker, Whitney Berard, Zvezdelina Stankova, and Barbara Li Santi. And thank you to my college friend group- Courtney Koetz, Alex Goodenough, Julia Spencer, Carrie Ghaffari, Sian Morris, Vanessa Cuevas, Emily Keller, Shoshana Moed and Amanda Cole. Without your influence I would not be the person I am today.

From Caltech I of course want to thank my advisor Prof. Mitchio Okumura. I've learned so much from Mitchio over the years, but the most valuable lesson he's imparted is the importance of immersing oneself deeply in the scientific literature. Whenever I feel uncertain or lack direction in a project, I've learned to return to the publications—to read

more deeply, more broadly, and more critically. That practice has become my compass, and for that, I am deeply grateful. I want to thank the entire literal and extended Okumura group. My first mentor, Elizabeth Lunny, who despite being right about to graduate was so patient and kind and never made me feel like I was taking too much of her time (even though I probably was). To the many friendly Okumurons I have gotten to know over the years including Prof. Tzu-ling Chen, Wen Chao, Leah Stevenson, Dr. Charlie Markus, Tyler Nguyen, Termeh Bashiri, Megan Woods and Makenna Herl, thank you for your camaraderie! One of my favorite grad school memories is frequently going to 85° bakery with Tzu-ling and Makenna. Thank you also to my committee, Drs. Scott Cushing, Ryan Hadt, and Melany Hunt for encouraging me and keeping me on track. I had the pleasure of working with Melany and her graduate student Ricardo Hernandez over the summer of 2024 (Chapter 4). It was one of the highlights of my PhD. In addition to his brilliance, Ricardo you are so incredibly kind and funny.

I want to thank Dr. John Seinfeld for allowing me to work in his laboratory (Chapter 1), and Dr. Rick Flagan for his continuing guidance over the years. From the Seinfeld and Flagan groups I would particularly like to thank Drs. Yuanlong Huang and Christopher Kenseth. Thank you for all your patience in training me on the chamber instrumentation and related code. Thank you Horoula Baliaka and Kat Ball from the Seinfeld lab as well for being your friendly and bubbly selves.

I want to thank the entire team over at Mitico for taking me in and giving me the opportunity to do leading-edge mitigation research and technology development with them (Chapters 2 & 3). Thank you Clément Cid, Léopold Dobelle and Alan Gu for your mentorship and unrivaled enthusiasm. Alan Gu, I will always appreciate you for taking a chance on me and “breaking me in” at my very first job. I had so much fun and am so proud to be your first employee. Also thank you Wuwei Mo, my colleague and snack buddy during my time at Mitico!

For much of my PhD I enjoyed living in a group house on Navarro Ave. in Pasadena with huge personalities. Thank you, Angela Gu, Sophia Lambrecht, Evie Harel and Andrew Nylander, for your antics that provided a much-needed break from science. Similarly thank you to my close friend and rehabber Cleo Watts for dragging me out of the laboratory basement every once in a while, to do something good for our local community. You are so crazy, and I love you for it.

Thank you to my large family- my parents, my grandparents “Meemaw and Peepaw,” my auntie Crissy Goldman, my late uncle Dave Goldman, my late cousin Samantha Mannina, my cousin Rodney Dimercurio, my cousins Uri and Gabe Lorvan, my uncle Dan Szentkuti, my adopted grandma Marcia Burtt, all the Verkozens, and my younger brother Niko Szentkuti. My grandparents Meemaw and Peepaw have always been my biggest supporters, and I could not have done any of this without them. Thank you, Niko, for being

my partner in crime. Getting to live with you as young adults together during this time and in Los Angeles was so special to me.

Thank you to my childhood friends- Evan Fontaine, Shoshana Moed, Grady Hovermale, Crista Mulhall, Merideth Stanley, Seon MontBlanc, Jack Womack, Henry Lancelle and Lesley Bode. My RPG group has been a continual source of release and distraction for me especially. Special thanks to my mice, of which I have had so many, but will all forever be in my heart. From courageous Chrysanthemum to the motherly Miss Cinnamon, or my current old man Cremini. And of course, to my piggies Jax and Gus who eat all my wages in luxury hay and vet bills, but I could not live without.

Huge thank you to my two grad school best friends, Drs. Gregory Jones and Douglas Ober. I have so many great memories in and outside of the Okumura group with you two. I can't wait to continue to see all the fantastic things that you do, both in and outside of science. I am so proud to call you my friends.

Lastly, thank you to my darling fiancé and life partner Austin Halter. Thank you for always putting up with me and supporting me through every challenge. You motivate me to be the best version of myself I can be. I can't wait to continue our life together and explore the world.

To all my past educators, mentors, colleagues, friends, family, and beloved pets—this is dedicated to you. Thank you.

A b s t r a c t

STUDYING AND MITIGATING ANTHROPOGENIC EMISSIONS

In all human history there has not been a more essential scientific -and political- endeavor than the prevention of the commencing climate catastrophe. Without swift and aggressive intervention, the upcoming century will see dramatic consequences for air quality, food security, and the habitability of entire regions across the globe. Because of the scale and complexity of the crisis, effective climate action must be multifaceted. A non-exhaustive list includes: support and development of green energy to replace combustion fuels, removal and storage of emitted or ambient carbon, reforestation, reducing energy consumption, monitoring and predicting emissions, and then regulation of said emissions. This dissertation contributes work to two of these key areas; monitoring and predicting emissions (Chapter 1) as well as carbon removal from the atmosphere (Chapters 2-4).

Chapter 1 presents experimental studies conducted in an environmental chamber, alongside mechanistic modeling, to quantify aerosol formation from the gas-phase pollutant cyclohexanol. While greenhouse gases like carbon dioxide and methane typically receive the most attention in climate modeling and global monitoring, atmospheric particles also play a critical role in Earth's radiative balance by absorbing and scattering light. Studies on black and brown carbon atmospheric aerosol (so named due to their strong absorption of visible light) indicate they contribute significantly to the global radiative budget, making them of growing interest to climate modelers. A specific class of these particles, secondary organic aerosols (SOA), forms in the atmosphere via the condensation of aged gas-phase emissions. Studies like this one quantify aerosol forming potential with the goal of informing and guiding regulatory policies. Solvents and chemical feed stocks, for example, with large aerosol forming potential should be more carefully stored to prevent evaporation or even replaced with analogous compounds. And unlike greenhouse gases, aerosol have short atmospheric lifetimes which means that proper regulation could result in almost immediate cooling effects once old brown aerosol rain or deposit out. In short, identifying gas-phase pollutants that result in SOA formation will enable faster phase-out of

problematic species from industrial and commercial processes, which if enacted will quickly improve global radiative budgets.

While Chapter 1 focuses on particulate emission prediction to assist in regulation, the following chapters explore novel methods to capture carbon dioxide, the largest single contributor to radiative forcing. Chapter 2 describes the construction and characterization of a mini-industrial scale packed-bed reactor, loaded with K_2CO_3-impregnated particles for CO_2 capture. Chapters 3 and 4 describe the formulation of durable high-capacity K_2CO_3-based sorbents using wet activated granulation and extrusion spheronization, respectively. These works were performed to assist in making point source capture economically feasible. While regulation of gas and particle phase emissions is critical to decelerate current heating trends, international infrastructures and energy networks are not prepared for complete decoupling from combustion yet. Thus, in the short-term future, it is necessary to develop supportive technologies that can remove combusted CO_2 from exhaust streams before they are emitted. While the sorbents studied in Chapters 3 and 4 are intended to be used in a point source capture system, like the reactor constructed in Chapter 2, given their favorable properties, K_2CO_3 sorbents also hold promise for deployment in ambient air capture systems.

TABLE OF CONTENTS

Acknowledgements……...……iii
Abstract……...……vi
Table of Contents…… ……...…..viii
List of Figures……..x
List of Tables……xiii

I. Cyclohexanol Chemistry and Aerosol Formation in an Environmental Chamber

Chapter 1: Cyclohexanol Oxidation and Aerosol Mass Yield……..…1
1.1 Abstract……..……1
1.2 Introduction……...……..……..…1
1.2.1 VOCs and Urban Air Pollution……...……...1
1.2.2 Cyclohexanol Sources and Significance……4
1.2.3 Previous Work…….…….……..5
1.3 Methods …...……..……..…….……5
1.3.1 Chamber and Instrument Descriptions…….…..5
1.3.2 Relative Rate Measurements……...…….13
1.3.3 Cyclohexanone Branching Fraction ……..…..13
1.3.4 Calibrations……..……15
1.3.5 Mass Yield Calculations ..…...……..…….……..15
1.3.6 Kinetic Model…….……16
1.4 Results and Discussion……...……..……..23
1.4.1 VOC Calibrations……..……...23
1.4.2 Measured Concentration Profiles…….……....25
1.4.3 Relative Rate Measurements……29
1.4.4 Cyclohexanone Branching Fraction…….…30
1.4.5 HO_2 and RO_2 Concentrations……...34
1.4.6 Product Identification……...38
1.4.7 Mass Yields……..…50
1.5 Conclusion……..…53
1.6 Future Works……...……54
1.7 Citations……..56

II. K_2CO_3-Based Sorbent Development and Testing in a Packed Bed Reactor for CO_2 Capture

Chapter 2: Centennial Reactor Design and Testing with K_2CO_3 Impregnated Zeolite.....60
2.1 Abstract……..…….60
2.2 Introduction……60

2.2.1 Carbon Capture……...……...60
2.2.2 K_2CO_3-Based Sorbents…….…….64

2.3 Methods……...66
2.3.1 Reactor Design and Construction……66
2.3.2 Gas Mixing Panel……69
2.3.3 Packed Bed Towers and Operational Procedures……71
2.3.4 Gas Analysis Panel……...75
2.3.5 Impregnated Zeolite, Preparation and Loading……...76
2.3.6 Calculations……..83
2.4 Results and Discussion……...87
2.4.1 Raw Data……..87
2.4.2 Capture Results……97
2.4.3 Additional Diagnostic Data……108
2.5 Conclusion……112
2.6 Future Works……113
2.7 Citations……....114

Chapter 3: K_2CO_3 Sorbent Development Via Wet-Activated Granulation…….....119
3.1 Abstract……119
3.2 Introduction……...119
3.2.1 Previous work on K_2CO3 Sorbents……119
3.2.2 Granule Manufacturing Strategies……122
3.2.3 Requirements for Industrial Scalability……125
3.3 Methods……126
3.3.1 Granulation Procedure……126
3.3.2 Additive Selection and Formulations……..128
3.3.3 Testing Procedure……131
3.4 Result and Discussion……...134
3.5 Conclusions……...144
3.6 Future Works……144
3.7 Citations……146

Chapter 4: Bentonite-K_2CO_3-Based Sorbents Made By Extrusion-Spheronization.....149
4.1 Abstract……149
4.2 Introduction……...……149
4.2.1 Extrusion-Spheronization Method……149
4.2.2 Previous Works……..151

4.3 Methods……154
4.3.1 Additive Selection and Formulations……..…..154
4.3.2 Testing and Calculations……158

4.4 Results and Discussion…….159
4.5 Conclusions……...169
4.6 Future Works…….170
4.7 Citations……171

LIST OF FIGURES

Chapter 1

1.1 General VOC oxidation model adapted from Kroll and Seinfeld……..……..…2
1.2 Carbon number versus aerosol mass yield, adapted from Cappa and Wilson.…....3
1.3 Diagram of the environmental chambers with accompanying instruments, including an SMPS, a DMA, CPC, NOx and O_3 monitors, GC-FID, and CIMS…6
1.4 Intensity spectrum from the atmospheric chamber lights……....8
1.5 Diagram of ammonium sulfate solution aerosolizer……...…….9
1.6 m/z 185 signal before and after oxidation is initiated, indicates why GC-FID was used instead of CIMS for quantifying cyclohexanol……..…11
1.7 Diagram of the GC-FID inlet, modified for continuous gas monitoring……...12
1.8 Dilution setup for GC-FID VOC calibrations……15
1.9 Cyclohexanol + OH mechanism, 1st and 2nd generation product formation……..19
1.10 Cyclohexanone + OH mechanism, 1st and 2nd generation product formation…...20
1.11 Alkoxy reaction(s) mechanism…….....21
1.12 Cyclohexene + OH reaction mechanism, adapted from Aschmann *et al*……..22
1.13 VOC FTIR plots fitted to PNNL reference data for calibration……...….24
1.14 Cyclohexanol decay curves, and cyclohexanone growth curves……...26
1.15 %Cyclohexanol reacted versus time……..27
1.16 Measured O_3, NO and NO_2 plots versus time...…….28
1.17 Relative rate log-log plots for cyclohexanol versus butanol and butanal……..29
1.18 Calculated OH profiles versus time……...30
1.19 Log of cyclohexanol plots fitted to 4th degree polynomials, used to calculated OH temporal profiles…….…...31
1.20 Cyclohexanone experimental data plotted against modeled data, varying cyclohexanone + OH reaction rate and φ……...33
1.21 Experimental cyclohexanol plotted against modeled cyclohexanol for optimal φ and cyclohexanone + OH rate……34
1.22 H_2O_2 measured, as m/z 120, signal plot…….35

1.23 Modeled HO_2 and RO_2 concentration versus time……..….36
1.24 Detected ions- m/z 56-175 for no-NO and NO trials…….39
1.25 Detected ions- m/z 176-295 for no-NO and NO trials……...40
1.26 Modeled versus measured concentrations for products A, B and D……..44
1.27 Modeled versus measured concentrations for products E, F and G……...45
1.28 Modeled versus measured concentrations for products I, L, C & H……..47
1.29 Modeled versus measured concentrations for products J, K, M, N, O, P……..48
1.30 Mass yield plots for Trials 3 & 6-9, with and without wall-loss corrections…….51
1.31 Mass yield results plotted against McDonald predicted value……...…52

Chapter 2
2.1 Picture of the Heirloom Carbon Capture facility in Brisbane, CA……..…….....62
2.2 CO_2 capture capacity for many multiple metal organic frameworks, borrowed from Younas *et al*……...63
2.3 Centennial Reactor Diagram- the gas mixing panel, the packed bed towers, the gas analysis panel, the cooling water tower, and the data logger……..66
2.4 Picture of the Centennial site prior to construction…….……..67
2.5 Picture of tower control panels and compressed gases…….....68
2.6 Picture of gas mixing and gas analysis panels…….……..68
2.7 Close-up picture of gas mixing panel and gas analyzer…….70
2.8 Close-up picture of reactor control panel and mounting skid……72
2.9 Valve flow diagram of a complete three-phase cycle……73
2.10 Close-up picture of gas analysis panel and RO water filters……76
2.11 Calculated pressure drops across the tower according to Ergun equation…….78
2.12 Picture of ADCOA and PureAir rock-type zeolite…….80
2.13 HEU and FAU crystal structures, borrowed from Gatta and Lotti and McCusker and Baerlocher, respectively……..82
2.14 Pressure and Flow profiles for Trial 2, Absorption 7…….……88
2.15 RH meter outputs along tower B during Trial 1, absorption 8……...89
2.16 Absorption breakthrough curve from Trial 2, absorption 5 as well as suboptimal regeneration from Trial 2, regeneration 2……..90
2.17 Volumetric flow exiting tower versus outcoming CO_2 concentration from Trial 2, regeneration 10……...93
2.18 Tower temperature during regeneration; expanded data from Figure 2.17……...95
2.19 Comparison of regeneration temperature for steam and N_2 purges……...96
2.20 Capture efficiency curves for all Trial 1 cycles…….99
2.21 Comparison of RH outputs for absorptions 2, 6, 7 and 8 from Trial 1- tower wetness is correlated to poorer capacity……..100
2.22 Bar graph comparing CO_2 captured across cycles 5-13 of Trial 2……..104
2.23 Absorption efficiency curves; comparing best cycles of Trial 1 to Trial 2……..105

2.24 Post-CO_2 regenerated efficiency curves from Trial 2 compared to those regenerated with N_2- CO_2 is a poor purge gas……105
2.25 Efficiency curves for cycles 8-13 of Trial 2- steam is a superior purge gas……106
2.26 pH of condensates during absorption phase for Trials 1 and 2……109
2.27 Tower temperature ramps during Trial 2 regenerations- observed large variability in rise time……...……110
2.28 Tower cooling temporal curves for Trial 2 cooling cycles……...111

Chapter 3
3.1 Diagram comparing wet activated granulation to impregnation methods……...123
3.2 Qualities of an economically viable and scalable sorbent……...126
3.3 Picture of wet activation formed granules baked at Mitico HQ……..127
3.4 Picture of mini-reactor and auto-cycler……...131
3.5 Kinetics and capacity plots as a function of %K_2CO_3……135
3.6 Picture of clumped and overly saturated sorbents……...137
3.7 Capacities for sorbents containing Al_2O_3 and CeO_2……138
3.8 Pictures of sorbent degradation due to repeated cycling……140
3.9 Samples C3-C6 after 33 cycles on the autocycler- addition of 13X as a desiccant appears to improve material longevity……141
3.10 Kinetic profile of sample C7 before and after cycling- improved rate after cycling attributed to microcracking……..142
3.11 Kinetic curves for sample B4 after being pre-wetted……..143

Chapter 4
4.1 Diagram of extrusion-spheronization method……150
4.2 Picture of extrudate exiting die and being spheronized, taken at Caltech.....…157
4.3 Picture of A1 and A4 formulations after baking……..159
4.4 Picture of A6 and A7 formulations after extrusion……..161
4.5 Calcined and uncalcined samples in water- calcination of bentonite makes insoluble particles……163
4.6 SEM images of pre and post-calcination samples with bentonite- all SEM performed by Ricardo Hernandez and Jordan Threat.....…163
4.7 Absorption curve for samples B2 and B3- calcination can result in lower capture capacity……164
4.8 SEM images of B4 surface before and after reaction with CO_2……..165
4.9 SEM images of particle surface after step-wise calcination……166
4.10 SEM images of potential zeolite formed from calcined bentonite……..167
4.11 Absorption curves for samples B4 and B5 before and after cycling……...168
4.12 SEM images of B4 and B5 after cycling……169

LIST OF TABLES

Chapter 1
1.1 All laboratory experiments……..7
1.2 Measured rate constants for OH reactions…….14
1.3 Branching fractions selected for model…….22
1.4 Calibration measurements for all VOCs……25
1.5 Relative rate data for cyclohexanol + OH…….29
1.6 Cyclohexanone rate vs. φ fit……..32
1.7 HO_2 and RO_2 Modeled Concentrations for Trials 6-9……...37
1.8 Observed masses from predicted mechanism……42
1.9 Cyclohexanol Mass Yield……..50

Chapter 2
2.1 Trials overview……..87
2.2 Trial details……91
2.3 Trial 1 Capture Capacities…….97
2.4 Trial 1 Calculated Kinetic Constants……...101
2.5 Trial 2 Capture Capacities……102
2.6 Trial 2 Calculated Kinetic Constants……...107

Chapter 3
3.1 Formulation details of all sorbents……...129
3.2 Capacities and rate constants of A1-A7……...134
3.3 Capacities and rate constants of B1-B8……...137
3.4 Capacities and rate constants of C1-C7……...140

Chapter 4
4.1 Summary of Extruded K_2CO_3-Sorbents from literature……..152
4.2 A and B series sorbent compositions and preparation conditions……155
4.3 B series capacity measurements and measured densities……162

[[This chapter is temporarily embargoed]

. C h a p t e r 2

CENTENNIAL REACTOR DESIGN AND TESTING WITH K_2CO_3 IMPREGNATED ZEOLITE

2.1 Abstract

In the following chapter the construction and validation of a prototype industrial scale "Centennial" reactor is discussed. The reactor is a two-tower system designed by Mitico, a carbon capture company founded in 2022 out of Caltech, to continuously capture CO_2. This is accomplished as one tower undergoes an absorption cycle, the other tower releases CO_2 in a regeneration cycle. Two different K_2CO_3-impregnated zeolite sorbents were tested and cycled; PureAir "rock-type" impregnated by the manufacturer and ADCOA spherical pellets impregnated on-site by Mitico. PureAir zeolite, was found to have the higher of the two capacities, with our highest trial capacity reaching 0.3 mmol g^{-1} sorbent capture for the 112 kg load. The impact of different regeneration temperatures and gas identities (N_2, CO_2, H_2O) on sample cyclability were also explored. It was found that steam can lower the required energy for regeneration, and results in a faster and more complete regeneration. While ultimately capture capacities were lower than desired, major design flaws and quirks were identified for the purpose of bettering future reactor designs.

2.2 Introduction

2.2.1 Carbon Capture

As the impacts of climate change become ever more prominent in political discussions, globally governments have made concerted efforts to minimize greenhouse gas emissions and find usage for them, i.e. storage through chemical fixation.[1] Of the many greenhouse gases, which includes fluorinated gases, nitrous oxide (N_2O) and methane, by far the most abundant is CO_2 which is expected to represent about 80% of annual emissions.[2] CO_2 is emitted in abundance for combustion energy and as a manner of eliminating unwanted materials. For example, CO_2 is emitted from coal and natural gas power plants, but it is also emitted when municipal solid waste is burned, a common practice in many countries.[3,4] CO_2 is also a by-product in many chemical reactions in industrial processes, like cement

production. Fossil fuel burning powerplants however, are estimated to be the single largest source of CO_2 production, representing a third of global annual emissions.[5]

As CO_2 sources are various and their originating processes are often challenging to replace with carbon neutral or negative alternatives, elimination of widespread CO_2 production is impossible, at least in the near future. Thus, it is necessary to find ways to capture CO_2, and store or utilize it. While capturing CO_2 may not naturally benefit corporate entities under an unregulated capital system, many governments have incentivized sequestration by offering carbon credits to companies who manage their emissions or delivering carbon tax penalties to those that do not.[6] In general, CO_2 capture can be categorized as ambient/direct air (DAC) or point source capture (PSC). Both capture types experience their own sets of challenges. In the case of DAC, the primary challenge is creating a system which can overcome the thermodynamic difficulty of reacting with a molecule that makes up less than 0.1% of the atmosphere. To increase the uptake rate of CO_2 into the reacting material, fans are used to pull in ambient air.

While green energy can be used to power these fans, operating costs for direct air capture are expected to be high as a result. Estimates for 2030 DAC systems are expected to range from $600-1,000 USD per net tonne of CO_2 captured.[7] Heirloom is one of the first to-market DAC companies; it is California-based and utilizes limestone tray stacks to chemically capture CO_2. Their earliest sales in 2021 is a good measure of current market limitations; with costs as high as $2000 per net ton captured.[8] The limestone, $Ca(OH)_2$, reacts with CO_2 to form $CaCO_3$. When $CaCO_3$ is heated, it releases CO_2 leaving behind CaO, which can be hydrated to reform $Ca(OH)_2$.[7] This chemical reactivation via temperature swing is a common strategy in both DAC and PSC.

PSC is as it sounds; sequestration of CO_2 from a point source emitter, most often flue stacks on top of powerplants. Flue stacks have very high exhaust flow rates, between hundreds and thousands of m^3ph depending on the design.[9] In addition, the CO_2 is present in much larger concentrations, typically between 4 and 15% by volume.[10] For this reason, the primary challenge to PSC is that absorbers must have very high capture capacities and reaction rates.

Figure 2.1 depicts the real Heirloom DAC facility in Brisbane California, 2023.[8] *$Ca(OH)_2$ powder is laid out on vertical stacks to minimize land requirements and maximize sorbent-air exposure from fans.*

Materials with low capture capacities pose concern to economic costs as they will need to be replaced/recycled more frequently or be used in larger quantities. Materials with low reaction rates necessitate long resonance times through the material, again increasing the size of the capture system (in the case of a reactor, the height) and compounding system complexity. While there are many materials under development that provide fast and efficient capture, other material qualities must be balanced as well. Properties that impact industrial feasibility include cost of material production, cost of regeneration and material lifetime (if the material is to be cycled) and toxicity to name a few. Two of the leading directions for selective CO_2 capture are metal organic frameworks (MOFs) and amine solvents. To illustrate the current state of the field of carbon capture, we will briefly discuss MOF and amine-based capture.

In the early 2000s, advancements in high porosity materials and synthetic tuning of pore environments allowed for MOFs to be applied to CO_2 related-problems.[11] Design elements that are common amongst MOFs intended for reversible CO_2 capture include square or hexagonal channels that are designed to allow CO_2 (and only CO_2) navigation, hydrophobic pores, open metal sites to interact with CO_2, and other heteroatom functionalization of the backbone like amino groups, again to interact with the CO_2.[11,12] Zeolites are an inorganic

silica and alumina based naturally occurring solid that can form in a variety of 3D structures. Zeolites are one of the earliest developed metal-oxide frameworks of interest to catalytic and capture technology.[13] Due to their high capacity and reversible absorption, zeolites are used as molecular sieves and structurally tuned depending on their application. Zeolites were one of the first simple materials with notable selective CO_2 capture and are often used as a basis of comparison to other capture materials. Zeolite 13X, for example, generally captures around 5mmol CO_2 per gram however they also capture other small gases like H_2O, O_2 and N_2.[14] MOFs can easily reach this capacity at standard pressures, and even higher capacities at higher pressures.[15] Unfortunately, MOFs also experience selectivity issues observed by zeolite. In addition to their high cost of production, insufficient CO_2 selectivity is one of the biggest challenges that prevent current use of MOFs for carbon capture.[15]

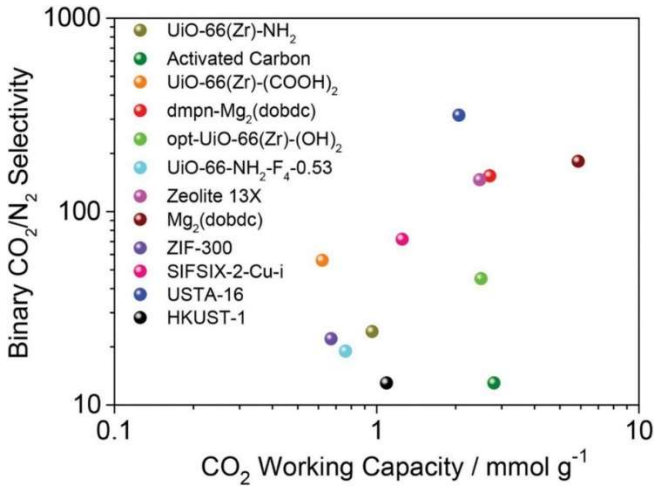

Figure 2.2 is borrowed from Younas et al and displays CO_2 capture capacity for a variety of studied MOFs against their selectivity in CO_2/N_2 mixtures.[15]

The most common carbon capture method that currently occupies about 60% of the carbon capture market is amine scrubbing.[16] Before its use in carbon capture to help mitigate climate change, amine scrubbing was used to purify industrial gas streams of compounds like hydrogen sulphide (H_2S) for safety reasons, which is why it is also called acid-gas decontamination. When amines react with CO_2, they do so according to lines 1 and 2; where line one displays formation of carbamate and line 2 displays formation of bicarbonate. The reaction preference between these two paths differs depending on the

amine identity, especially if it is primary, secondary or tertiary. Tertiary amines, for example, can only undergo the reaction 2.[17]

1. $2R_1R_2NH + CO_2 \leftrightarrow (R_1R_2NH_2^+)(R_1R_2NCOO^-)$
2. $R_1R_2NH + CO_2 + H_2O \leftrightarrow (R_1R_2NH_2^+)(HCO_3^-)$

Amine scrubbing is currently the most economically viable method of CO_2 capture, as amines are cheap and easy to produce, and controlled release of the CO_2 requires only a small temperature swing. Capture typically occurs between 40 and 70°C, while release occurs between 100 and 150°C, a temperature that can easily be achieved at most industrial plants by repurposing waste-heat.[18] Despite these advantages, amine scrubbing cannot be the only long-term solution to CO_2 management because accidental release of amines presents its own environmental concerns. While amine towers utilize traps to minimize losses, amine vapours and aerosol still readily escape. Additionally as amines degrade over time due to oxidation, they also form other compounds such as organic acids, ammonia, and amides which corrode equipment and are themselves environmentally hazardous.[17,19]

2.2.2 K_2CO_3-Based Sorbents

New materials are needed to replace amine-based CO_2 capture to prevent future environmental complications brought on by amine emissions. To be able to compete with amine scrubbing, the capture material must possess many properties including cheap and simple production, a low-cost regeneration, and a long use time before needing to be replaced to name a few. Solid alkali-metal based sorbents have been identified and begun to be explored in the last few decades.[20] Some metal oxides and carbonates that have been considered include MgO, CaO, and K_2CO_3.[20,21] In the following work we explored the capture capability and feasibility of K_2CO_3-based sorbents on a small industrial scale (a small packed bed reactor, not a bench scale measurement). K_2CO_3 is considered over other alkali-metal materials due to its comparably low regeneration temperature. Most metal oxides are heated to >500°C, while in comparison under atmospheric conditions K_2CO_3 regenerates at around 120°C+ depending on the utilized support and gas conditions, but typically hovering around 155°C.[22,23] The simplified reaction is provided in line 3; K_2CO_3 reacts with CO_2 under humid conditions to reversibly form $KHCO_3$.[20]

3. $K_2CO_3 + CO_2 + H_2O \leftrightarrow 2KHCO_3$

The biggest challenge to K_2CO_3-based sorbents is that despite their high theoretical capacity of 7.25 mmol CO_2/g K_2CO_3 (compare this to zeolite, around 5 mmol CO_2 per gram), actual CO_2 conversion often is capped at around 50% that. This is primarily due to poor morphological structure of the raw K_2CO_3 that results in pore-clogging.[24] In addition, due to the very deliquescent nature of K_2CO_3 salt, their stability in humid environments is often quite low.[22] For these two reasons, support structures are needed to provide ample surface area for reaction, and to prevent dissolution of the material and thus mass loss while cycling. Recently most efforts in developing K_2CO_3-based solid sorbents have been focused on finding a viable support for industrial scalability. Some of the options considered in the literature include carbon nanofibers, TiO_2, Al_2O_3, SiO_2, cement and clay.[24]

There are primarily two approaches to adhering K_2CO_3 to its support. Wet-activated granulation, like what is primarily used for clays and cements, describes a process in which support/binding dry powders are mixed with K_2CO_3 and water. The slurry can then be shaped into pellets then dried or dried to be crushed and sieved into the appropriate size particles. When dried low temperatures superficial water is baked off, and at high temperatures (>300°C) calcination may even convert carbonates and hydroxides to metal-oxides, or recrystalize the mixture, increasing material strength.[25] Alternatively, impregnation describes a process in which a covalently bonded network, typically a metal oxide particle like Al_2O_3, is submerged in K_2CO_3 solution. Dissolved K_2CO_3 slowly traverses the pores until the solution reaches an equilibrium. The particles are then removed from the solution and dried. While there are many benefits to granulation-formulated materials, as will be discussed in Chapter 3, for the purpose of testing the Centennial reactor we chose to utilize impregnated zeolite beads. The primary benefit of utilizing an impregnated media is that there is no concern the structure the K_2CO_3 is adhered to will dissolve or break apart. As this work involves the construction and calibration of the new reactor system, it was important that the testing material be as chemically simple as possible by providing a strong support for the K_2CO_3.

2.3 Methods

2.3.1 Reactor Design and Construction

The Centennial packed bed reactor, with which this work was performed, is the first industrial prototype that utilized Mitico's potassium carbonate-based sorbent. It is the test-system of a family of reactors which will be installed on top of industrial exhaust vents to capture CO_2 from post-combustion flue gas. The entire structure referred to as the Centennial reactor is multiple tandem systems that make controlled capture and release of CO_2 possible. The system generates a laboratory "flue gas," controls that flue gas composition and flow rate, regulates temperature, pressure and humidity in the tower, and detects and captures data related to CO_2 capture and release. Generation of the laboratory flue gas mimic was a non-trivial aspect of the work, as will be explained in the following section. Figure 2.3 provides a simplified diagram of the main points of interest in the centennial system.

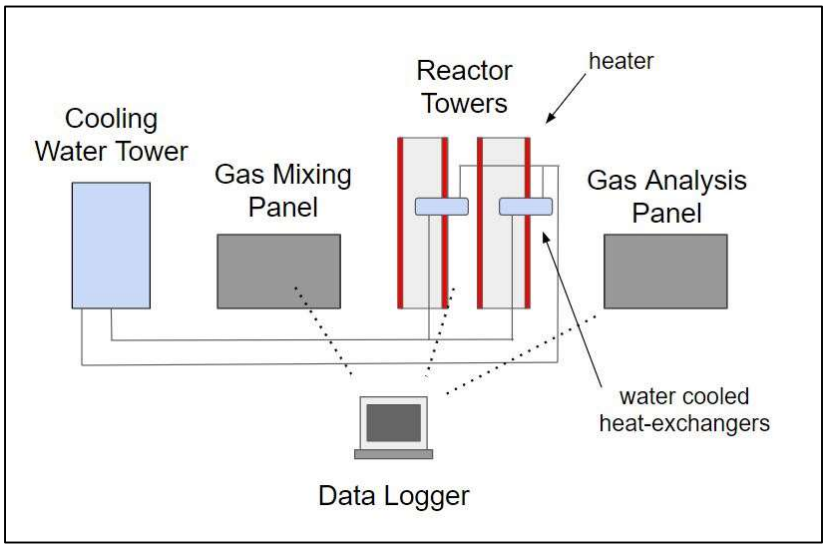

Figure 2.3 displays an overview of the most critical components to the Centennial reactor. The three subsystems that will be explored in more detail in the following sections are the gas mixing Panel, the packed bed towers, and the gas analysis panel. Also shown in the above image is the cooling water system, the internal tower heater, and the data logger.

Centennial was assembled at Mitico's 2023-2024 headquarters, an industrial warehouse in Los Angeles, California. Assembly began Spring of 2023 and was completed Fall of that year, excluding some minor modifications carried out in late 2023 and early 2024. The two

reactor towers were purchased from a commercial supplier and mounted on a modular process skid for easier mobility. All other system components were constructed around the skid, which was placed near the black “X” in Figure 2.4. To make the reactor work requires an elaborate network of electronics, plumbing and gas regulation subsystems, not all of which will be discussed in detail. For example, to generate enough steam to provide humid flue gas at high flow rates necessitated utilization of a commercial steam generator which itself requires a deionized water source. A water sampling network with multiple reverse osmosis filters are maintained to provide the steam generator with a constant flow of clean water. Another subsystem not explored in this thesis is wastewater management. When the towers are in operation, lines must be continuously drained of any condensed vapours resulting from absorption or regeneration. However, the site did not allow for easy gravity drainage from all active sites, thus electronic drains were installed to collect and move wastewater. In the following sections we will explore in further detail the flue gas generation at the gas mixing panel, the packed bed towers, and the gas analysis panel.

Figure 2.4 shows the Centennial site prior to construction. Black tape was used to outline the approximate total system size. The black “X” indicates the approximate site the skid-mounted towers were placed. Component placement was optimized according to the location of the water supply (the white sink), site drainage (the black tube by the sink), and power supply (transformer and electrical control panels, grey).

Figures 2.5 and 2.6 display the complete Centennial system from two different angles. The cooling tower is around the open door (1) in Figure 5, and thus not displayed. In Figure 5, the tower control panels (2) are displayed on the reactor front, as well as compressed gases on the right (3), which are used to generate different flue gas conditions. In between the towers and cylinders sits a steam generator (4) used primarily to humidify the flue gas. Occasional trials were conducted where steam was also utilized for CO2 regeneration. In Figure 6 the gas mixing (5) and gas analysis (6) panels are visible. An in-line heater (7) is available near the tower control panels and provides extra temperature control for injected flue gas. One of the water-cooled heat exchangers (8) also illustrated in Figure 2.3, is visible to the left of the gas mixing panel.

2.3.2 Gas Mixing Panel

Centennial is designed to be flue gas agnostic, meaning that it can capture CO_2 from many industrial processes. For example, in a natural gas combined cycle powerplant CO_2 concentrations are very dilute, about 4% in the outlet stream. Alternatively, a pulverized coal power plant may have exiting CO_2 concentrations as high as 15%.[10] Powerplants, depending on their energy source and combustion conditions, can also be highly humidified, with most post-combustion streams having absolute humidities between 5 and 15% H_2O.[26] One challenge to creating carbon capture materials is though they must be employed under a variety of industrial conditions, the composition of the gas can affect the performance of the material in many ways. For example, pure K_2CO_3 has a lower capture capacity at lower concentrations of CO_2 because of a shift in the reaction equilibrium. This was observed by Luo *et al.*, who found an absorption capacity of 6.24 mmol g^{-1} when the flue gas was 1% CO_2 and a capacity of 6.92 mmol g^{-1} while at 100 %CO_2.[27] Hydration levels of the material, active or inactive, may also impact the rate at which CO_2 is captured. If H_2O is blocking pores, dissolving material, and overall creating greater flow resistance it can impede reaction with CO_2. On the other hand, readily accessible water may expedite the 3-molecule reaction to form bicarbonate.[27]

Since the material performance will vary depending on the flue gas composition, it is important for any study to have a well-defined flue gas. To accomplish this, we constructed a flue gas mixing panel. The panel was constructed of a perforated carbon steel sheet for its easy mounting capability and large weight capacity. During initial system testing, which included leak testing and monitoring gas flows through the tower, two Omega FMA-1600 series mass flow controllers were utilized to mix CO_2 and N_2 from Airgas compressed gas cylinders. During this phase only low flow rates between 5 and 25 lpm were needed. Figure 2.7 shows this initial set-up, including a sampling line that sends mixed but not yet humidified flue gas to a Servomex 4900 Multigas (CO_2) Analyser. While it is redundant to send samples of known mixtures through to the CO_2 analyser, later compressed air was utilized to increase flow to industrially relevant rates greater than 50 lpm and necessitated use of an external concentration measurement. Once the gas was mixed and verified against the CO_2 analyser, it was humidified and sent to the reactor inlet.

Figure 2.7 shows the original perforated panel design. Two mass flow controllers set the flow of CO_2 (1) and N_2 (2) coming from pressurized cylinders. Around 2 lpm of the mixed "flue" gas is sent to a CO_2 analyser (5) via another mass flow controller (4) to monitor composition changes in real time. Again, this is not as necessary when flue gas is generated by controlled gas mixes, but later compressed ambient air was used instead of N_2 to increase flow rates. A pressure relief valve (3) can be used in case of an emergency shutdown. Once the gas is mixed and analysed it is sent to a junction (6) that introduces water vapor from the steam generator.

As previously stated, industrial flue gas absolute humidities span between 5 and 15% water, and reaction kinetics and sorbent capacity are dependent on humidity levels. However, maintaining near constant humidity levels in gas streams, especially at high flow rates is not trivial. The Antoine equation[28] for water dictates that at 50°C, air can hold a little over 10% water. Thus, we hoped to generate flue gas of around 50°C or more. It should be noted that gas greatly above the optimal absorption temperature of 65°C, which can hold up to 25% water, would also introduce issues, as it would shift the equilibrium towards the reverse (regeneration) reaction.

The heat from the steam injected into the line was not on its own enough to heat the gas stream to 50°C so heating tape was wrapped around the humidification junction depicted

in Figure 2.7. The Cellkraft E-1500 Precision Steam generator can produce steam at a set flow rate, or it can be set to an operating mode that uses a hygrometer and internal Proportional-Integral-Derivative (PID) loop to maintain an average set humidity. It was determined that temperature fluctuations in the warehouse and flow rate fluctuations from the air compressors introduced too much instability to use a set steam flow rate, thus we utilized PID operation mode.

Before actual packed-bed absorption testing the original mixing panel shown in Figure 2.7 was used for general operational testing. First, N_2 between 0 and 25 lpm was injected into the tower under different operational configurations (to be explained in the following section) to test for leaks. Leaks were identified by comparing entering tower flow rates to exiting tower flow rates and located on the skid by bubble test method. CO_2 containing samples were then injected to ensure that no unexpected empty tower absorption unto surfaces occur, again by comparing the concentration at the inlet to that at the exit. Lastly, humidified samples were injected into the tower to ensure tower drainage was functional and properly removing condensed vapours.

As we increased testing flow rates to mimic industrial flue gas conditions, it was clear that it was not possible to replace N_2 tanks fast enough. Thus, when this initial round of testing was complete, the compressed N_2 was replaced with compressed air from two 15-gallon DeWalt Electric Air compressors. Additionally, all the quarter inch lines displayed in Figure 2.7 were replaced with half inch lines.

2.3.3 Packed Bed Towers and Operational Procedures

Centennial was designed to continuously cycle absorbing material, therefore after an absorption phase saturated material must be regenerated in the tower (opposed to being unloaded and regenerated elsewhere). But because the capture system must continuously capture CO_2 exiting an industrial vent, while saturated material is regenerating a fresh reactor bed must be available for capture. Thus, to perform continuous CO_2 capture necessitates (at minimum) a two-tower system, which we will refer to as “A” and “B.”

In short, while tower A is performing capture, Tower B can regenerate its sorbent and prepare for another absorption period. To accomplish this, a collection of valves is controlled by the tower's operating system and progress each tower through 3 phases: absorption, regeneration, and cooling.

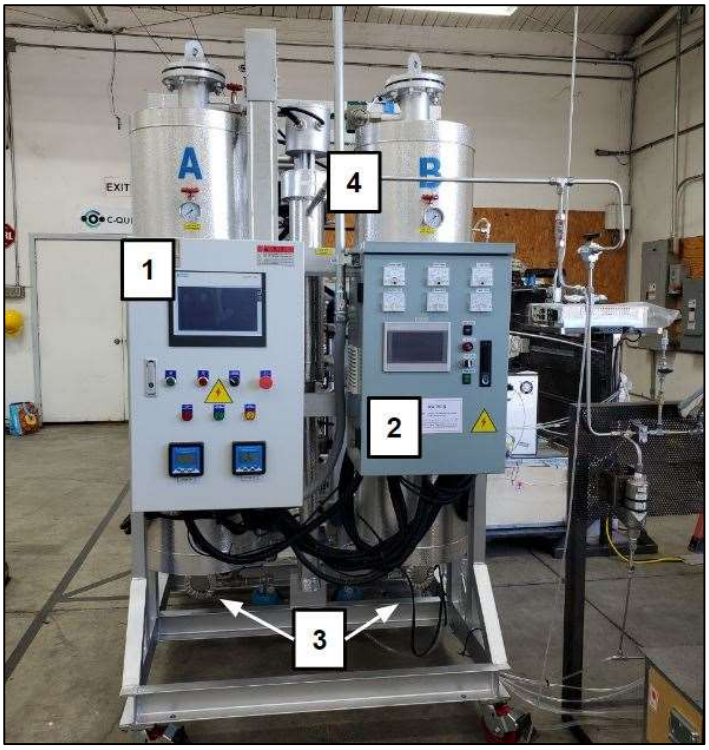

Figure 2.8 displays the front of the two-tower reactor on its mounting skid. The left control panel (1) is used to set and monitor each towers operating phase (absorption, regeneration, and cooling). The right control panel (2) sets the towers' temperatures. At the bottom of the tower, a set of matching pressure relief membranes are visible (3) that open when tower exceeds pressures of 20 atmospheres. In between towers A and B is an inline heater (4) that can be used to maintain or increase flue gas temperature.

To simply explain typical Centennial operation, we will describe a complete cycle within a singular tower. During the absorption phase the tower is heated, usually to 65°C, at which point the flue gas is injected. In the trials performed here, ~100kg loads of K_2CO_3-impregnated zeolite were found to absorb for approximately 1 to 3.5 hours (variation will be explained in the results and discussion section). Saturation is observed when outgoing CO_2 concentration equals that of the incoming concentration on the CO_2 analysers.

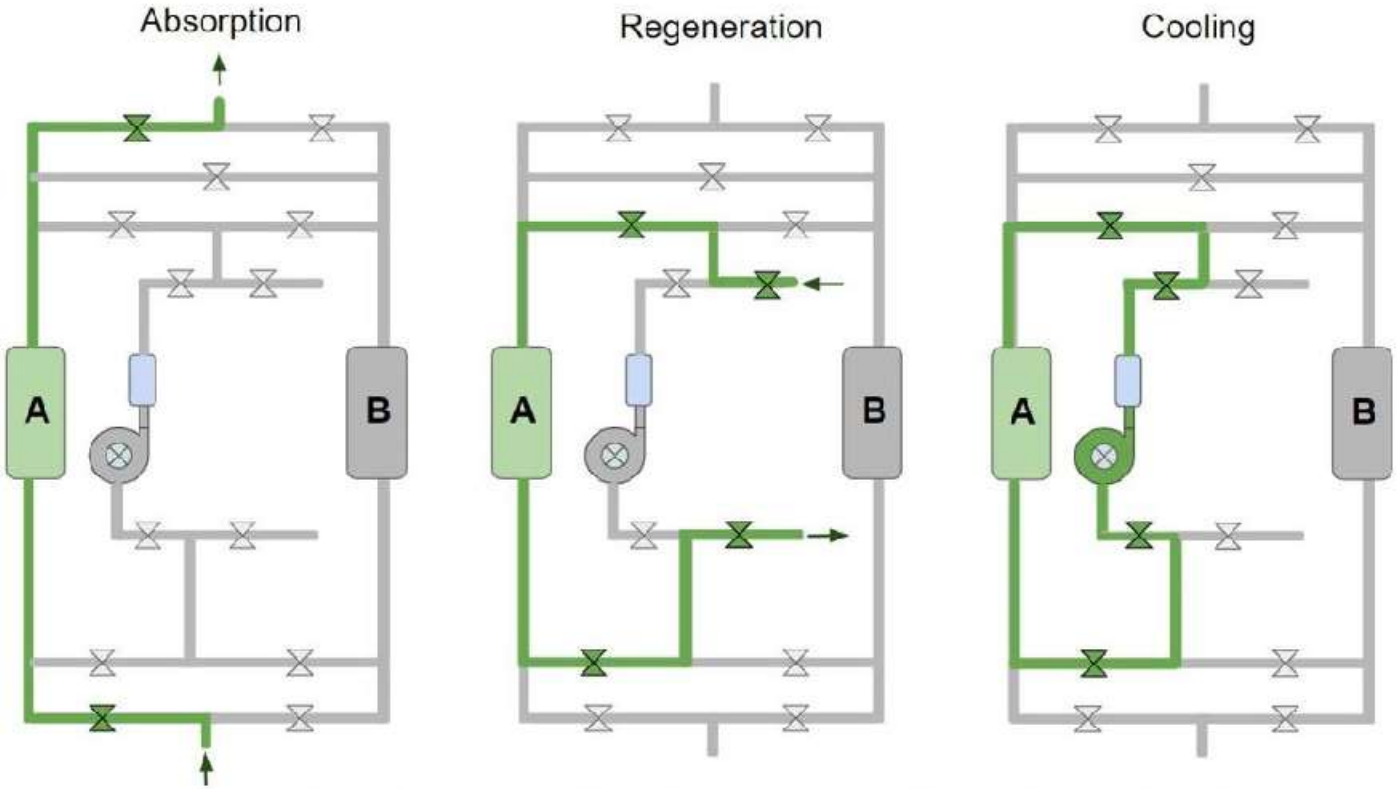

Figure 2.9 visualizes the three phases of a complete cycle in reference to tower A. Valves are illustrated by the hourglass shape, and the cooling fan and heat-exchanger are located between towers A and B and highlighted in green during the cooling phase. The tower is designed such that flue and purge gases enter and exit through different channels to allow for simultaneous running of the towers. During the absorption phase flue gas enters through the bottom of the tower and exits through the top of the tower, while during the regeneration phase purge gas enters through the top and exits through the bottom. During the cooling phase the air is circulated.

Typically, the absorption phase is held for at least half an hour after the CO_2 analysers first indicate sample saturation. When the absorption phase ends, flue gas injection in that tower is halted, and the tower is heated to prepare for sorbent regeneration. Once the tower has reached the desired regeneration temperature (can vary, will be explained in the results section), a purge gas can be injected. While in an ideal open-air system a purge gas may not be necessary, the reactor has long and narrow lines that may trap CO_2 during regeneration. During the regeneration phase once the purge gas is introduced the outcoming CO_2 is again monitored on a Servomex analyser. Regenerated CO_2 is observed as an increase in CO_2 concentration/volume of the exiting gas.

Typically, regeneration is the longest step as it takes multiple hours to heat the tower, especially depending on how much moisture the sorbent absorbed due to the high heat capacity of water. Challenges in accurately measuring low CO_2 concentration towards the end of regeneration phases made it difficult to assign when regeneration was truly "complete." For this reason, the length of regeneration period varied sometimes taking as long as 40 hours for N_2 and CO_2, but taking only about an hour with steam, as explained in the results section. After the regeneration phase ends the tower is at around 160°C and must be cooled before another absorption cycle can begin. During the cooling phase the tower heater shuts off, and the system valves reconfigure to create a loop as shown in Figure 2.9. An internal fan (Redbo 2GH210-H16) circulates tower air at 98 m^3ph, through one of the water-cooled heat exchangers. The rate at which the tower can be cooled is primarily determined by the fan rate and the water temperature, which for our system was about 20°C.

During operation, sensors inside the towers help assess system and material performance. Each tower has a cylindrical reactor region that is 1.8 meters long with an inner diameter of 0.27 meters. Surrounding these reactors are the heating elements, which are then surrounding with a layer of fiberglass insulation. At the very bottom of each tower is a condensate trap that is monitored via pH meter. The pH probe was installed to monitor sorbent leaching which occurs due to condensation that dissolves K_2CO_3 and will be discussed further in the results section. At the top, middle and bottom of each tower are thermocouples, pressure gauges, as well as humidity sensors. At just the top and bottom of

the towers are mass flow meters. The thermocouples were used primarily to monitor tower heating and cooling rates during the regeneration and cooling phases. The thermocouples, for example, helped identify heat sinks that would prevent sorbent from regenerating to completion. In early tests runs, it was determined that the middle of the tower heated much faster than the top and bottom, despite the heating elements running the full reactor length. Thus, extra fibre glass insulation was installed on both the top and bottom to minimize the temperature differential. The RH probes assist monitoring in two ways. During the absorption phase, the RH meters assure that flue gas is properly humidified upon arrival to the reactor. During the regeneration and cooling phases, the RH meter should be monitored to evaluate sample "wetness." A sample that is very wet, which will read as a high or even 100% RH, will take longer to heat due to the high heat capacity of water. In addition, when the sorbent is too wet it risks losing active material due to the previously mentioned issue of leaching. The pressure gauges should be monitored regularly to ensure that the reactors do not become dangerously over-pressurized from a lapse in procedure or system malfunction. They are also used to measure the sorbent-dependent pressure drops. Lastly, flow rate measurements are necessary to calculate total absorbed CO_2.

2.3.4 Gas Analysis Panel

During the absorption and regeneration phases, the exiting gas streams are navigated towards a gas analysis panel. As can be seen in Figure 2.9, it is necessary to have the treated and regenerated gas exit through different paths so that both towers can be run simultaneously. Ideally, the gas analysis panel would be equipped with two CO_2 analysers so that exiting treated flue gas and regenerated gas can also be analysed simultaneously while both reactors are loaded. At the time of data collection however, the gas analysis panel was equipped with one CO_2 analyser, labelled (6) in Figure 2.10. For this reason, during the data collection described in this chapter, only one tower was run at a time. The PureAir and ADCOA zeolites were run in towers B and A, respectively, so that both reactors were tested for potential system issues.

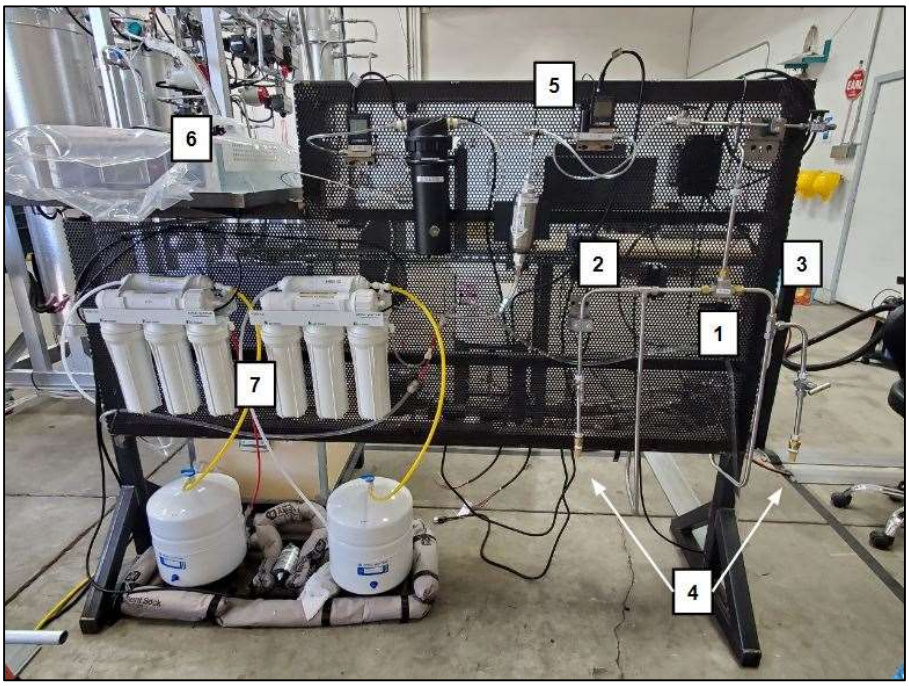

Figure 2.10 displays the gas analysis panel at the start of testing. The valve (1) is switched to select the exiting treated flue gas (3) or the regenerated CO_2 (2). Since the CO_2 analyser, which is this picture is bagged, (6) can only measure flow rates of up to 2.5 lpm, vent valves (4) were installed to release excess gas. Due to the vary large flow exiting the towers during the absorption phase, positive pressure prevents outside air from mixing significantly with sampled gases. A flow controller (5) sets the analyser (6) flow rate. Condensers and desiccants were installed after the flow meter (5) to protect the analyser. The tower humidity meters indicated that treated flue gas was almost completely dry by the time it exited the towers. On the other hand, regenerated gas was quite wet, and later another larger condenser/drying tube was installed near (2).

2.3.5 Impregnated Zeolite, Preparation and Loading

At the time that these towers were constructed and tested, a higher capture capacity sorbent was being developed in parallel via wet activated granulation method, as explained further in Chapter 3. For the purpose of tower testing and development, a first-generation material was utilized; K_2CO_3 impregnated zeolite beads. To keep K_2CO_3 in the solid phase requires at minimum some sort of support material. This is because K_2CO_3 is very deliquescent in humid conditions and has an incredibly high solubility, of over 1 g/mL at room temperature. In addition to resistance to moisture, supporting material should also provide porosity. While K_2CO_3 has a very high theoretical capture capacity of 7.24 mmol CO_2 g^{-1} K_2CO_3, measured capture capacities of pure K_2CO_3 tend to be substantially lower due to

poor pore formation during crystallization.[27,29] For example, K_2CO_3 calcined from the hydrate ($K_2CO_3 \cdot 1.5H_2O$) at 200°C with no support only achieves about half of the theoretical capture efficiency.[29] Alternatively, K_2CO_3 supported by 65 mass percent γ-alumina has been observed to increase that capture to 70% the theoretical value.[25] As will be further explored in chapters 3 and 4, the support material and how it is bonded to K_2CO_3 (water content, calcination temperature, material density etc.) can alter sorbent capacity, sometimes allowing it to reach near theoretical values.

Impregnated zeolite was selected for first generation sorbent testing primarily because of its high surface area and known resilience in humid environments. For example, 3μm diameter 13X zeolites prepared from bentonite clays have an observed surface area of around 900 m^2g^{-1}. Assuming a crystal (non-bulk) density of around 1.5 g cm^{-3}, a nonporous material of the same diameter would have a surface area of around 1 m^2g^{-1}. Thus, the zeolite microstructure increases the surface area by about 3 orders of magnitude! Due to its use in many industrial and commercial systems as a molecular sieve, zeolite beads are also relatively cheap, making it amenable to large-scale (multiple kg) testing. Again, due to their popular use, zeolite beads are commercially available in many sizes.

Sorbent particle size must be carefully matched to the tower design. On one hand, smaller particles are preferable due to higher surface area:volume ratio, which results in slightly faster chemical reactions. On the other hand, particles which are smaller can create too much frictional resistance, resulting in large pressures drops according to the Ergun Relation, equation 4.[30] Pressure drops are an issue for a couple of reasons. First, to increase pressure usually requires greater energy consumption by using electric pumps. Pressure drops also correspond to a decrease in reactor resonance time, which in turn results in lower reaction efficiencies. Lastly, too great of pressure drops can result in channelling, leading to uneven reaction conditions.

4. $$-\frac{dP}{dx} = \alpha \frac{(1-\varepsilon)^2 \mu}{\varepsilon^3 D_p^2} v + \beta \frac{(1-\varepsilon)\rho}{\varepsilon^3 D_p} v^2$$

The Ergun equation predicts pressure drop (P) of a given material packing length (x). The pressure drop is dependent on the particle diameter ($D_{p)}$, the porosity or void fraction of the bed (ε), the incoming fluid velocity or superficial velocity (ν), as well as the fluid (flue gas) density (ρ), fluid viscosity (μ), and viscous resistance (α) and formal resistance (β) coefficients of 150 and 1.75. Most of these variables cannot be modified for the system as they are inherent properties of the flue gas. The tower height must be selected according to the anticipated capture efficiency of the material. For example, slower reacting materials will need a comparably taller tower than quickly reacting materials to obtain a similar capture efficiency as they need to interact with more material. Thus, the simplest variable to adjust to reduce pressure drop is D_p.

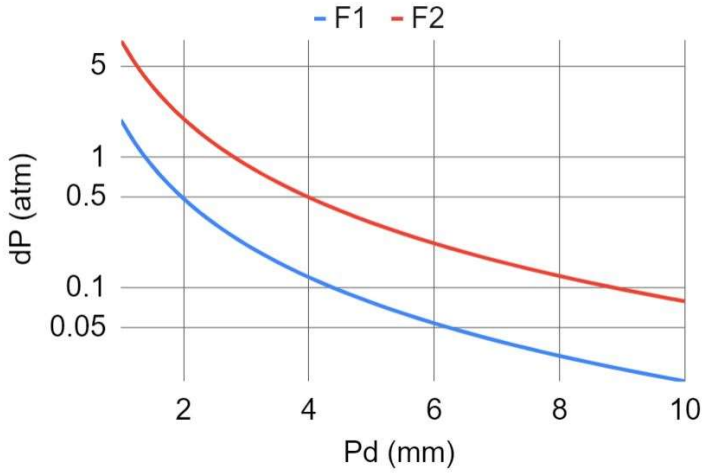

Figure 2.11 displays the expected pressure drop curve according to the Ergun equation for two different flow rates in the centennial tower. F1 and F2 are equal to 6 and 12 m^3ph. They were converted to linear flow by dividing by the reactor cross-sectional area as well as the void fraction. These curves were calculated assuming a 40% void fraction.

The relationship between D_p and pressure drop for two different flow velocities is expressed in Figure 2.11. The incoming velocity for most trials we performed is approximately 6 m^3ph, which with a reactor diameter of 0.266 m and assumed void fraction of 40% corresponds $\nu = 0.075$ m s^{-1}. μ and ρ of the flue gas can be approximated to that of ambient air, so 1.8×10^{-5} kg $m^{-1}s^{-1}$ and 1.2 kg m^{-3}, respectively. Considering a reactor height of 1.8 m, we can plot the pressure drop as a function of P_d. The pressure drop relation for a total flow rate of 6 m^3ph is labelled Flow 1 or "F1." Flow rates exiting power plant flue

stacks can easily be double that, so we also plot the pressure drop curve for 12 m^3ph, labelled “F2.” Higher flow rates result in larger frictional forces, thus, to obtain similar pressure drops towers with higher flow rates will require larger particles. For example, in Figure 2.11 the 6 m^3ph flow observes a pressure drop of 0.1 atm for a particle around 4 mm, while the 12 m^3ph tower will observe the same drop for a 9 mm particle.

In an ideal system, where no chemical reactions are happening, the change in pressure will directly result in a change in flow rate according to conservation of mass, equation 5. Here, m_{in} (and similarly out) is mass flow rate, A is the cross-sectional area, v_{in} is the linear velocity, and ρ_{in} is the gas density. Thus, the change in the linear velocity of the fluid can be estimated to be inversely proportional to the density change in the fluid. The change in density is, at constant temperature, proportional to the change in pressure. So, a decrease in pressure of 10% results in an increase in flow rate by 10%. Again, this is assuming conservation of mass, which we know is not true for our system where both CO_2 and H_2O are reacting.

5. $$m_{in} = m_{out} = Av_{in}\rho_{in} = Av_{out}\rho_{out}$$

In conclusion, to prevent substantial pressure drop a support bead size of at least 4mm was selected for impregnation. Impregnation of zeolite samples is theoretically a simple procedure; expose the support material to the active material by submerging it in concentrated K_2CO_3 solutions, then dry them before use.[31] Ideally, K_2CO_3 can penetrate the entire depth of the particles and multiple layers adhere to its surface. Impregnation duration and solution concentration can both impact the resultant activated particle capacity and kinetics. Too concentrated of a solution causes fast adhesion onto the particle once it is submerged, and this creates thick but superficial impregnation. Superficial impregnation means that the active material resides mostly on the surface and makes the material more susceptible for leeching and thus material loss. This is not ideal, since the sorbents are meant to be cycled potentially hundreds of times. Additionally, superficial and fast adhesion can contribute to pore clogging, which reduces surface area and thus also reduces sample capacity and kinetics. On the other hand, solutions which are not concentrated enough do not adhere enough active material to the support material. Lastly, it takes time

for active material to attach to the support surface. To ensure proper adhesion all sorbents formed at Mitico were submerged for around 24 hours which is standard for incipient wetness impregnation.[31,32]

To verify the solution concentration selected for large-scale sorbent testing was optimized, small-scale samples were tested and compared in terms of their capacities. For impregnation of small-scale samples, 100g of 4mm ADCOA 13X zeolite beads, shown in Figure 2.12, were submerged in 500g solutions ranging between 15 and 45g K_2CO_3 g^{-1} H_2O. After 24 hours samples were drained and superficially dried for an hour at 95C, and then more thoroughly dried at 190°C for two hours. This two-step drying method was selected as rapid initial drying before the addition of the 95°C step caused the particles to crack, likely due to explosive water release. The zeolite impregnation was visually confirmed as the beads changed colour from beige to paler beige (K_2CO_3 is white).

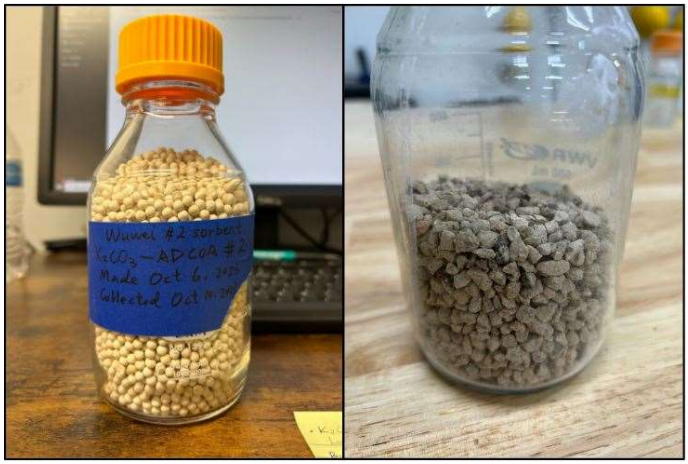

Figure 2.12 displays the Mitico-prepared ADCOA spherical zeolite (left) as well as the PureAir-prepared rock-type zeolite (right).

In addition to the Mitico-prepared spherical 13X zeolite beads another sample comprised of Clinoptilolite zeolite, which we refer to as rock-type, was purchased and impregnated by PureAir to be tested. The impregnation methods for the rock-type Clinoptilolite zeolite thus are proprietary. The goal in testing two different zeolite samples is to quantify the effect of zeolite source and impregnation method on resultant sorbent capacity and kinetics. Despite both the spherical and rock-type sorbents being zeolites, we do not expect them to have the same capture properties. Zeolites can vary greatly in both structure and chemical

composition, which results in differences in colour, density, pore size, and compressive strength.[33,34]

Zeolites are similar to clays in that they are aluminosilicates containing exchangeable cations. They also have the ability to hold large amounts of water, up to 20% of their mass in humid environments.[33] However clays are phyllosilicates, meaning that they are 2D sheets that make 3D structures by layering.[34]

Unlike clays, zeolites have crystallographic 3D order, specifically zeolites are tetrahedral.[34] Connected tetrahedra can form a variety of unique structures, but they all fall under a system that can be used to classify them according to their structural elements, known as the Meier and Olsen framework.[33] This framework identifies secondary building units that makes different crystals more easy to identify. For example, clinoptilolite (the PureAir rock-type) is primarily made up of the 10-node 4-4-1-1 subunit, also known as the heulandite subunit.[35] These subunits are primarily connected via mirror planes forming what is known as the heulandite series (IUPAC code HEU). Heulandite is structurally the same as clinoptilolite except heulandite contains samples with Si:Al< 4 and the clinoptilolite series refers to those with Si:Al > 4.[36] Clinoptilolite, as a member of the HEU series, contains 3 types of large channels made up of 8 and 10-membered rings, depicted in the top panel of Figure 2.13.[36] Clinoptilolite is also naturally occurring, and contains both primary and secondary porosity, where the primary porosity refers to that determined by crystal structure and secondary refers to natural imperfections like fractures.[37]

Zeolite 13X on the other hand, which the ADCOA beads are made of, is industrially made and primarily composed of structural unit called a sodalite or β-cage in an arrangement that forms what is called the faujasite series (IUPAC code FAU).[33] Sodalite cages are defined by a surface which is composed of six 4-rings and eight 6-rings. In the FAU series sodalite cages are joined together via double-six rings, like carbon in a diamond. This creates a “super cage” with four 12-ring openings as shown in the bottom of Figure 2.13. Zeolite X refers to a synthetic FAU with lower Si:Al, typically around 1. As Si-O bonds are shorter than Al-O bonds, ~1.6 vs 1.8 Å, enriching zeolites in either Si or Al modifies the pore size. 13X is often called NaX as it is also primarily composed of sodium ions.

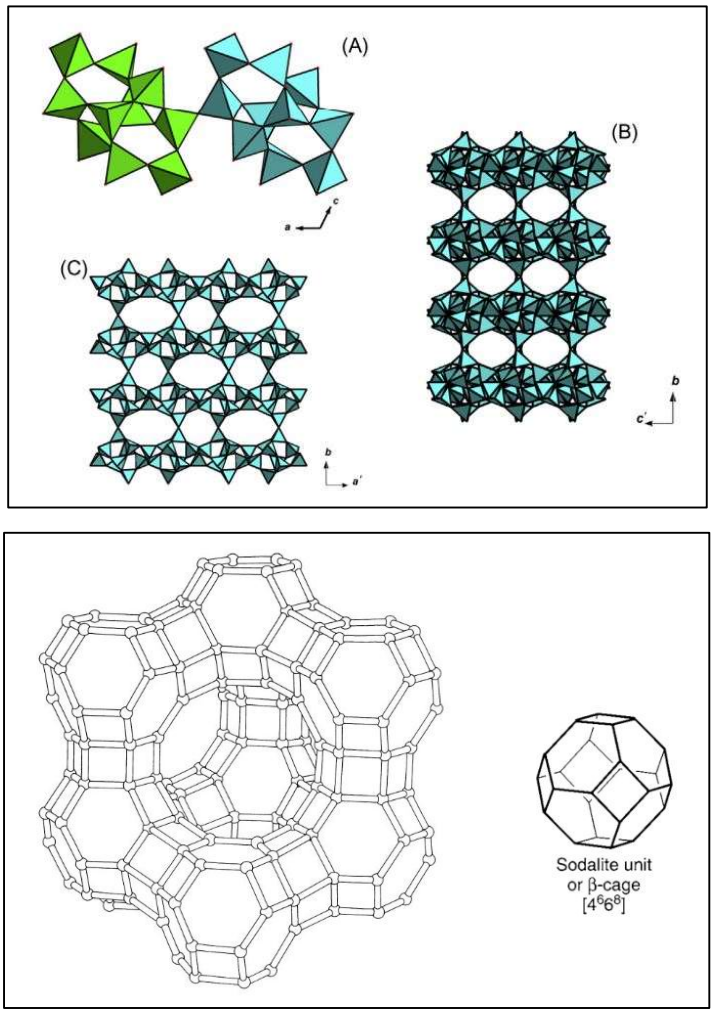

The top panel of Figure 2.13 is borrowed from Gatta and Lotti and depicts the HEU series from 2 different orientations (B and C). Also shown in the top panel is two heulandite subunits side by side (A).[36] *The bottom panel of Figure 2.13 depicts a sodalite unit, borrowed from McCusker and Baerlocher, as well as the full FAU super cage.*[33]

These structural and compositional differences result in different pore sizes and effective surface area. Clinoptilolite tends to secondary porosity that is more mesoporous, with pores on the order of 50nm,[37] while zeolite 13X is considered to be microporous with pores on the order of around 1nm. We expect these differences, especially the pore size, to impact many aspects of the impregnated product. Differences we expect include how much active material can be loaded, how deeply the active material can penetrate the particles, how fast the loaded K_2CO_3 can react with CO_2, how fast and how completely the $KHCO_3$ can be regenerated to K_2CO_3. These effects may be caused by simple sterics (larger openings makes for better mobility) or chemical effects (for example, larger pores may hold larger

amounts of water). We even expect differences in the longevity of the material; differences in pore size may result in substantial variation in material leaching.

As mentioned in Section 2.3.4, the rock-type and ADCOA 13X zeolites were run in separate trials in towers B and A respectively. The ADCOA impregnation method resulted in beads which had taken up 20% their original dry mass in K_2CO_3 after optimization. This means for every 100 g ADCOA beads, 20 g of K_2CO_3 can be loaded resulting in a dry mass of 120 g after impregnation and drying. The rock-type loading efficiency is unknown due to its proprietary nature, but PureAir said to have also optimized their loading efficiency. Future work on Clinoptilolite samples would benefit from noting the loading efficiency to know the total mass of active material loaded into the tower. These samples were loaded using cotton long underwear to gently convey particles into the reactor bed, preventing fragmentation. Minimal fragmentation was visually confirmed when the towers were later unloaded. The entire 1.8m reactor length was loaded for both trials, to normalize is respect to volume. The rock-type and ADCOA beads ultimately had total loaded masses of 111.6 and 100.8 kg, respectively.

2.3.6 Calculations

The sensors before, along, and past the reactor (discussed in sections 2.3.2-2.3.4) were ultimately used to characterize and quantify the effectiveness of the absorption and regeneration cycles. The raw sensor data was primarily used to calculate three types of data; capture efficiency, total CO_2 captured, and a 2^{nd} order kinetic rate constant. Capture efficiency compares the amount of CO_2 injected to how much was absorbed at a single point in time. Ideally, around 100% capture would occur for almost the entire capture period with a very steep transition to 0%. This sort of efficiency curve is correlated to, but not the same as, the capture kinetic constant. A fast overall absorption rate constant should result in a high capture efficiency, unless for some reason there is little CO_2 or H_2O available in the flue gas stream. CO_2 captured is put simply, the total injected CO_2 minus the exiting (non-captured) CO_2.

To calculate **capture efficiency** (moles captured/moles injected, shown in equation 8 requires the amount of CO_2 injected at a point in time (N_{inj}) as well as the moles captured

at that same point in time (N_{capt}). It should be noted that the gas that enters at some time "t" really exits the tower and is sampled at some point "t+dt" where "dt" is the resonance time through the reactor and entering/exiting lines. The reactor (~0.1 m^3 packing volume) resonance time at the flow rates used (~5 m^3/hr^{-1}) was estimated to be about 1.5 minutes. We estimate the total "dt" for the gas stream entering at time "t" to exit is about 2 minutes. Since absorption usually occurs over several hours, the error associated with sampling injected and exiting CO_2 at the same time was considered minimal. To be clear; for capture efficiency calculations, each injected and exiting pair was calculated for the same time "t."

Sampling is done in 10 second intervals, thus moles injected during a sampling period is defined by equation 6, where $F_{CO2,inj}$ is the volumetric flow rate, 4 slpm, which is always the same in our trials as it is injected via flow controller. t_{samp} is the sampling period, which when multiplied by the flow rate determines the volume of flow injected in litres and can be converted to moles via relationship with the ideal gas constant, R. Since the flow is in slpm, P and T are standard pressure and temperature.

Moles captured is moles injected, determined by equation 6, minus moles exiting. The moles exiting the tower is calculated according to equation 7. This equation takes the same form as equation 6, except that the flow rate of CO_2 exiting the tower must be determined by the total flow exiting the tower, F_{tower} and the fraction of CO_2 in the stream, $\%_{CO2}$, measured on the exiting gas panel via CO_2 analyser. Condensers (Figure 2.10) and later desiccant tubes were installed prior to the analyser inlet to protect it, thus the $\%_{CO2}$ is inherently a RH = 0 measurement. This did become an issue later when we attempted to calculate regenerated CO_2 as the exiting stream is inherently wet. This means that the $\%_{CO2}$ is artificially higher during regeneration cycles than it is in reality as water vapor was intentionally removed. However, for absorption cycles, RH meters at the tower exit confirmed the gas stream was always dry once exiting the column at the location where F_{tower} is measured. This is not unexpected as the absorption reaction requires both CO_2 and H_2O, and zeolite is a known desiccant, meaning it physisorbs water.

6. $N_{inj} = F_{CO2,inj}\,(\,t_{samp})\,(\frac{P}{RT})$

7. $N_{exit} = F_{tower}\,(\%_{CO2})\,(t_{samp})\,(\frac{P_{tower}}{R\,T_{tower}})$

8. $N_{eff} = \frac{N_{capt}}{N_{inj}} = \frac{N_{inj} - N_{exit}}{N_{inj}}$

To calculate **CO_2 captured**, we can utilize equations 6 and 7, i.e. $N_{capt} = N_{inj} - N_{exit}$. It is important to note this calculation determines CO_2 captured over the 10 second sampling period. Total capture is calculated by summing over the total absorption period. CO_2 captured can be expressed in moles, kg, kg kg^{-1} sorbent or kg m^{-3} reactor. While academic literature often normalizes capture by the mass of sorbent, in an industrial setting it is often more useful to consider the volume of material that can be loaded, since the reactor size is fixed once it is constructed but the material density can change.

In addition to these two calculations, we attempted to determine a **2nd order rate constant** for each absorption cycle of the two trials. This calculation was performed early in the cycle at the point of highest observed absorption to better accommodate our assumptions, which includes that there was negligible diffusion limitation, the available reacting solid K_2CO_3 is constant, and there is no back reaction. If we assume that the absorption is 3-body one-step mechanism but with a constant solid K_2CO_3 (K_2CO_3 activity is assumed unchanging) then equation 3 implies equation 9, a bimolecular rate. As will be explored more thoroughly later in section 2.4, there is significant evidence that H_2O hydration does not occur simultaneously with CO_2 addition. We acknowledge that this framework, though necessary to attempt to quantitatively compare rates across and within trials, ultimately simplifies a very complex chemical mechanism.

9. $\frac{d[CO2]_t}{d_t} = \frac{d[H2O]_t}{d_t} = -k[CO_2]_t\,[H_2O]_t$

Equation 8 is ultimately used to derive equation 16, which can be utilized to calculate a 2nd order rate constant, k. First, equation 9 is simply rearranged and integrated to form equation 10. Without more information equation 10 is very challenging to integrate; however, if we consider the stoichiometric relationship in equation 3, equation 11 follows. Using equation 11 we can rewrite equation 10 as equation 12. Equation 12

simplified is of the form shown in equation 13, where c = $[H_2O]_0 - [CO_2]_0$. Expression 14 yields equation 15 when $[H_2O]_t$ is substituted back in. As is shown in equation 16, utilizing this framework of assumptions we can calculate a bimolecular rate constant for the absorption reaction in the tower using only the initial and final concentrations of CO_2 and H_2O (mol m^{-3}).

10. $$\int \frac{1}{[CO_2]_t\,[H_2O]_t}\, d[CO_2]_t = \int -k\, dt$$

11. $$[H_2O]_t = [H_2O]_0 - (\,[CO_2]_0 - [CO_2]_t\,) = [H_2O]_0 - [CO_2]_0 + [CO_2]_t$$

12. $$\int_{[CO_2]_0}^{[CO_2]_f} \frac{1}{(\,[CO_2]_t\,)([CO_2]_t + [H_2O]_0 - [CO_2]_0\,)}\, d[CO_2]_t = -k(\tau - 0)$$

13. $$\int \frac{1}{x(x+c)}\, dx = \int \frac{c^{-1}}{x} + \frac{-c^{-1}}{(x+c)}\,\mathrm{dx} = \frac{\ln(x) - \ln(x+c)}{c}$$

14. $$\frac{(\,\ln[CO_2]_f - ln[CO_2]_0 + ln([CO_2]_0 - [CO_2]_0 + [H_2O]_0) - \ln[CO_2]_f + [H_2O]_0 - [CO_2]_0)}{([H_2O]_0 - [CO_2]_0)} = -\mathrm{k}\,\tau$$

15. $$\frac{(\,\ln[CO_2]_f - ln[CO_2]_0 + \ln[H_2O]_0 - \ln[H_2O]_f)}{([H_2O]_0 - [CO_2]_0)} = \text{-k}\,\tau$$

16. $$\mathrm{k} = \left\{ \ln\left(\frac{[CO_2]_0}{[H_2O]_0}\right) + \ln\left(\frac{[H_2O]_f}{[CO_2]_f}\right)\right\} ([H_2O]_0 - [CO_2]_0)^{-1}\,\tau^{-1}$$

The initial undiluted CO_2 concentration ($[CO_2]_{und}$, mol s^{-1}) is given by the mass flow controller connected to the CO_2 compressed gas cylinder. The initial diluted concentration ($[CO_2]_0$, mol m^{-3}) needed to calculate k is dependent on the total flow (F_{total} m^3 s^{-1}), which is measured at the bottom of the reactor after the CO_2 stream is mixed with air and hydrated via the steam generator described in section 2.3.2. The initial H_2O concentration can be determined by the RH meter and temperature probe at the bottom of the reactor. The August–Roche–Magnus, equation 18, can be used to approximate the saturation vapor pressure in hPa, where T is in kelvin. Then the absolute vapor pressure is proportional to the measured relative humidity. The initial H_2O concentration ($[H_2O]_0$, mol m^{-3}) can be calculated according to equation 19.

17. $$[CO_2]_0 = \frac{[CO2]_{und}}{F_{total}}$$

18. $$VP_{sat} = 6.11\exp\left(\frac{17.63}{T+243.04}\right)$$

19. $$[H_2O]_0 = VP_{sat}\left(\frac{\%RH}{100}\right)\left(\frac{1}{RT}\right)$$

Lastly, the final concentrations of CO_2 and H_2O are needed to calculate the rate constant. The final concentrations can both be calculated if the amount of CO_2 reacted is known. The amount of CO_2 reacted ($\Delta[CO_2]$, mol m^{-3}) is determined by the signals on the CO_2 analysers according to equation 20 where the signals before and after reactor are noted S_0 and S_f, respectively. Due to stochiometric equivalence, $\Delta[CO_2]$ is the same as $\Delta[H_2O]$. Then the final concentrations of both CO_2 and H_2O are just the initial minus the amount reacted, written for CO_2 in equation 21.

20. $\Delta[CO_2] = [CO_2]_0 \left(\frac{S_i - S_f}{S_i} \right) = \Delta[H_2O]$

21. $[CO_2]_f = [CO_2]_0 - \Delta[CO_2]$

2.4 Results and Discussion

2.4.1 Raw Data

The rock-type operation, labelled Trial 1 in table 2.1, ran from 9/25-10/20/23 in tower B. There was a total loaded sorbent mass of 111.6 kg, completing 8 cycles. Trial 1 was terminated early because it was determined that further insulation was required to prevent condensation during steam regeneration, which was attempted for the first time in Trial 1, cycle 7. The ADCOA beads, noted Trial 2, ran from 10/24-12/11/23 in tower A with a total loaded mass of 100.8 kg, completing 13 cycles. Two more steam regenerations were attempted in Trial 2 (after modifications to prevent condensation), with an added drying step before cooling down. This drying step utilized a 30-minute burst of compressed air to liberate excess water from the reactor walls as well as superficial water from the sorbent.

Table 2.1: Trials overview

Trial	Material	Impregnation	Tower Tested	Mass loaded	Run Dates	Cycles
1	“rock-type” Clinoptilolite	by PureAir	B	111.6 kg	9/25-10/20/23	8
2	spherical beads 13X ADCOA	by Mitico	A	100.8 kg	10/24-12/11/23	13

*Impregnation of the ADCOA beads and loading procedure for both Trials 1 and 2 are described in section 2.3.5

During the absorption period around 5 to 6 m^3ph of mixed flue gas was injected into the bottom of the tower. The compressed air tanks do generate some variation in the flow rate, as shown in Figure 2.14, on the bottom panel. As the flue gas enters the bottom of the tower, we measure a pressure less than one atmosphere. Since the flue gas is generated in a closed system using a steam generator it is possible to form flue gas below atmospheric pressure. There may also be some sort of vacuuming force between the mixed flue gas and the tower bottom. Since the reactor is full of a hydroscopic sorbent, and the flue gas is between 15-25% H_2O at any time, we hypothesize this may result in a low-pressure region at the tower bottom.

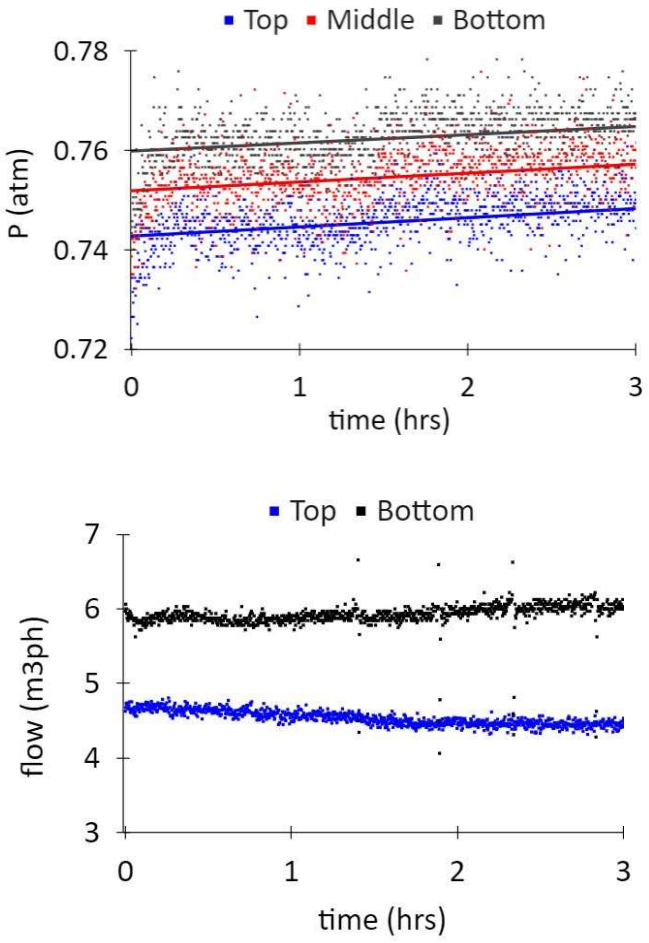

Figure 2.14 displays the pressure and flow profiles for Trial 2, Absorption 7. These profiles are typical of what was observed across all trials and absorption cycles. The top panel displays the pressure profile measured along the tower. The bottom panel shows that instead of a flow rate increase, we observed a decrease.

A pressure drop on the order of 1500-2500 pa, or 0.015-0.025 atm is observed from the bottom to the top of the tower for both trials (both sorbents), which makes sense given that despite being different shapes the materials are of similar size. For 4 mm diameter spheres with an initial volumetric flow rate of 6 m^3ph, we calculated a drop in pressure of approximately 0.1 atm or around 10,000 Pa when the void fraction is assumed to be 40% (see Figure 2.11). As our measured pressure drop is around an order of magnitude smaller, we expect that our void fraction is much higher than 40%. If we assume a void fraction of 50%, we calculate a pressure drop of approximately 3000 Pa, which is much closer to our measured value which fluctuates between 1500 and 2500 Pa. A void fraction of around 50% is on the higher end of what can be expected for a typical cylindrical reactor packing when the material randomly loaded, and indicates that a more optimal packing procedure is probably desired for industrial setting to optimize the mass loaded.[38]

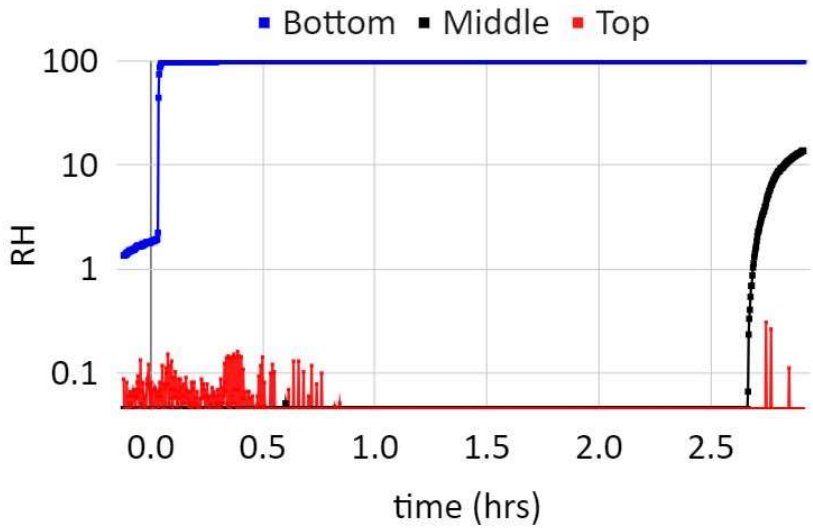

Figure 2.15 displays the RH meter outputs from along tower B during Trial 1 absorption 8. The plot shows the few minutes prior to start of the absorption period (time < 0), and the rapid increase in RH at the bottom of the tower once the flue gas is injected. Despite some minor variations in the baseline at the start and end of the trial, the top RH sensor consistently detects an essentially dry stream throughout the absorption period, meaning that the exiting gas was dry. The middle sensor began to increase towards the end of the trial, indicating that after about 2.5 hours the bottom-middle of the tower was becoming saturated with water.

Under a non-reacting flue gas system, we would expect the flow rate to increase as the pressure drops. Instead, we observe a drop in volumetric flow rate from 6 to around 4.5 m^3ph. This corresponds well to a loss in CO_2 and H_2O from the flue gas due to uptake by the coated zeolite; CO_2 and $H_2O_{(g)}$ comprise about 5 and 10-25% of the volume, respectively. While the sorbent very quicky becomes saturated with CO_2, as shown by the data collected on the CO_2 analyser (Figure 2.16, left panel), the zeolite can absorb water for much longer before it becomes saturated (assuming it was dried before recycling). The slow saturation of the zeolite was observed by the RH meters along the tower, for example Figure 2.15.

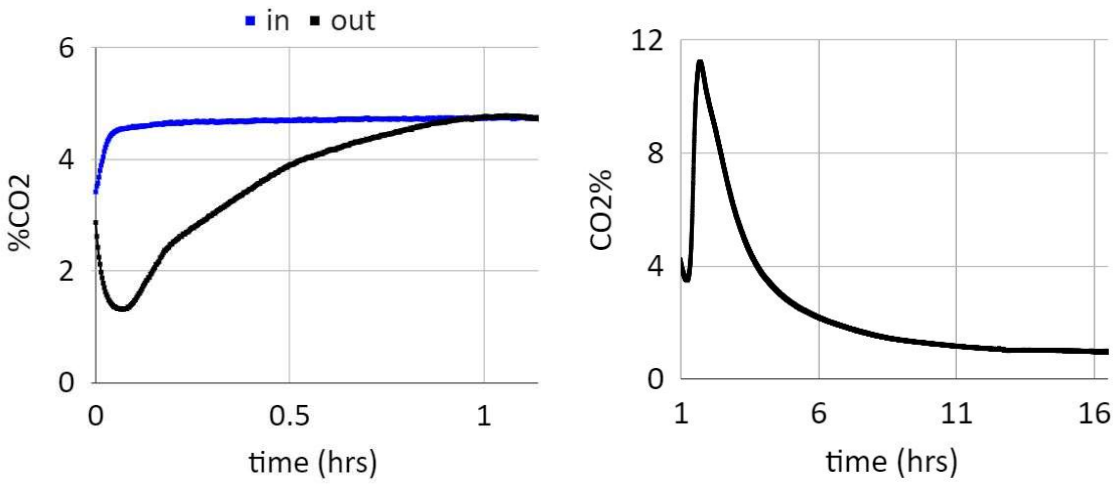

Figure 2.16 displays an example of the absorption breakthrough point on the left panel. The data is taken from Trial 2, absorption 5, and is also an example of sub-optimal capture as the outgoing CO_2 concentration never drops near 0 (100% capture efficiency). The right panel shows the CO_2 exponential decay resulting from regeneration with N_2 as a purge gas. The data is taken from Trial 2, regeneration 2. The slow decrease towards 0% made it challenging to determine a clear cut-off to end regeneration. Regeneration length was varied to determine its impact on the following absorption cycle.

The total length of each period (absorption, regeneration and cool down) was not constant across cycles. The length of the absorption period was held at minimum until "breakthrough," where the final and initial signals on the CO_2 analysers are the same. An example of the breakthrough is shown in Figure 2.16 on the left panel. While absorption indicates completion in a clear manner, regeneration depending on the purge gas identity, is more challenging to determine.

For this reason, a variety of regeneration lengths were tested in both Trial 1 and 2, as shown in Table 2.2. The regeneration durations listed include time required to heat the tower, which was especially important in the case of steam.

Table 2.2: Trial details

Trial	Cycle	Regen Details	Trial	Cycle	Regen Details
1	1	CO_2 @ 5 slpm, 36 hrs	2	4	CO_2 @ 5 slpm, 51 hrs
	2	CO_2 @ 5 slpm, 42 hrs		5	N_2 @ 5 slpm, 24 hrs
	3	CO_2 @ 5 slpm, 31 hrs		6	CO_2 @ 5 slpm, 18 hrs
	4	CO_2 @ 5 slpm, 27 hrs		7	N_2 @ 5 slpm, 28 hrs
	5	N_2 @ 5 slpm, 66 hrs		8	H_2O @ 65 gpm, 1.5 hrs
	6	CO_2 @ 5 slpm, 67 hrs		9	N_2 @ 5 slpm, 40 hrs
	7	H_2O @ 65 gpm, 3.5 hrs		10	H_2O @ 65 gpm, 2.5 hrs
2	1	N_2 @ 5 slpm, 73 hrs		11	N_2 @ 5 slpm, 28 hrs
	2	N_2 @ 5 slpm, 17 hrs		12	N_2 @ 5 slpm, 28 hrs
	3	N_2 @ 5 slpm, 24 hrs			

In both Trials 1 and 2 three different gases were used to regenerate the sorbent, N_2, CO_2 and steam. While the heating of the reactor to 160°C+ will initiate the regeneration reaction, a purge gas is needed to push gaseous products (CO_2 and H_2O) through the lines. In theory, no purge gas is needed if infinite time is available for products to diffuse out, but this is not possible in an industrial setting. In addition, for commercial reactors no gas can be used as a purge unless it is easily removed after the sorbent is regenerated or does not reduce the purity of the final product significantly. For this reason, the two purge gases that are being considered for scale-up are CO_2 and H_2O. A small flow rate of CO_2 in theory can

help push released CO_2 out of the reactor without reducing the stream purity. At a substantially high temperature, the backwards reaction should be minimal, so the CO_2 should not be recaptured. Alternatively, steam can be used and condensed out of the stream once the CO_2 is regenerated. Use of steam does necessitate active prevention of condensation in the tower, making its use a little more challenging to engineer. The obvious benefit of using steam instead of CO_2 in an industrial setting is that no CO_2 is reused in the regeneration process. For our studies N_2 is used as standard because it does not partake in the capture reaction and should go right through the material (it also minimally physisorbs to zeolites).

For regeneration using N_2, the analyser was calibrated to 10% CO_2. The accuracy of the CO_2 analyser is dependent on how close the experimental value is to the calibration point. As regeneration nears completion, and closer to 0%, the analyser becomes less accurate/sensitive to the small decreases in CO_2 concentration. In the case of regeneration trials when N_2 is used as a purge gas, outgoing CO_2 % curve is an exponential decay, shown in Figure 2.16 on the right panel. This made it very challenging to determine when the regeneration should be considered complete. The impact of the length of regeneration phase (which at the same time is also a drying phase as the material is heated) for N_2 purge is more thoroughly explored in section 2.4.2. A flow rate of 5 slpm was selected as higher flow rates caused substantial heat dissipation from the tower, resulting in longer heating times and temperature fluctuations.

The same flow rate of 5 slpm was used to purge with CO_2. The CO_2 analyser could not be used to approximate the end of the regeneration as it was for purge with N_2 (shown in Figure 2.16, right panel) as it will always show around 100%. Instead, a flow meter was installed after a desiccant tube on the gas analysis panel (Figure 2.10) to measure changes in the total amount of CO_2 exiting the tower. The flow rate initially (first few hours) sits well below 5 lpm, indicating the possibility of further absorption by the material. While at first this may seem unreasonable, as we observed CO_2 breakthrough (like in Figure 2.16, left panel) it should be recalled that the absorption capacity of K_2CO_3 has been found to be dependant on the amount of CO_2 in the gas stream. As was mentioned in section 2.3.2, *Luo et al.* found an absorption capacity of 6.24 mmol g^{-1} when the flue gas was 1% CO_2 and a

capacity of 6.92 mmol g^{-1} while pure CO_2 due to a shift in the reaction equilibrium.[27] Thus we would anticipate that during the pure CO_2 flush, the material will absorb about 10% more CO_2 before reaching its new higher capacity. Additionally, while the CO_2 was flushed in the tower at t=0, the tower did not reach its maximum temperature for regeneration of 160C until about 2 hours in.

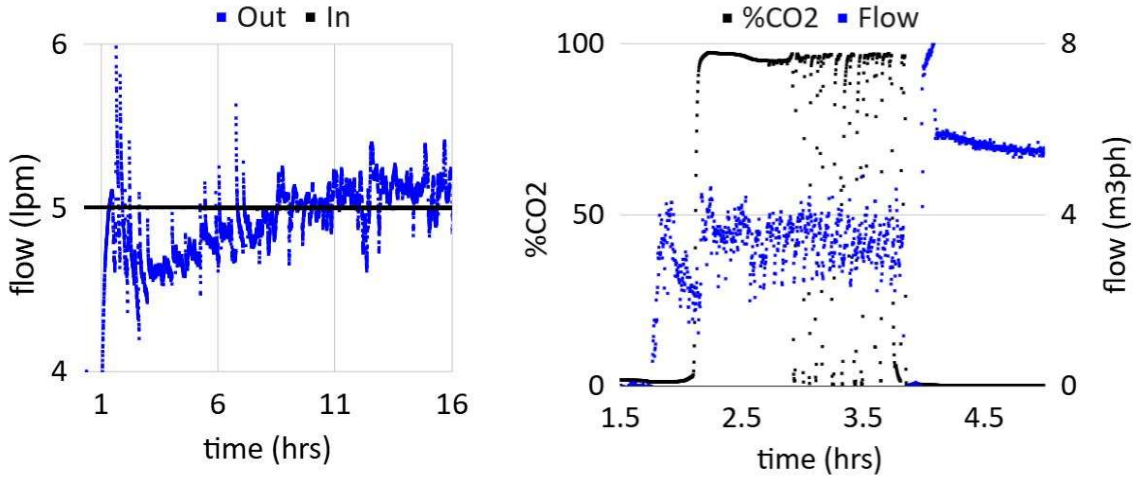

Figure 2.17 on the left panel displays the flow profile exiting the tower from Trial 2 cycle 6 during a CO_2 purged regeneration. As is discussed further in the main text, there is a small period in which the flow rate exiting is below 5 lpm, indicating further CO_2 absorption. This however, can be expected due to an increased absorption capacity at higher concentrations of CO_2. On the right panel, a steam purged regeneration from Trial 2 cycle 10 is displayed. The steam flows for about 15 minutes before a change is observed in the exiting CO_2%. A near 100% CO_2 flow was observed on the analyser for over an hour before dropping down to 0. This indicates a fast and efficient regeneration.

Due to this extra absorption period when CO_2 is used to purge the regeneration, like the N_2 purge it appears that a complete regeneration takes many hours to complete under these conditions. Industrial scalability requires that the regeneration phase take a similar length to complete as the absorption phase. The raw data suggests that absorption for these trials take on average less than 3 hours, while N_2 and CO_2 purged regenerations take 10+ hours. This will be discussed further in the capture results section, 2.4.2. It may be possible to increase the regeneration efficiency and decrease the phase length by increasing the purge gas flow rate. But as was described earlier, above about 5 lpm caused substantial heat

dissipation with this reactor design. Future study of purge gas flow rate on purge efficiency would require injected purge gas to be closer to 160°C; for these measurements it was closer to 100°C. In fact, the temperature of the entering purge gas likely has a significant effect on the regeneration as well. One can imagine that cold purge gas will steal heat from the hotter sorbent upon collision, potentially slowing the regeneration of the sorbent. The K_2CO_3 system and absorption/regeneration mechanism are clearly quite complex and depend on surrounding gas conditions, as evidenced by the change is absorption capacity with $\%CO_2$. The impact of purge gas flow rate as well as temperature clearly requires further study, but is beyond the scope of the current work.

In addition to CO_2, in this work steam was also considered as a potential industrially scalable purge gas for the regeneration phase. The raw data from one of the steam regeneration trials is presented in the right panel of Figure 2.17. It should be noted that the actual steam did not get injected until about 1.5 hours into the phase. During this time the tower was being heated from its absorption phase temperature of 70°C to about 110°C. This temperature was selected as the minimum temperature to begin steam injection to reduce the possibility of condensation in the tower. Once this was reached, steam was injected at a steam generator set point of 65 gpm, which corresponded to a measured flow rate of approximately 4 m^3ph, or more than 60 lpm. This high flow rate was selected as the steam generator used had an optimal injection rate between 50 and 100 gpm, with a more stable rate at around 65+ gpm setting. Figure 2.17 right panel shows that there was a short, 15-minute delay after steam was injected before the CO_2 began appearing on the exiting analyser at around 100% purity. Then, after about 1.5 hours of high purity CO_2 showing up on the exiting analyser, the $\%CO_2$ dropped. To confirm that the regeneration was complete, the steam generator was then set to 100 gpm which can be observed in Figure 2.17 right panel as an increase in flow rate, while $\%CO_2$ remained at 0. Based off these raw data, steam regeneration appears preferable over CO_2 as a purge gas for industrial use. This is due to the clear end (compared to Figure 2.17 left panel) and complete regeneration, as well as the phase's brevity. In section 2.4.2, the regeneration conditions' impact on following capture capacities will be discussed, and further compare the industrial scalability of CO_2 to steam.

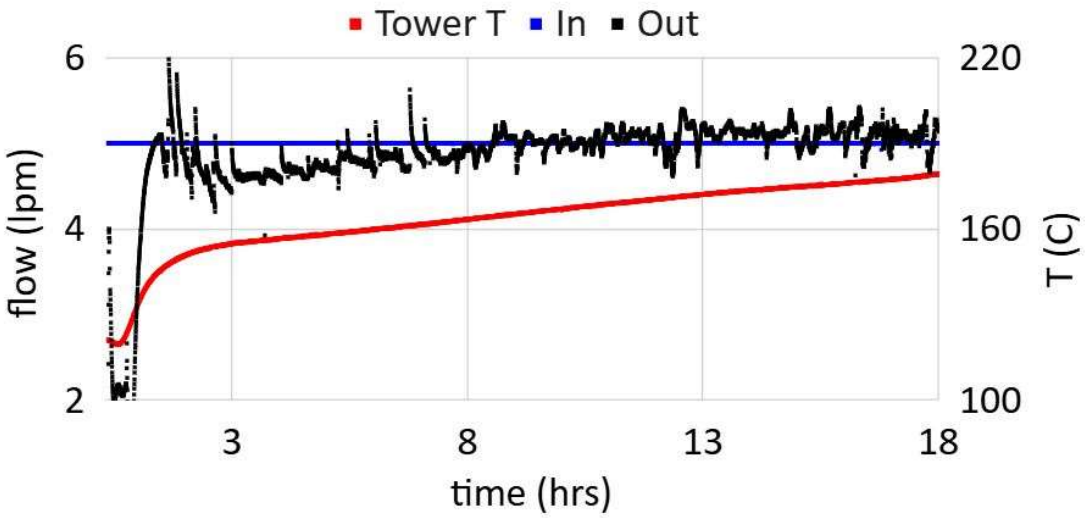

Figure 2.18 shows an expanded version of the data from Figure 2.17, on the left panel. From 8 to 18 hours there is no significant or obvious increase in the flow rate of CO_2 exiting the tower compared to that entering (shown in blue), indicating, if any, a very slow regeneration. This profile can be more directly compared to the 5 lpm N_2 purge shown in Figure 2.16, right panel. Despite using the same flow rate, N_2 appears to purge the regenerated gas faster than CO_2.

It should be noted that the 60+ lpm of steam is clearly a lot higher than the 5 lpm CO_2 and N_2 injections, which complicates the comparison of the purge gas identity on regeneration efficiency. It is possible that at 60+ lpm, CO_2 would be just as efficient at purging the regenerated CO_2 as steam. However, a 60 lpm purge of CO_2 for just an hour (assuming the length to completion is similar or better than steam) would require injecting around 7 kg of CO_2 into the tower. As will be discussed further in section 2.4.2, this is even larger than the amount captured during one cycle during these experiments. Recycling captured CO_2 for purge purposes, especially in such large quantities, may pose engineering challenges for scalability.

One of the biggest challenges we observed when using CO_2 as a purge gas is determining when the regeneration was complete. This is better depicted in Figure 2.18, an expanded view of the data from Figure 2.17, left panel. The same strange absorption region previously discussed in Figure 2.17 is displayed before the 8-hour mark, but from 8 to 18 hours the exiting CO_2 hovers around 5 lpm (the initial purge flow rate). At 5 lpm, it appears

that the regenerated CO_2 does not significantly add to the overall measured CO_2 flow, indicating a slow and steady regeneration. This will be further quantified in section 2.4.2. However, it indicates a clear challenge; future studies which want to use CO_2 as a purge need to be able to measure a clear end of regeneration, which may require a substantially higher purge flow rate to speed up the process. For comparison, the N_2 regeneration was performed at the same low 5 lpm flow rate, but experienced an obvious maximal regeneration point, depicted in Figure 2.16 on the right panel. While the "end" of regeneration was still challenging to determine from the Figure 2.16 decay curve, there was a much more obvious maximal regeneration region between 1 and 6 hours.

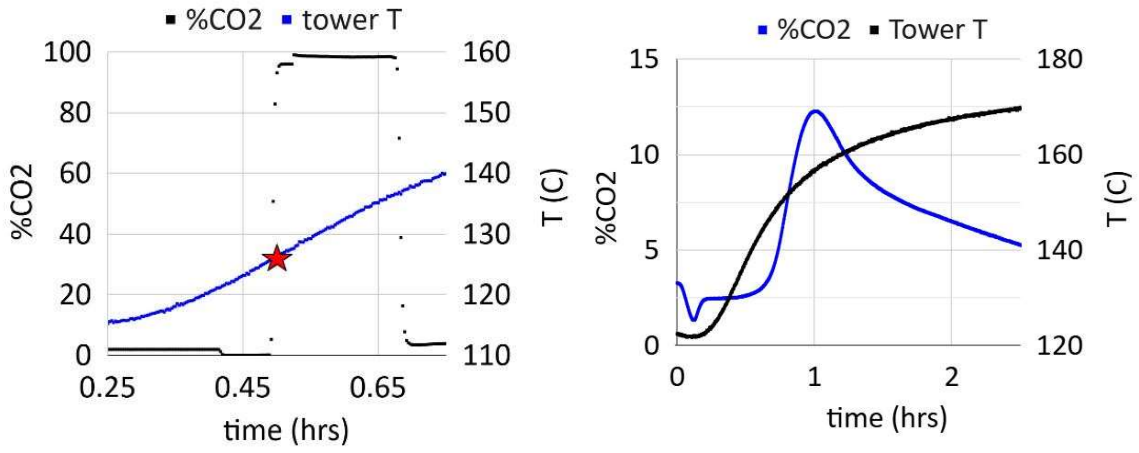

Figure 2.19 compares the temperature needed to regenerate the material under steam (left panel) versus N_2 (right panel) purge gas. The left panel and right panel data is taken from Trial 2 cycle 8 and Trial 2 cycle 1, respectively. In both panels, the CO_2 profile exiting the tower (black) is displayed against the temperature profile (blue), and tower temperature refers to the temperature taken in the middle of the tower. The red star in the left panel indicates the region where a burst of CO_2 began to exit the tower, which occurred at a tower temperature of around 125°C. When N_2 was used as a purge some regeneration occurred at around 130, but substantial regeneration begins at 140°C+.

Another benefit we found to using steam as a purge gas was that regeneration was noted to occur at a significantly lower temperature than anticipated. During the N_2 purged regenerations, our zeolite-supported K_2CO_3 sorbents typically began to substantially desorb at temperatures above 140°C. An example of this is shown in the right panel of Figure 2.19. On the other hand, when steam was introduced, we saw fast regeneration occur

at a temperature of around 125°C, depicted in the left panel of Figure 2.19. Literature on the K_2CO_3 reaction mechanism gives insight to this purge-gas dependent desorption temperature. As will be discussed further in Chapter 3, there is substantial evidence that reaction 3 occurs in a multistep mechanism, with potentially multiple hydrated intermediates. One reaction pair that has been considered is presented in equations 22 and 23 below.[39] Zhao *et al.* suggested saving energy of regeneration by reforming $1.5H_2O{\cdot}K_2CO_3$ instead of K_2CO_3. It should be noted that K_2CO_3 hydrates are complex, as they can dehydrate at temperatures above 100°C depending on the pressure and humidity conditions.[40] Despite this, humidity swing to decrease the regeneration temperature is feasible, as Rodríguez-Mosqueda *et al.* were able to successfully regenerate 50% of captured CO_2 with wet air at bench scale.[41] Thus, there is precedence in the literature to observe, as we did, a decrease in the required temperature for regeneration when substantial water is present.

22. $K_2CO_{3(s)} + 1.5H_2O_{(g)} \leftrightarrow 1.5H_2O{\cdot}K_2CO_{3(s)} \quad \Delta H_{60°C} = -99 kJ\ mol^{-1}$

23. $1.5\ H_2O{\cdot}K_2CO_{3(s)} + CO_{2(g)} \leftrightarrow 2KHCO_{3(s)} + 0.5H_2O_{(g)} \quad \Delta H_{60°C} = -44 kJ\ mol^{-1}$

2.4.2 Capture Results

While the raw sensor data gives some insight into the effectiveness of each regeneration, in this section we will present capture capacities, capture efficiencies, and calculated capture kinetics during the maximal efficiency period to compare regeneration conditions in a quantitative manner. In addition to being able to more directly compare the impact regeneration conditions have on the following absorptions, with these data we will also be able to observe the effects of cycling on material durability.

Table 2.3: Trial 1 Capture Capacities

Cycle	1	2	3	4	5	6	7	8
CO_2 Capt. (kg)	0.32	+0.21[a]	0.52	- [b]	0.57	0.94	1.4	0.28
Cap. (kg m^{-3})	3.2	+2.1[a]	5.2	- [b]	5.7	9.4	14.	2.8

[a] note that the CO_2 compressed gas cylinder ran out before breakthrough occurred
[b] data acquisition for cycle 4 crashed; the data was lost

Table 2.3 displays the captured CO_2 as well as the capture capacity for Trial 1, the rock-type zeolite. The capture capacity is simply the CO_2 captured divided by the tower volume; it can be used to estimate how large a tower may need to be scaled in future designs. It should be considered that tower dimensions must be scaled carefully to avoid pressure drop and flow tunnelling, but this is beyond the scope of the current work.

The first obvious trend in this data is that over many cycles (excluding for a moment, cycle 8) the material does not drop in capacity. The material could lose activity over time if disintegration/degradation causes pore closure or if the material leeches K_2CO_3. These data affirm that the current tower design and support material does not cause substantial degradation/leeching within 8 cycles. It is challenging to quantify exactly how long the material would need to last without replacement for it to be commercially viable. The lifetime of the material impacts the cost of capture, but further, even if a material is very cheap, operating a tower becomes cumbersome if it requires frequent loading/loading. Conversations with potential customers indicate that materials that have a lifetime less than about a month are undesirable. Assuming a tower completes 2 cycles a day, the material would need to last about 60 cycles.

There are essentially two groupings of capacities that were measured in Trial 1. Cycles 1-5 and 8 captured about half a kg of CO_2 or less, while cycles 6 and 7 stood out with higher capacities. Unfortunately, the data for cycle 4 was lost as the data acquisition device crashed. Additionally, the captured CO_2 for cycle 2 is a lower bound, as the CO_2 cylinder ran out in the middle of the absorption cycle. The efficiency curve for cycle 2 (Fig 2.20) shows that the material was close to saturation regardless. Absorptions 1-5 and 8, despite having similar low capacities, had prior regenerations performed with all three purge gas types (see Table 2.2). While the goal was to determine the impact (if any) of different purge gases on the regeneration efficiency, we determined that for Trial 1 other factors may have obscured any potential differences across cycles. We attribute the lower capacities seen in cycles 1-5 and 8 to primarily two factors: incomplete regeneration and overly wet material, both of which result from us not yet optimizing operating procedures. For example, the first absorption was performed after the material was loaded into the tower. Before

absorption 1, the material was dried for over a day with a purge gas flow rate of 2 lpm N_2, during which the tower hovered around 140°C. This drying was intended to drive off water, as the RH meters indicated the loaded material was wet, but in retrospect it is highly likely that during manufacturing/packaging/traveling the material also became somewhat saturated with CO_2. This was rectified in Trial 2 by increasing the purge flow rate to 5 lpm and tower set temperature to 190°C before the first absorption.

During Trial 1, we also were still optimizing procedure related to the absorption phase. While we observed CO_2 breakthroughs typically around 3 or less hours into absorption, we allowed the flue gas to flow for up to 12 hours in some cases to test other tower subunits. During prolonged absorption phases, eventually the material became quite wet, as evidenced by the RH meter data for the middle tower probe, shown in Figure 2.21. The regeneration phase if long enough, could help dry the material. This was likely true in the case of cycles 6 and 7, which had 65+ hours each of drying (Table 2.2).

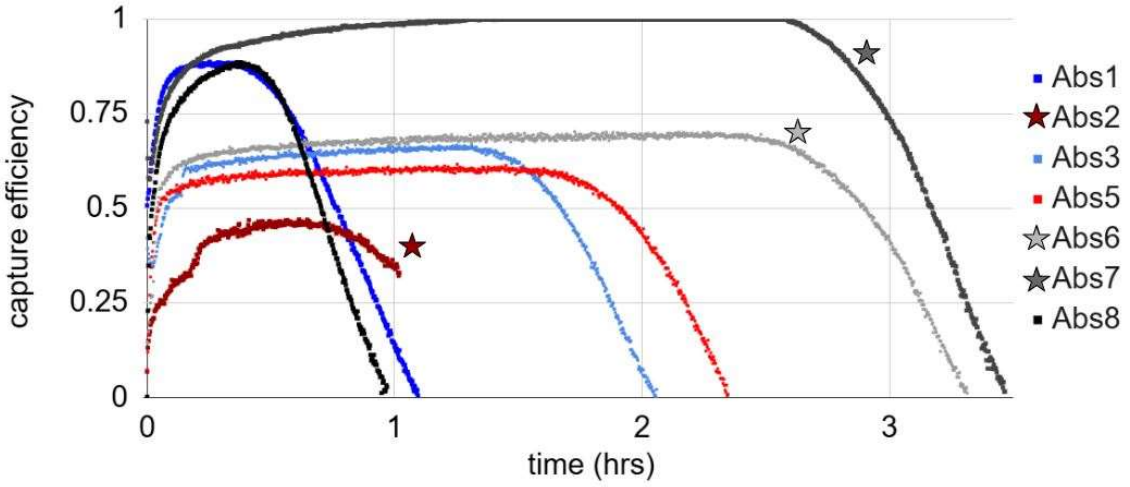

Figure 2.20 displays the efficiency curves for each of the absorption cycles in Trial 1. Cycles 6 and 7 observed the longest capture periods, with maximal capture efficiency occurring for about 3 hours. Alternatively, cycle 2 performed the worst, with the lowest maximal efficiency of less than 50%, and dropping at less than one hour into the absorption period.

Alternatively cycle 8, which performed very poorly, occurred after our first attempt at steam regeneration (regeneration 7) which appeared to have condensation issues. Thus, in conclusion, while Trial 1 absorption 1 likely performed poorly due to CO_2 saturation during manufacturing/packaging/shipping, cycles 2-5 and 8 appear to have performed poorly due to water saturation of the sorbent. How increase in absorbed water reduces capacity cannot be studied thoroughly with this system, but most likely is related to pore blocking. More complex analytical techniques are necessary to diagnose what physical/chemical mechanisms are driving this capacity drop and should be explored in future works.

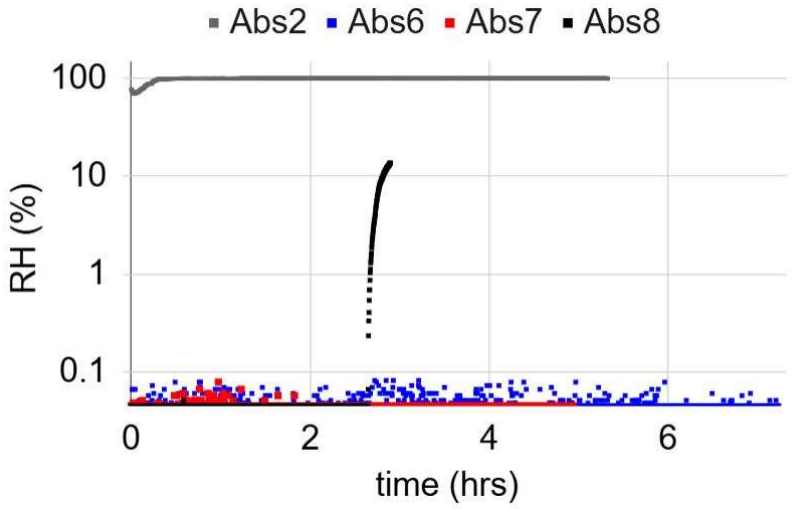

Figure 2.21 displays the RH data from the middle tower sensor during Trial 1, absorption phases 2, 6, 7, and 8. Absorption 2 performed the worst in terms of efficiency and capacity of any cycle in Trial 1 and was the most wet by far. The middle RH meter (grey) sat near 100% during the entire absorption 2 period. Absorption 8 occurred after a steam regeneration and began to display signs of water saturation at the tower midpoint at around 2.5 hours (black). Absorption 8 also performed poorly in terms of capacity and efficiency. In comparison, absorptions 6 and 7 performed the best in terms of total capacity and did not indicate signs of water saturation during their entire phases.

The decrease in sorbent activity can also be observed as changes in the capture efficiency profile (Figure 2.20) or the calculated 2nd order rate constant (Table 2.4). As is explained in more detail in section 2.3.6, the efficiency profile shows what fraction of the injected CO_2 at a given moment was taken up by the tower. If all mass injected at a given moment was absorbed (the CO_2 analyser on the tower exit reads 0%), then the efficiency will be 1.

In addition to having the largest capture capacity cycle 7 also showed the greatest maximal efficiency, reaching near 1 for most of the absorption phase. Interestingly, cycles 8 and 1 have the second and third highest maximal efficiencies, but only for a short period of time before they drop, thus explaining their low capacities. Cycle 2 had the lowest maximal efficiency; at its best capturing less than 50% of the injected CO_2. The kinetic data in Table 2.4 is in general agreement with the trends observed in the capture data and efficiency profiles. We had hoped that these data may also be used to discriminate optimal tower temperature for this system, but there unfortunately were no clear trends between calculated rate and middle-tower temperature. This may be further evidence that the one-step mechanism in which H_2O and CO_2 are simultaneously reacted is a poor assumption.

Table 2.4: Trial 1 Calculated Kinetic Constants

Cycle	1	2	3	4	5	6	7	8
k[a] ($m^3mol^{-1}s^{-1}$)	1.4(0.5)[c] E-2	5.2(0.9) E-3	4.5(0.8) E-3	-	8.5(0.8) E-3	1.2(0.5) E-2	2.0(0.6) E-1	7.6(0.8) E-3
Temp[b] (°C)	45.5 (0.7)[c]	46.3 (0.9)	55.1 (1.0)	-	43.3 (0.6)	42.3 (0.7)	34.1 (0.6)	56.0 (0.5)

[a] note that the kinetic constant can be calculated at any point in the absorption. We chose times near the start of the maximal efficiency period
[b]temperature of reaction is assumed to be that measured at the middle tower probe
[c]uncertainty is the standard deviation of 4 measurements, 1 minute apart

While the RH meters have proven quite critical in monitoring tower operations, future tower designs would benefit from minor changes to their layout. The bottom tower RH meter is located right by the flue/purge gas entrance and basically indicates the humidity of the entering gas stream. The next RH meter is in the middle of the tower and was used to determine when the material became saturated with water. Unfortunately, it measures the RH of the gas surrounding the material, not the wetness of the material itself. Because zeolite is a very good desiccant, the RH meter only appears to read non-zero values when the zeolite is almost fully water saturated. Additionally, if no gas is being moved through the tower (flow rate = 0), then the RH meter also reads 0, even when the material is very wet. The RH meter at the very top of the tower almost always reads 0, because the tower

saturates from the bottom up. For this reason, to help monitor tower wetness, it would be useful to mount an RH meter between the bottom and middle of the tower. Future designs may even investigate more direct manners of monitoring material wetness.

Table 2.5 displays the capture capacities measured for Trial 2, the 13X ADCOA bead zeolite. During Trial 1, many operational issues were identified and resultantly avoided or modified for Trial 2. To avoid over-wetting the sorbent, once capture was completed (indicated by the exit CO_2 concentration equalling that entering the tower) the flue gas was immediately shut off. During N_2 and CO_2 purged regeneration cycles, RH was closely monitored to ensure significant drying had occurred. As previously mentioned, the middle tower RH meter was our best indicator of material wetness. After CO_2-purged regenerations, a final compressed air pulse was used to evacuate remaining CO_2 before the tower entered the cooling phase. This was to prevent reabsorption of the CO_2 remaining in the tower after CO_2-purged regeneration. Lastly, after steam-purged regenerations compressed air was utilized again, but in this case to evacuate water that might condense during the cool down phase. While during N_2 and CO_2 purged regenerations drying occurs over many hours at a low flow rate, during steam-purged regenerations the following compressed air pulse spurs drying. In summary, multiple procedural changes were instituted so that Trial 2 had more consistent sorbent conditions than Trial 1. As a result, we were better able to compare the regeneration abilities of the different purge gases, N_2, CO_2 and steam.

Table 2.5: Trial 2 Capture Capacities

Cycle	1	2	3	4	5	6	7	8
CO_2 Capt. (kg)	0.56	0.52	0.43	0.51	0.14	0.33	0.20	0.33
Cap. (kg m^{-3})	5.6	5.2	4.3	5.1	1.4	3.3	2.0	3.3

Cycle	9	10	11	12	13
CO_2 capt. (kg)	0.37	0.32	-[a]	0.25	0.27
Cap. (kg m^{-3})	3.7	3.2	-[a]	2.5	2.7

[a]data acquisition for cycle 11 crashed; the data was lost

Despite our optimized procedure, the best performing cycle of Trial 2 observed a total CO_2 capture of 0.56 kg, which is less than half that of Trial 1, which was 1.4 kg. Since the Trial's total sorbent mass loaded were similar (111.6 and 100.8 kg for Trial 1 and 2 respectively), we hypothesize that the rock-type Clinoptilolite had a higher mass percent of K_2CO_3 than the 13X (which was around 20%). Unfortunately, the supplier did not provide the mass loaded, however it would not be unreasonable to expect Clinoptilolite to support more K_2CO_3 a than 13X. As discussed in section 2.3.5, 13X is a commercial produced zeolite with very regular primary structure and pores that are around 1nm. On the other hand, clinoptilolite is a naturally occurring zeolite with secondary structure and has a range of pore sizes, scaling as large as 50nm.[37] Larger pores may enable clinoptilolite to hold more K_2CO_3 than 13X. In addition, larger pores may prevent pore clogs during absorption (pore clog/closure will be discussed further in Chapter 3), increasing availability and activity of K_2CO_3.

Unlike Trial 1, Trial 2 observed a decrease in material activity over cycling, with a starting capacity of 0.56 kg CO_2 and a final cycle 13 capacity of 0.27 kg. The capacity drop appears to occur around cycle 5. Notably, the regeneration 4, which occurred directly before cycle 5, was the first regeneration of Trial 2 without a N_2 purge. Cycles 1-4 were all performed after a N_2 purge to determine the variation in measured capture under conditions which were as similar as possible. The standard deviation across cycles 1-4 was 0.05 kg, 11% of the average. It can be extrapolated that most of our capacity measurements have an error of around 10%. Cycles 5 and 7, which occurred after CO_2 regeneration, had the lowest capacities of the Trial. While cycle 9, which occurred after steam regeneration, also had a low capacity, it compares well to neighbouring post-N_2 cycles. This is depicted in Figure 2.22. While cycle 11 was also performed after a steam regeneration, unfortunately the data acquisition device again malfunctioned, and the data for that cycle was lost. Capacity measurements from cycles 12 and 13, both performed after N_2-purged regenerations, did not decrease significantly. Thus, we can still conclude that steam regeneration under these new procedures did not harm material activity overtime.

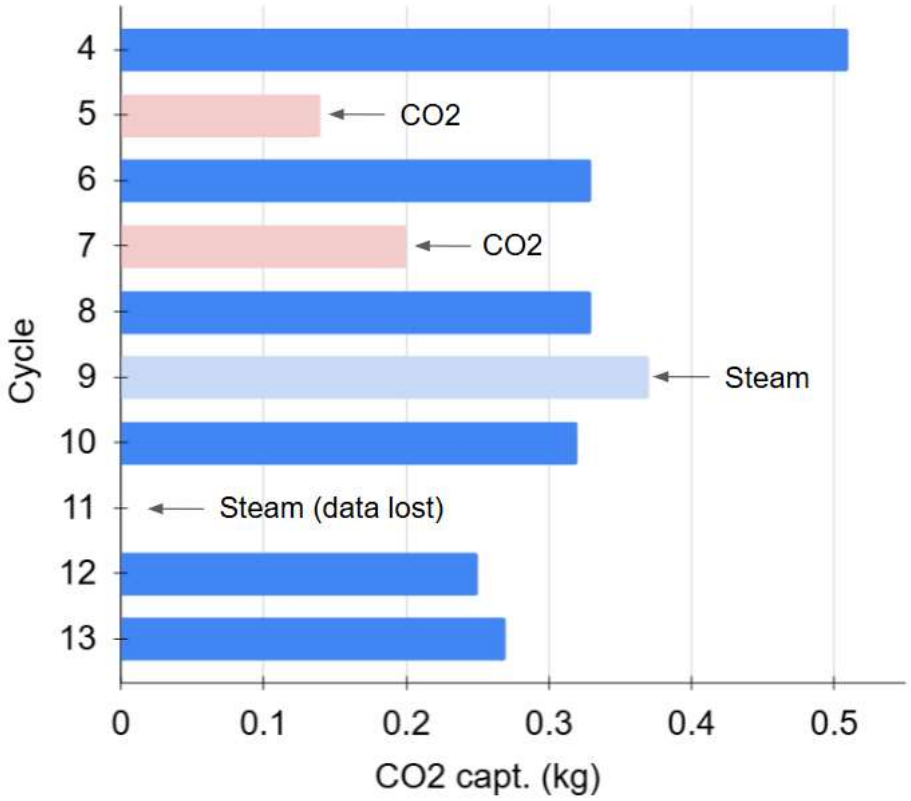

Figure 2.22 visualizes the CO_2 captured for cycles 5-13 from Table 2.5. The post-N_2 regenerated cycles are shown in blue, post CO_2 and steam cycles are shown in light red and light blue respectively. Unfortunately, the second post-steam cycle data, cycle 11, was lost. As the material does appear to degrade in activity overtime, the post-N_2 cycles in-between CO_2 and steam regeneration cycles can be used for comparison to observe the impact of these two purge gases. Cycles 4, 6, and 8 neighbour the post-CO_2 cycles while 8 and 10 neighbour the post-steam cycle. Using these as comparison, steam performs similarly to N_2, while CO_2 does worse by nearly 50%.

Figures 2.23, 2.24 and 2.25 display capture efficiency curves for Trial 2. Unlike the Trial 1 curves (Figure 2.21), whose trends are overshadowed by issues with tower wetness, Trial 2 data shows differences in regeneration effectiveness according to purge gas type. First, Figure 2.23 displays the first four cycles, all post-N_2 purge, and contrasts them to a curve from Trial 1. The four Trial 2 curves are very similar in shape, which agrees well with their similar capture capacities. Notably, their maximal efficiency region is short lived and drops consistently throughout absorption in comparison to Trial 1. This may be evidence of pore-clogging, which makes K_2CO_3 in the particle center harder to access.

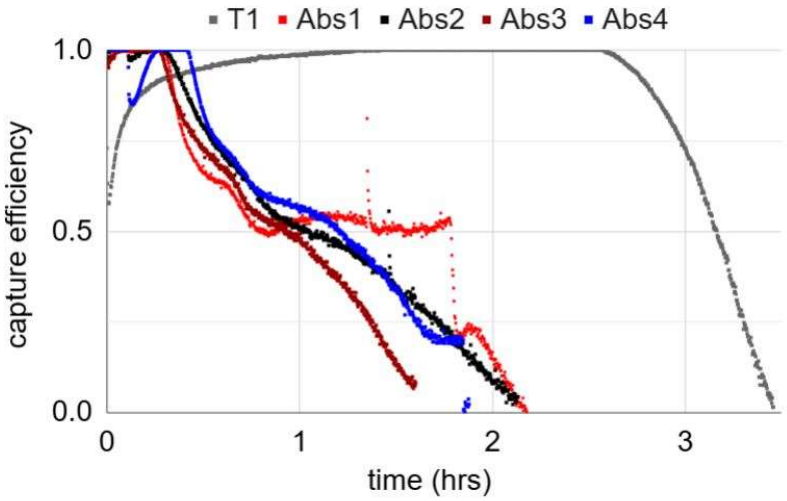

Figure 2.23 compares the first four cycle efficiencies of Trial 2 to each other, as well as the highest performing absorption of Trial 1, which was cycle 7 (labelled T1). Absorptions 1-4 are very similar in profile, which agrees with their similar absorption capacities listed in Table 2.5. They contrast greatly with the profile from Trial 1, which is very smooth and proceeds for over 3 hours where most of the cycle observes a fairly unchanging measured efficiency.

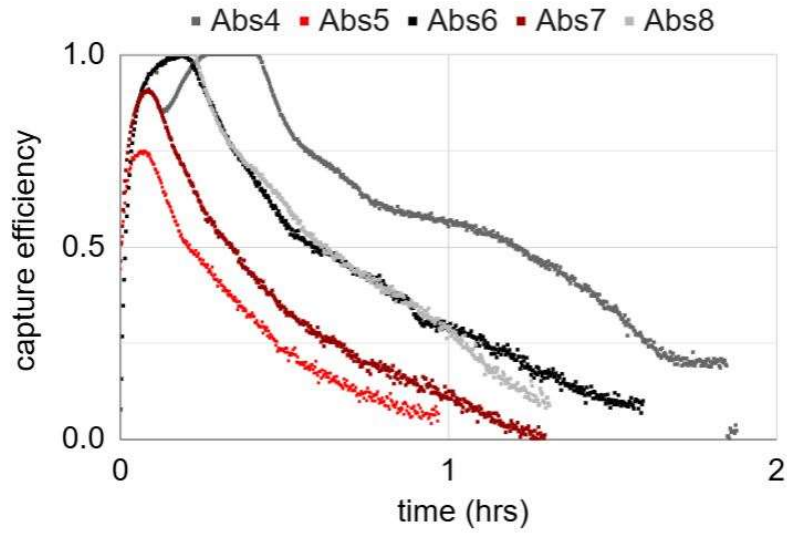

Figure 2.24 displays the post-CO_2 absorption efficiency profiles, Abs5 and Abs7, shown in light and dark red respectively. They are directly compared against the neighbouring post-N_2 cycles Abs4, Abs6 and Abs8. While Abs4 (in medium grey) outdoes all other presented cycles, likely because it was performed earliest and the material appears to degrade over cycling, absorptions 5 and 7 both perform substantially worse than the latest presented cycle, cycle 8 (in light grey).

In Figure 2.24, the efficiency curves for the post-CO_2 regenerated absorptions are directly compared against the neighbouring post-N_2 absorptions. Interestingly, the shape of the profiles are quite similar; a sharp increase with a short-lived maximal efficiency period, followed by a slow decay to 0%. Notably, both post-CO_2 curves indicate the material performed worse than even the latest neighbouring absorption cycle, cycle 8. Figure 2.25 compares the only post-steam cycle with surviving data, Abs9, against its neighbouring post-N_2 curves. The data from Abs11 (the other post-steam cycle) was unfortunately lost, but the Abs12 and Abs13 curves which immediately followed continued to observe similar efficiencies as those prior, indicating that no substantial material change occurred due to steam-regeneration. While issues from Trial 1 gave us concern that steam regenerations give opportunities for condensation and thus leaching of K_2CO_3, the largest drop in capacity and efficiency occurred between Abs4 and Abs5, when the first CO_2 purge of Trial 2 was performed. It is possible that the CO_2-purge initiated significant material degradation, but how is currently unclear without material characterization techniques such as Brunauer–Emmett–Teller (BET) or Scanning Electron Microscopy (SEM).

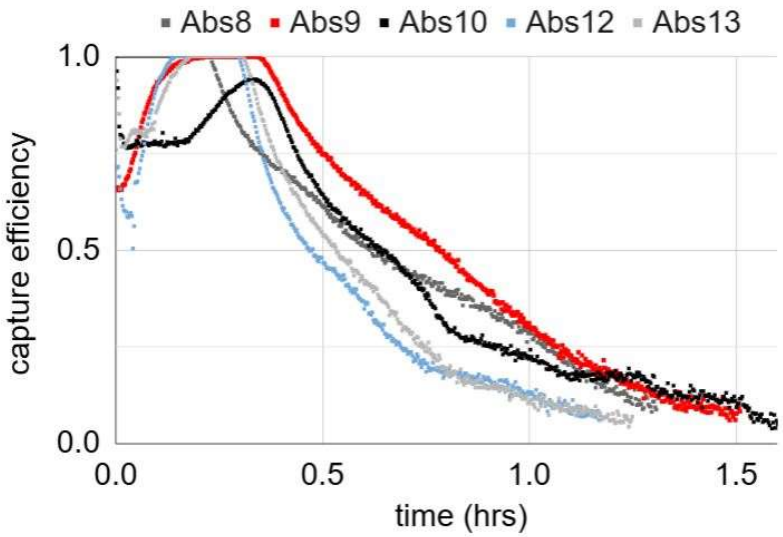

Figure 2.25 displays the efficiency curves for absorptions 8-13. Absorptions 9 and 11 were performed after steam-purged regenerations but unfortunately the data from absorption 11 was lost. Abs9 outperformed its prior and successive absorptions, 8 and 10, indicating that steam as a purge was very effective. While the data from Abs11 was lost, the following absorption efficiency curves appear very similar to all those prior.

Table 2.6: Trial 2 Calculated Kinetic Constants

Cycle	1	2	3	4	5	6	7
k[a] ($m^3mol^{-1}s^{-1}$)	1.3(0.2)[c] E-2	5.7(1.2) E-2	2.9(0.1) E-2	2.7(0.1) E-2	3.3(0.2) E-3	1.0(0.4) E-2	1.8(0.1) E-3
Temp[b] (°C)	27.4 (0.1)[c]	50.1 (0.2)	46.0 (0.3)	41.0 (0.1)	41.3 (0.2)	43.0 (0.2)	40.5 (0.1)

Cycle	8	9	10	11	12	13
k[a] ($m^3mol^{-1}s^{-1}$)	5.8(0.9) E-3	9.6(0.4) E-3	3.5(0.2) E-3	-	3.8(1.4) E-2	1.3(0.3) E-1
Temp[b] (°C)	40.4 (0.2)	41.2 (0.1)	38.0 (0.3)	-	47.9 (0.1)	48.0 (0.2)

[a] calculated at times near the start of the maximal efficiency period
[b]temperature of reaction is assumed to be that measured at the middle tower probe
[c]uncertainty is the standard deviation of 4 measurements, 5 seconds apart. These are notably more closely spaced than points selected for Table 2.5. This is because the maximal efficiency period was much shorter.

Table 2.6 shows the calculated rate constants for these absorptions. Like Table 2.4, the rate was calculated at the region of highest efficiency, which for each cycle in Trial 2 lasted just a few minutes. Also, like Table 2.4 the results are not elucidating in the same way that the capacity measurements and efficiency profiles are. For example, cycles 12 and 13 both occurred after N_2-purge regenerations and occurred at the same measured mid-tower temperature but have rates that are an order of magnitude apart. It is possible that there was a temperature gradient in the tower, meaning that the reaction doesn't occur at the reported temperature, it occurs under a temperature range. The bottom and top probes typically measure different values than the mid tower probe that are more indicative of the temperature of the gas stream entering and exiting the tower. Thus, to be more confident in the temperature distribution of the material more probes may be useful in future designs. On the other hand, as mentioned earlier, it may be that the single-step capture mechanism is a very poor assumption. A more complex mechanistic model may be necessary to accurately compare cycle kinetics.

The theoretical capacity of pure K_2CO_3 is 7.25 mmol g^{-1}, and the expected mass loaded of the 13X was about 20% based on the density change after impregnation. The total mass loaded during Trial 2 was 100.8 kg, meaning that 20.16 kg of K_2CO_3 was present. Assuming all of this was available for capture, this would result in a captured CO_2 mass of 6.43 kg. Our highest observed CO_2 mass captured was 0.56 kg, meaning that we captured only about 9% of the theoretical capacity of this material was reached.

Typical pilots plants capturing point source carbon from powerplants hope to capture about 1-tonne (1000 kg) of CO_2 a day.[42] Even if the material is cycled every hour, this system would capture less than one tenth that goal at its current size. Comparatively, the clinoptilolite (Trial 1) captured 1.4 kg during its best run, absorption 7. Additionally, as previously discussed Trial 1 operating conditions were not yet optimized, meaning that it may have performed even better. It appears that clinoptilolite may provide a better support than 13X zeolite. We hypothesize that the bigger pores, provided via naturally forming secondary structure, allows for greater mass loading and availability of K_2CO_3.

2.4.3 Additional Diagnostic Data

In addition to CO_2 capture data, we monitored other operational variables during these trials that will impact future designs. One variable of great importance is the pH of the condensed liquids exiting the tower bottom. While condensation should be avoided as much as possible, as the flue gas contains around 15% $H_2O_{(g)}$ and we performed some regenerations with superheated steam; ultimately, some liquid will condense and exit out the tower bottom. In addition to rusting of the tower, two chemical processes will impact the pH of the exiting liquid: leaching and acidification. Material leaching describes carbonate ion dissolution, resulting in a pH increase according to reactions 24 and 25. Alternatively, acidification occurs when gaseous CO_2 dissolves into the liquid water according to equation 26.

24. $K_2CO_{3(s)} \rightarrow 2K^+_{(aq)} + CO_3^{2-}{}_{(aq)}$

25. $CO_3^{2-}{}_{(aq)} + H^+ \rightarrow HCO_3^-{}_{(aq)}$

26. $H_2O_{(aq)} + CO_{2(g)} \rightarrow H^+_{(aq)} + HCO_3^-{}_{(aq)}$

By monitoring the pH exiting the tower, we hoped to identify if there were specific phases (absorption, regeneration and cooling) or purge gas conditions that exacerbated either of these processes. We anticipated seeing an increase in pH due to leaching during the cooling phase or during steam regeneration. We also expected a decrease in pH due to acidification during CO_2-purged regeneration. Instead, we observed rapid changes in pH during the absorption phases in which pH generally increased, indicative of leaching. Absorption phases occur at temperatures less than the boiling point of water (typically less than 70°C), while regeneration occurs at 100°C+, and cooling begins at temperatures of 100°C+. Thus, it makes sense that more condensation occurs during the absorption phase comparatively, which results in greater leaching of carbonate ions from the sorbent. It would be beneficial in the future to measure the volume condensed after each phase, even collecting these samples for further analysis. This is clearly not reasonable to do for day-to-day industrial working conditions but would be useful to optimize operational procedures before regular use.

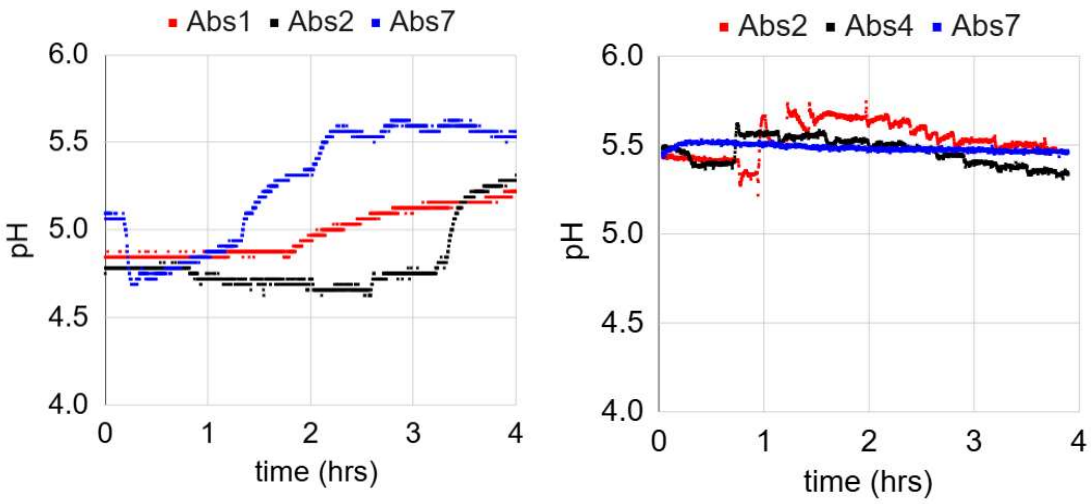

Figure 2.26 shows data from Trial 1 on the left panel and Trial 2 on the right panel. They are presented with the same scale of pH 4 to 6 for the first four hours of absorption.

In addition to finding that larger pH changes occurred during absorption phases, we also found that Trial 1 observed significantly larger pH increases than Trial 2. This agrees with our understanding that the material during Trial 1 was generally more wet due to flaws in operational procedure. This difference is visualized in Figure 2.26.

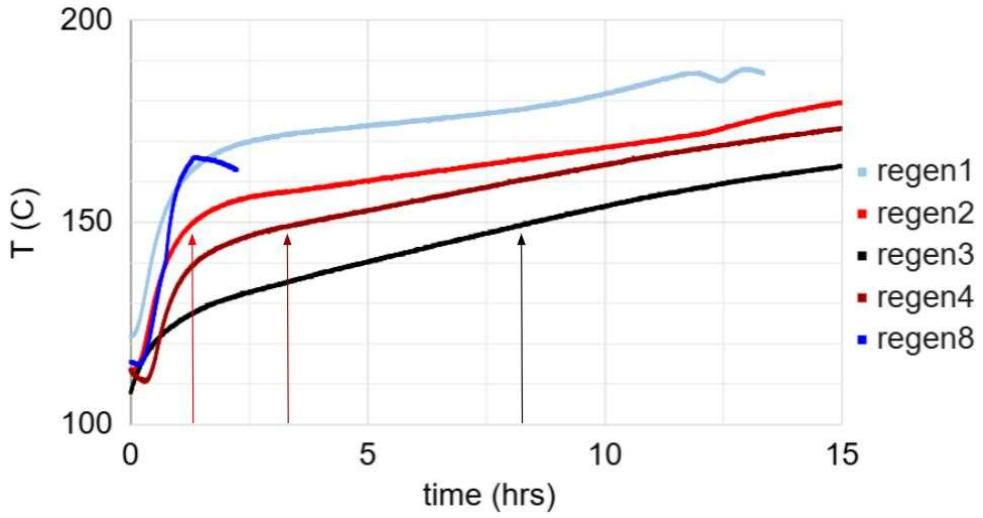

Figure 2.27 displays some mid-tower temperature ramps during the regeneration of sorbent from Trial 2. Regenerations 1-3 were performed with N_2 at 5 lpm, regeneration 4 was performed with CO_2 also at 5 lpm, and regeneration 8 was performed with steam at 65 gpm. Even across regenerations 1-3 (which utilized the same purge gas and flow rate) we observed large variability in time for the tower to warm to 150°C. The fastest tower heating of all 13 cycles occurred via steam-induced regeneration (dark blue) and took less than an hour. The wiggle-curve at the end of regen1 is the result of the tower heater turning off and on to maintain an average temperature of 185°C.

One of the greatest challenges to providing similar regeneration conditions is setting tower temperature. During Trial 1 the in-tower heater was initially set to 165°C, but it was determined that by setting it to a higher temperature the heating occurred significantly faster, thus for all Trial 2 runs the in-tower heater was set to 185°C. While the heater could reach 250°C, the RH meters throughout the tower are only viable to temperatures up to 200°C, after which they break. In general, it is difficult to find RH meters that can withstand high temperatures; this may be a challenge for manufacturing if larger temperature gradients are needed to heat the tower more quickly.

There was a large variability in the time it took for the tower to reach the minimum temperature in which regeneration could be expected, which should be around 150°C. We expect flow rate and purge gas identity to impact the heating time, as gases have different thermal conductivities and het capacities. However, even across the three N_2 cycles presented in Figure 2.27 we see a large variability in the time to heat to 150°C. Fast tower

heating is highly desirable to increase the number of cycles (thus total CO_2 captured) a tower is capable in a day. It is also important that the length of the absorption phase vs the regeneration and following cooling phase be very similar to maximize tower efficiency. One can imagine, for example, that if an absorption only requires two hours but to regenerate and cool the material requires a total of twenty, there is a lot of idle time in which the tower is not absorbing. So, while the mere 30 minutes to heat up observed for regenerations 1 and 8 are very scalable, the longer heating times, for example eight hours for regeneration 3, may cause an issue. It is possible that the temperature of the warehouse had an impact on the heat up time of the tower, as during the operational period the temperature could fluctuate between 5-30°C, which is quite large. While this may appear problematic for a laboratory study, it does resemble real conditions as reactor towers will be installed outdoors on top of flue stacks and will be subjected to variable temperatures. It is also possible that while we attempted to dry the tower to similar degrees throughout Trial 2, that we ultimately were not entirely successful. Increased water content in the sorbent would increase its heat capacity, causing an increase in the time to heat the material. More work is necessary to pinpoint the primary causes of this variability. However, another benefit to using steam as the purge gas is that it is highly efficient at transferring heat.

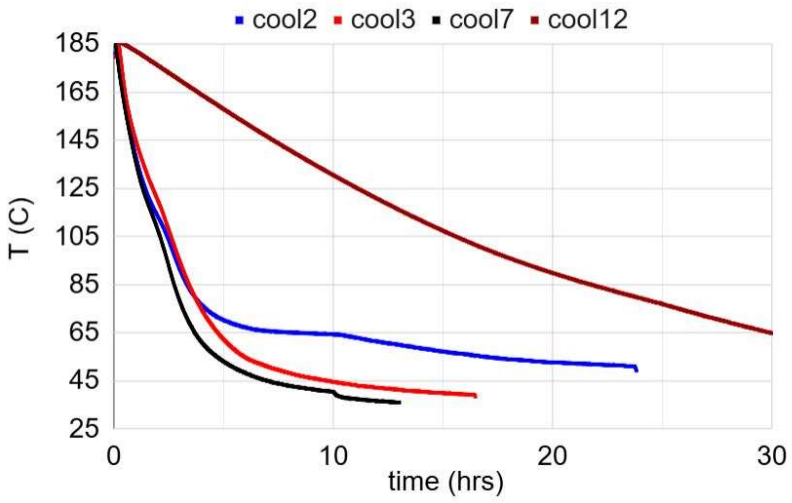

Figure 2.28 displays some cooling profiles from Trial 2. Tower temperature should be a maximum of 65°C before flue gas is injected for absorption. Cooling phases 2, 3, and 7 were performed with the cooling fan and heat exchangers while cooling phase 12 did not.

Lastly, to maximize the number of daily full tower cycles, the cooling phase must also be optimized. For the current tower design, sorbent composition, and flue gas flow rate absorption phases typically require about three hours to completion. Assuming steam is used as the purge, regeneration phases typically take about one hour to complete at which point they will need to be cooled before a new absorption can occur. Thus, for the current design, a cooling period of around 2 hours to 65°C is optimal. As previously mentioned, (section 2.3.3), the cooling phase is currently assisted by an internal fan (Redbo 2GH210-H16) which circulates tower air at 98 m^3ph, while two water-cooled heat exchangers (shown in Figure 2.3) remove system heat at a water flow rate of approximately 0.8 m^3h^{-1} and a total heat exchanging area of 0.1m^2. The water used in this system comes from the exit of a cooling water tower circuit (we recycle the cooling water), which is about 10-20°C depending on ambient conditions. When the fan is inactive, and the tower is allowed to cool naturally, it takes up to 30 hours. As depicted in Figure 2.28, when the cooling phase is active it takes between 5 and 10 hours for the material to cool from 185 to 65°C. To cut idle time larger heat exchanging area may be necessary to reduce cooling time in future adaptations.

2.5 Conclusion

A two-tower packed bed reactor for the purpose of K_2CO_3-based carbon capture was constructed and tested. The towers are a little smaller than industrial size, approximately 1.8 m tall, 0.1 m^3 internal volume, with the capability of holding around 100 kg of impregnated zeolite sorbent. Two Trials, each utilizing a different type of zeolite, clinoptilolite and 13X, were cycled under varying conditions. Both temperature and humidity swing regenerations were attempted at temperatures ranging between 125 and 200°C. It was determined that steam assisted in lowering the temperature needed for material regeneration, which has been observed at the laboratory scale for other K_2CO_3 based sorbents. Sorbent dampness appears to negatively affect material capacity, which may continue to challenge future tower designs and operational procedures. Of the two materials the natural zeolite, clinoptilolite, observed higher performance, which may be a result of larger pores. A total of 8 and 13 cycles were successfully completed without large

losses of material activity, indicating potential of zeolite as a support in the future of K_2CO_3-based capture.

2.6 Future Works

While sorbent formulation improvement is still under development, some immediate changes can be made to the reactor diagnostics systems. It was determined that the internal reactor humidity levels and overall saturation levels of the sorbent greatly impacted absorption capacity and kinetics. More humidity meters can be added along the reactor length to assist in monitoring these levels. Unfortunately, the model used here appeared sensitive to the operational temperatures, which can reach as high as 200°C, breaking the sensors. A more robust sensor model would be ideal, otherwise the sensor ports will need to be redesigned to isolate them from high temperatures. If this proves to be a challenge, it may even be necessary to design particle sampling ports along the length of the reactor. Then, throughout operation small particle samples can be directly removed and analysed for water content. On the bench scale, each sorbent formulation will need to be characterized, to determine the saturation levels at which performance suffers, defined by the mass of water absorbed by a given mass of dry particles. The “drying” phase will need to be added in between regeneration and cooling phases (or added into an extended regeneration phase) to bring particles below the identified maximal saturation level. It is possible that flue gas streams may even need to be somewhat dried to prevent quick oversaturation of sorbent with water. While some amount of water is necessary for the capture to proceed, the optimal flue stream humidity has yet to be determined. Similarly, the impact of total flow rate and CO_2 partial pressure on the sorbent is another avenue that requires investigation.

2.7 Citations

(1) Yu, K. M. K.; Curcic, I.; Gabriel, J.; Tsang, S. C. E. Recent Advances in CO2 Capture and Utilization. *ChemSusChem* **2008**, *1* (11), 893–899. https://doi.org/10.1002/cssc.200800169.

(2) US EPA, O. *Overview of Greenhouse Gases*. https://www.epa.gov/ghgemissions/overview-greenhouse-gases (accessed 2024-07-29).

(3) Kumari, K.; Kumar, S.; Rajagopal, V.; Khare, A.; Kumar, R. Emission from Open Burning of Municipal Solid Waste in India. *Environmental Technology* **2019**, *40* (17), 2201–2214. https://doi.org/10.1080/09593330.2017.1351489.

(4) Krecl, P.; de Lima, C. H.; Dal Bosco, T. C.; Targino, A. C.; Hashimoto, E. M.; Oukawa, G. Y. Open Waste Burning Causes Fast and Sharp Changes in Particulate Concentrations in Peripheral Neighborhoods. *Science of The Total Environment* **2021**, *765*, 142736. https://doi.org/10.1016/j.scitotenv.2020.142736.

(5) Choi, S.; Drese, J. H.; Jones, C. W. Adsorbent Materials for Carbon Dioxide Capture from Large Anthropogenic Point Sources. *ChemSusChem* **2009**, *2* (9), 796–854. https://doi.org/10.1002/cssc.200900036.

(6) Bhardwaj, M. M.; Prakash, A.; Prakash, D. N.; Sharma, D. S.; Sharma, M. P. Study the Impact of Carbon Credit on Accounting and Taxation of Companies' Profitability - An Indian Perspective. *Journal of Positive School Psychology* **2022**, *6* (3), 5416–5421.

(7) Abanades, J. C.; Criado, Y. A.; White, H. I. Direct Capture of Carbon Dioxide from the Atmosphere Using Bricks of Calcium Hydroxide. *CR-PHYS-SC* **2023**, *4* (4). https://doi.org/10.1016/j.xcrp.2023.101339.

(8) Henderson, P. Climate Tech Company Heirloom Opens US Commercial Carbon Capture Plant. *Reuters*. November 9, 2023. https://www.reuters.com/sustainability/climate-energy/climate-tech-company-heirloom-opens-us-commercial-carbon-capture-plant-2023-11-09/ (accessed 2024-07-29).

(9) Chen, K.; Huang, Y.; Wang, S.; Zhu, Z.; Cheng, H.; Yuan, Q. Integrated Technology for Dust Removal and Denitration of High-Temperature Flue Gas in Coal-Fired Power Plants. *Fuel* **2023**, *342*, 127687. https://doi.org/10.1016/j.fuel.2023.127687.

(10) Raganati, F.; Miccio, F.; Ammendola, P. Adsorption of Carbon Dioxide for Post-Combustion Capture: A Review. *Energy Fuels* **2021**, *35* (16), 12845–12868. https://doi.org/10.1021/acs.energyfuels.1c01618.

(11) Trickett, C. A.; Helal, A.; Al-Maythalony, B. A.; Yamani, Z. H.; Cordova, K. E.; Yaghi, O. M. The Chemistry of Metal–Organic Frameworks for CO2 Capture, Regeneration and Conversion. *Nat Rev Mater* **2017**, *2* (8), 1–16. https://doi.org/10.1038/natrevmats.2017.45.

(12) Millward, A. R.; Yaghi, O. M. Metal−Organic Frameworks with Exceptionally High Capacity for Storage of Carbon Dioxide at Room Temperature. *J. Am. Chem. Soc.* **2005**, *127* (51), 17998–17999. https://doi.org/10.1021/ja0570032.

(13) Li, Y.; Yu, J. New Stories of Zeolite Structures: Their Descriptions, Determinations, Predictions, and Evaluations. *Chem. Rev.* **2014**, *114* (14), 7268–7316. https://doi.org/10.1021/cr500010r.

(14) Chen, C.; Park, D.-W.; Ahn, W.-S. CO2 Capture Using Zeolite 13X Prepared from Bentonite. *Applied Surface Science* **2014**, *292*, 63–67. https://doi.org/10.1016/j.apsusc.2013.11.064.

(15) Younas, M.; Rezakazemi, M.; Daud, M.; Wazir, M. B.; Ahmad, S.; Ullah, N.; Inamuddin; Ramakrishna, S. Recent Progress and Remaining Challenges in Post-Combustion CO2 Capture Using Metal-Organic Frameworks (MOFs). *Progress in Energy and Combustion Science* **2020**, *80*, 100849. https://doi.org/10.1016/j.pecs.2020.100849.

(16) Meng, F.; Meng, Y.; Ju, T.; Han, S.; Lin, L.; Jiang, J. Research Progress of Aqueous Amine Solution for CO2 Capture: A Review. *Renewable and Sustainable Energy Reviews* **2022**, *168*, 112902. https://doi.org/10.1016/j.rser.2022.112902.

(17) Dutcher, B.; Fan, M.; Russell, A. G. Amine-Based CO2 Capture Technology Development from the Beginning of 2013—A Review. *ACS Appl. Mater. Interfaces* **2015**, *7* (4), 2137–2148. https://doi.org/10.1021/am507465f.

(18) Rochelle, G. T. Thermal Degradation of Amines for CO2 Capture. *Current Opinion in Chemical Engineering* **2012**, *1* (2), 183–190. https://doi.org/10.1016/j.coche.2012.02.004.

(19) Eide-Haugmo, I.; Brakstad, O. G.; Hoff, K. A.; Sørheim, K. R.; da Silva, E. F.; Svendsen, H. F. Environmental Impact of Amines. *Energy Procedia* **2009**, *1* (1), 1297–1304. https://doi.org/10.1016/j.egypro.2009.01.170.

(20) Hirano, S.; Shigemoto, N.; Yamada, S.; Hayashi, H. Cyclic Fixed-Bed Operations over K2CO3-on-Carbon for the Recovery of Carbon Dioxide under Moist Conditions. *Bulletin of the Chemical Society of Japan* **1995**, *68* (3), 1030–1035. https://doi.org/10.1246/bcsj.68.1030.

(21) Wang, S.; Yan, S.; Ma, X.; Gong, J. Recent Advances in Capture of Carbon Dioxide Using Alkali-Metal-Based Oxides. *Energy & Environmental Science* **2011**, *4* (10), 3805–3819. https://doi.org/10.1039/C1EE01116B.

(22) Meis, N. N. A. H.; Frey, A. M.; Bitter, J. H.; de Jong, K. P. Carbon Nanofiber-Supported K2CO3 as an Efficient Low-Temperature Regenerable CO2 Sorbent for Post-Combustion Capture. *Ind. Eng. Chem. Res.* **2013**, *52* (36), 12812–12818. https://doi.org/10.1021/ie4017072.

(23) Boonprasop, S.; Chalermsinsuwan, B.; Piumsomboon, P. Effect of the Operating Parameters on the CO2 Capture Capacity of Potassium Carbonate Supported on Gamma Alumina (K2CO3/γ-Al2O3) Using Conventional Heat Regeneration. *Journal of the Taiwan Institute of Chemical Engineers* **2017**, *78*, 282–289. https://doi.org/10.1016/j.jtice.2017.06.016.

(24) Guo, Y.; Sun, J.; Wang, R.; Li, W.; Zhao, C.; Li, C.; Zhang, J. Recent Advances in Potassium-Based Adsorbents for CO2 Capture and Separation: A Review. *Carbon Capture Science & Technology* **2021**, *1*, 100011. https://doi.org/10.1016/j.ccst.2021.100011.

(25) Qin, C.; Yin, J.; Ran, J.; Zhang, L.; Feng, B. Effect of Support Material on the Performance of K2CO3-Based Pellets for Cyclic CO2 Capture. *Applied Energy* **2014**, *136*, 280–288. https://doi.org/10.1016/j.apenergy.2014.09.043.

(26) Xu, D.; Zhang, J.; Li, G.; Xiao, P.; Webley, P.; Zhai, Y. Effect of Water Vapor from Power Station Flue Gas on CO2 Capture by Vacuum Swing Adsorption with Activated Carbon. *Journal of Fuel Chemistry and Technology* **2011**, *39* (3), 169–174. https://doi.org/10.1016/S1872-5813(11)60016-9.

(27) Luo, H.; Chioyama, H.; Thürmer, S.; Ohba, T.; Kanoh, H. Kinetics and Structural Changes in CO2 Capture of K2CO3 under a Moist Condition. *Energy Fuels* **2015**, *29* (7), 4472–4478. https://doi.org/10.1021/acs.energyfuels.5b00578.

(28) Informatics, N. O. of D. and. *Water*. https://webbook.nist.gov/cgi/cbook.cgi?ID=C7732185&Mask=4&Type=ANTOINE&Plot=on (accessed 2024-07-08).

(29) Zhao, C.; Chen, X.; Zhao, C. Carbonation Behavior of K2CO3 with Different Microstructure Used as an Active Component of Dry Sorbents for CO2 Capture. *Ind. Eng. Chem. Res.* **2010**, *49* (23), 12212–12216. https://doi.org/10.1021/ie1018035.

(30) Pang, M.; Zhang, T.; Meng, Y.; Ling, Z. Experimental Study on the Permeability of Crushed Coal Medium Based on the Ergun Equation. *Sci Rep* **2021**, *11* (1), 23030. https://doi.org/10.1038/s41598-021-02524-4.

(31) Miranda, C.; Mansilla, H.; Yáñez, J.; Obregón, S.; Colón, G. Improved Photocatalytic Activity of G-C3N4/TiO2 Composites Prepared by a Simple Impregnation Method. *Journal of Photochemistry and Photobiology A: Chemistry* **2013**, *253*, 16–21. https://doi.org/10.1016/j.jphotochem.2012.12.014.

(32) Chang, F.-W.; Kuo, M.-S.; Tsay, M.-T.; Hsieh, M.-C. Hydrogenation of CO2 over Nickel Catalysts on Rice Husk Ash-Alumina Prepared by Incipient Wetness Impregnation. *Applied Catalysis A: General* **2003**, *247* (2), 309–320. https://doi.org/10.1016/S0926-860X(03)00181-9.

(33) McCusker, L. B.; Baerlocher, C. Chapter 2 - Zeolite Structures. In *Studies in Surface Science and Catalysis*; Čejka, J., van Bekkum, H., Corma, A., Schüth, F., Eds.; Introduction to Zeolite Science and Practice; Elsevier, 2007; Vol. 168, pp 13–37. https://doi.org/10.1016/S0167-2991(07)80790-7.

(34) Bish, D. L. Chapter 14.2 - Parallels and Distinctions Between Clay Minerals and Zeolites. In *Developments in Clay Science*; Bergaya, F., Lagaly, G., Eds.; Handbook of Clay Science; Elsevier, 2013; Vol. 5, pp 783–800. https://doi.org/10.1016/B978-0-08-098258-8.00026-2.

(35) Popovici, E.; Sulitanu, N.; Dvininov, E.; Misaelidis, P. Preparation and Characterization of Palladium Supported on Heulandite. In *Studies in Surface Science and Catalysis*; Xu, R., Gao, Z., Chen, J., Yan, W., Eds.; From Zeolites to Porous MOF Materials - The 40th Anniversary of International Zeolite Conference; Elsevier, 2007; Vol. 170, pp 2134–2140. https://doi.org/10.1016/S0167-2991(07)81111-6.

(36) Gatta, G. D.; Lotti, P. Chapter 1 - Systematics, Crystal Structures, and Occurrences of Zeolites. In *Modified Clay and Zeolite Nanocomposite Materials*; Mercurio, M., Sarkar, B., Langella, A., Eds.; Micro and Nano Technologies; Elsevier, 2019; pp 1–25. https://doi.org/10.1016/B978-0-12-814617-0.00001-3.

(37) Kowalczyk, P.; Sprynskyy, M.; Terzyk, A. P.; Lebedynets, M.; Namieśnik, J.; Buszewski, B. Porous Structure of Natural and Modified Clinoptilolites. *J Colloid Interface Sci* **2006**, *297* (1), 77–85. https://doi.org/10.1016/j.jcis.2005.10.045.

(38) Marek, M. Numerical Modeling of Random Packed Beds of Various Packing Densities with a Sequential Deposition Algorithm. *AIP Conference Proceedings* **2019**, *2078* (1), 020015. https://doi.org/10.1063/1.5092018.

(39) Zhao, W.; Sprachmann, G.; Li, Z.; Cai, N.; Zhang, X. Effect of K2CO3·1.5H2O on the Regeneration Energy Consumption of Potassium-Based Sorbents for CO2 Capture. *Applied Energy* **2013**, *112*, 381–387. https://doi.org/10.1016/j.apenergy.2013.06.018.

(40) Duan, Y.; Luebke, D. R.; Pennline, H. W.; Li, B.; Janik, M. J.; Halley, J. W. Ab Initio Thermodynamic Study of the CO2 Capture Properties of Potassium Carbonate Sesquihydrate, K2CO3·1.5H2O. *J. Phys. Chem. C* **2012**, *116* (27), 14461–14470. https://doi.org/10.1021/jp303844t.

(41) Rodríguez-Mosqueda, R.; Bramer, E. A.; Roestenberg, T.; Brem, G. Parametrical Study on CO2 Capture from Ambient Air Using Hydrated K2CO3 Supported on an Activated Carbon Honeycomb. *Ind. Eng. Chem. Res.* **2018**, *57* (10), 3628–3638. https://doi.org/10.1021/acs.iecr.8b00566.

(42) Vinjarapu, S. H. B.; Neerup, R.; Larsen, A. H.; Jørsboe, J. K.; Villadsen, S. N. B.; Jensen, S.; Karlsson, J. L.; Kappel, J.; Lassen, H.; Blinksbjerg, P.; von Solms, N.; Fosbøl, P. L. Results from Pilot-Scale CO2 Capture Testing Using 30 Wt% MEA at a Waste-to-Energy Facility: Optimisation through Parametric Analysis. *Applied Energy* **2024**, *355*, 122193. https://doi.org/10.1016/j.apenergy.2023.122193.

Chapter 3

K_2CO_3 SORBENT DEVELOPMENT VIA WET-ACTIVATED GRANULATION

3.1 Abstract

In the following chapter, we present bench-scale testing results for several prototype granulated (uncalcined) K_2CO_3-based formulations developed by Mitico. Optimized formulations are desired for eventual scale-up and use in a packed bed reactor system for point source carbon capture, as described in Chapter 2. While many categories of additive materials were considered, including binders and potential catalysts, we found that sorbents composed primarily of the active material, inert supports, and desiccants resulted in materials that had simultaneous sufficient activity and material durability. Material activity was evaluated via capacity and kinetic evaluation over multiple cycles. Material durability was defined by its ability to maintain particle structure over cycling and exposure to humidity. We present our findings on the beneficial effects of adding Al_2O_3, CeO_2, $CaCO_3$ (supports and fillers), $CaCl_2$, and Zeolite 13X powder (desiccants) to K_2CO_3 granulate sorbents. Na_2CO_3, $MgCl_2$, Clinoptilolite zeolite powder, and a Mg-Al silicate were also considered, but found to be less effective than their analogues.

3.2 Introduction

3.2.1 Previous work on K_2CO_3 sorbents

Hot carbonates, in addition to other solvents, have been used for decades in oil refineries, ammonia manufacturing, and coal and natural gas purification plants to remove acidic gases in a process called gas "scrubbing" or "sweetening."[1] In fact, amine scrubbing for CO_2 and H_2S removal from acidic gas streams was patented in 1930, but wasn't significantly applied to small scale coal and gas-fired power plants until the 1980s and 1990s.[2] As discussed in Chapter 2, temperature requirements to swing amine solutions are minimal, but other environmental impacts of amine use are significant. Accidental release of amines and their oxidized/degraded products make such systems hazardous, and thus an unideal solution to the carbon capture problem.[3,4] Alternatively, the Benfield process, currently utilized in hundreds of plants globally, uses 20-30% by mass solutions of non-

toxic non-volatile K_2CO_3 and is less environmentally detrimental. Unfortunately, K_2CO_3 solutions observe slower reaction kinetics.[5,6] Assuming potassium or sodium carbonates are the sole reacting species present the net reaction is presented in line 1, where of all steps (2-4) the rate limiting step is line 3.[6,7]

1. $CO_{2(g)} + CO_3^{2-}{}_{(aq)} + H_2O_{(l)} \rightarrow 2HCO_3^-{}_{(aq)}$
2. $H_2O_{(l)} \rightarrow H^+{}_{(aq)} + OH^-{}_{(aq)}$
3. $CO_{2(g)} + OH^-{}_{(aq)} \rightarrow HCO_3^-{}_{(aq)}$
4. $CO_3^{2-}{}_{(aq)} + H^+{}_{(aq)} \rightarrow HCO_3^-{}_{(aq)}$

To enhance the rate of line 3, promoters are added to the solution, reactor temperature is increased, and most importantly reactor vessels are pressurized to around 70 atmospheres.[5,8] Thus, while the Benfield process does not emit toxic gases to the degree that amine based processing does, pressurizing hot corrosive solutions comes with its own set of safety and environmental concerns.

As K_2CO_3-based solutions have expanded in usage for carbon capture, simultaneously interest in the solid-phase reaction with CO_2 has increased, showing much potential. In the past two decades significant work has been made in elucidating the more complex “dry” chemistry, which is notably much faster. Note, dry chemistry refers to the fact that the K_2CO_3 sorbent is in the solid phase, opposed to being dissolved as in the Benfield process, but in fact is still exposed to water vapor. Recall from Chapter 2 that K_2CO_3 reacts in the presence of water with CO_2 to form $KHCO_3$ via the net reaction, line 5. The forward rate is maximal around 60°C while the forward reaction is initiated at temperatures as low as 120 °C, but typically around 155°C.[9,10]

5. $K_2CO_{3(s)} + CO_{2(g)} + H_2O_{(g)} \leftrightarrow 2KHCO_{3(s)}$
6. $K_2CO_{3(s)} + 1.5H_2O_{(g)} \rightarrow K_2CO_3 \cdot 1.5H_2O_{(s)}$
7. $K_2CO_3 \cdot 1.5H_2O_{(s)} + CO_{2(g)} \rightarrow 2KHCO_{3(s)} + 0.5H_2O_{(g)}$
8. $2K_2CO_{3(s)} + 2.5H_2O_{(g)} + CO_{2(g)} \rightarrow K_4H_2(CO_3)_3 \cdot 1.5H_2O_{(s)}$
9. $K_4H_2(CO_3)_3 \cdot 1.5H_2O_{(s)} + CO_{2(g)} \rightarrow 4KHCO_{3(s)} + 0.5H_2O_{(g)}$
10. $2K_2CO_3 \cdot 1.5H_2O_{(s)} + CO_{2(g)} \rightarrow K_4H_2(CO_3)_3 \cdot 1.5H_2O_{(s)} + 0.5H_2O_{(g)}$

Earlier (mid-1990s) work on the K_2CO_3 dry reaction mechanism by Hirano *et al.* and Hayashi *et al.* showed X-ray Diffraction (XRD) evidence of a stable K_2CO_3-hydrate intermediate, $1.5H_2O{\cdot}K_2CO_3$ (reactions 6-7).[11,12] Further work and XRD assignments by Zhao *et al.* gave evidence for a second reaction mechanism (lines 8-9) through hydrate $K_4H_2(CO_3)_3{\cdot}1.5H_2O$.[13] Both hydrates were verified by Luo *et al.*, and are hypothesized to form together under most relevant flue gas conditions.[14] Luo *et al*. suggest that the overall reaction might progress through a two-step hydration instead, according to line 10.[14]

Currently, there does not appear to be conclusive work which can predict branching fractions for the two (possibly three) paths. Due to the complexity of this mechanism, it is very difficult to define a kinetically accurate rate law that can be used to calculate rate constants to be compared across differing reaction conditions. As a flawed rate law/constant derivation is better than none what-so-ever, the following work continued to use the bimolecular rate constant derivation described in Chapter 2 Section 3.6 to compare sorbent reaction rates.

These mechanistic insights do however indicate that excess humidity, despite its challenges to sorbent structure/durability, may positively impact the speed of reaction. In short, if the material is fully hydrated (via line 6) before any flue gas is introduced, then initial hydrate formation step may be "skipped." Unfortunately, reaction kinetics are not only defined by the chemical mechanism. Luo *et al.*, like many others, have seen that physical accessibility of reacting material is also a great challenge to the K_2CO_3 system. For example, they observed via SEM imaging that at higher CO_2 concentrations, the surface reacted so quickly that the interior K_2CO_3 became inaccessible due to pore clogging. Thus, even though theoretically we would chemically expect higher CO_2 capacities at higher CO_2 concentrations (due to equilibria shift described in Chapter 2 Section 3.2), we might observe lower reaction rates depending on the pore structure.

Due to the deliquescent nature of K_2CO_3 as well as its naturally low porosity, current work on K_2CO_3-based sorbents focuses on formulating materials that can provide adequate support (to minimize material leaching, observed as capacity/mass loss) and maximize surface area. Metal oxides and carbon bonded networks are quite common in the literature.

CaO, MgO, TiO_2, ZrO_2, Al_2O_3, SiO_2, activated carbon, carbon nanotubes, and carbon honeycomb just to name a few, have all been considered and studied.[9,10,15–17] For example, in their work with TiO_2 and ZrO_2 Lee *et al.* generated impregnated beads and found that to maintain their physical properties over cycling, including bulk density and attrition resistance, they needed to be first calcined at temperatures above 500°C.[16] Unfortunately, calcination of the TiO_2 resulted in the formation of K-Ti alloys, significantly reducing the capacity.[16] Despite the benefits of thermal stability, ZrO_2 currently is not ideal to be the bulk material support as high purity ZrO_2 can be twice as expensive as TiO_2 and similar metal oxides.[18,19] Additionally, impregnation methods generally have lower K_2CO_3 loading maximums; it appears ZrO_2 was found to load about 30% K_2CO_3 by mass.

Meis *et al.* found that activated carbon, which is essentially charcoal and thus is very economical, observed decently high capacities on first absorption. However charcoal loses about half its capacity on successive cycling (regeneration of 150°C).[10] They found better regeneration using carbon nanofibers grown from synthesis gas using a Ni/SiO_2 catalyst to approximately 1mm in length (much smaller diameter).[10] Small batch preparation of carbon nanofibers make it unclear how such a material would be scaled. Of those materials studied, Al_2O_3 seems a very promising support with good regenerability, high mass loading capability, high porosity (translating to fast kinetics) and low cost.[15,20–22] There is some variability in the material traits depending on which Al_2O_3 phase is used (commonly used are α, γ and δ). While some success has been made, thus far none of these additives alone, prepared as described in the literature, are an obvious solution to the deliquescent nature of K_2CO_3.

3.2.2 Granule Manufacturing Strategies

While solid particulate sorbents for the purpose of CO_2-capture are emerging technologies, many other commercial products take the form of small granules, including but not limited to prescription drugs, fertilizer, detergents, pet litter, and feed pellets for livestock. Uniform particle generation strategies developed for these other commercial products can be utilized for carbon capture sorbent scale-up. However, it is not as simple as taking a particle production method and simply applying it to the K_2CO_3 system. As will be further described in this chapter, as well as Chapter 4, material processing can have a large impact

on the final properties of a sorbent, including durability/strength, capacity and kinetics. Additionally, some processes are more expensive than others. The cost-intensive nature of other aspects of carbon capture (like storage and mobilization) currently rules out more expensive methods.

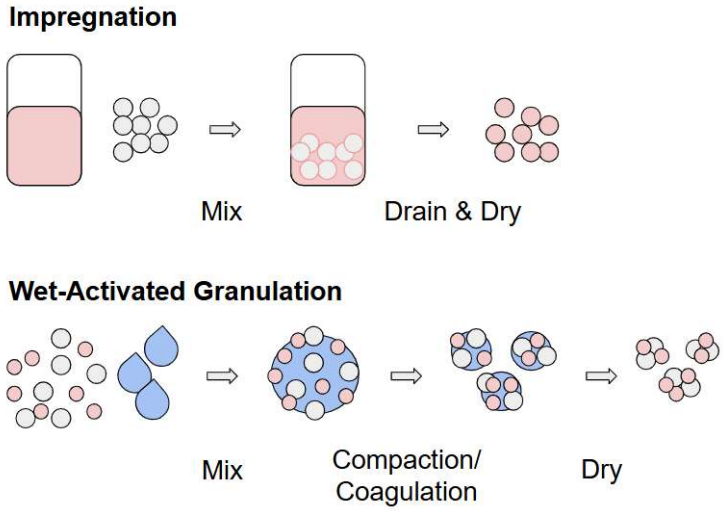

Figure 3.1 visually contrasts two methods for supporting active materials on uniform particles. Impregnation describes the process of soaking already prepared uniform porous particles in solvent concentrated with the active material (shown in light red). Wet-activated granulation takes dry active material and support material and mixes them with a solvent, eventually compacting it and forming particles. These can then be dried of the solvent.

In Chapter 2 Section 2.2, we briefly describe the difference between impregnation and wet granulation, which employ very differing strategies to support an active material on/in uniform particles.[23] Impregnation, which is far more common in the literature, takes already prepared (ideally durable, porous, uniform and inert) particles and submerges them in a solution concentrated with the dissolved material of interest, i.e. active material. The mixture is allowed time to settle, during which the dissolved active material slowly deposits onto the particles. Ideally if they are porous enough, the active deposits throughout their entire depth and not just superficially. On the other hand, wet granulation takes a powder/dust support material and mixes with the dry active in the presence of some solvent. In wet granulation active material is bonded into the support material in a "native" manner; the active material is already present when the particle is formed. The solvent is often water

but can be other liquids such as alcohols or acetone. The purpose of the solvent is to physically bring the dry materials closer together and initiate van der waals and/or ionic bonding. Afterwards the material is dried so that the solvent evaporates. To help strengthen the material a binder is often added. Additionally, the material can be heated at a higher temperature during a process often referred to as calcination. If higher temperatures are utilized, the particles may continue to strengthen via new (covalent) bonds formed during phase changes. Calcination temperatures must be carefully selected, as if an additive melts it may destabilize the particle structure.

While in theory impregnation is arguably simpler to streamline on a large scale and can be very cost effective, it comes with many limitations. First, impregnated particles cannot easily be recycled as they deteriorate over time. If leaching of the active material was the only problem, the material could simply be reimpregnated, but fast heat cycling does eventually cause cracking/dunting for most metal-oxides (like clays and zeolites).[24] If the material cracks and deteriorates it must be discarded and replaced.

Secondly, impregnated materials may have less activity due to clogging and insufficient active loading. As the active material is not "native" to the particle, sufficient deposition is required for significant mass loading onto the support medium. Inherently, the dissolved active material interacts with the superficial layers of the particle first and must traverse porous channels to deposit deeper into the particle. Unfortunately, each active material/particle system is different, and it is challenging to avoid clogging. At lower active dissolved concentrations, it is easier to avoid clogging (allowing material to potentially penetrate deeper into the particle), however lowering the concentration may decrease the amount of active that deposits overall by shifting the deposition equilibrium. In short, it is challenging to achieve a very large mass loading as well as deep penetration at the same time. Shallow penetration results in increased leaching of active material, and low mass loading reduces activity. In the case of the Mitico-developed 13X zeolite investigated in Chapter 2, a mass loading of only about 20% was achieved when the solvent solution concentration was optimized. To reduce size requirements for future CO_2-capturing packed bed towers, it is necessary to increase the sorbent's K_2CO_3 mass loaded.

Alternatively, during granulation, any amount of K_2CO_3 can be loaded into the material, if when mixed it will granulate. Wet granulation is the most common granulation method due to its simplicity and flexibility. It should be noted that dry granulation is also used in some commercial processes. For example, pharmaceutical "slugs" are created through compression of dry powder into slug molds. Most dry granulation techniques are done in small batches and require complex industrial machinery that necessitate larger industrial space and maintenance.[25] While this process lends itself to drug manufacturing, the costs and complications make it less desirable for CO_2 capture. Technically there are also many variations to the simple wet granulation presented in Figure 3.1. For example, some utilize freeze/spray granulation, which takes a wetted granulation mixture and sprays droplets into liquid N_2.[25,26] It is also possible, for certain more malleable formulations, to extrude the wetted mixture and spheronize it into beads.[27] This process will be further explored in Chapter 4.

3.2.2 Requirements for Industrial Scalability

Considering the benefits of wet-activated granulation, which includes increased loading potential, this process was selected for the next phase of Mitico sorbent development. While the primary goal these studies was to identify formulations with increased absorption capacity, it is critical to always keep in mind other necessary traits for a sorbent to be economically viable for scale-up. Any additives must be cheap (or used in very small quantities); ideally the most expensive material in the sorbent would be K_2CO_3. In the third quarter of the 2024 fiscal year, for example, K_2CO_3 powder cost around 1500-1600 USD per metric ton in the United States and Europe.[28] In comparison, TiO_2 during that same period cost 2500+ USD per metric ton in the US and Europe, and thus would not make for an ideal additive.[29]

Ideally, the material additives or the processes required for production will be non-toxic. One of the major downsides to other popular forms of carbon capture, like amine scrubbing, is their environmental impact. Non-toxic materials also make loading and unloading protocols easier, and thus more desirable for commercial use.

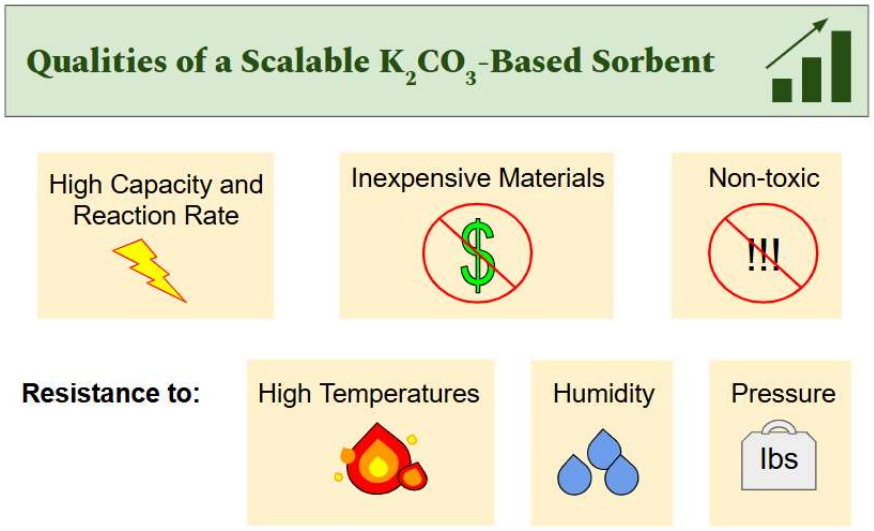

Figure 3.2 visualizes the primary challenges that must be addressed to design an economically viable and competitive K_2CO_3-based sorbent. While current academic literature focuses heavily on achieving high capacity and reaction rates, the sorbent must possess many other physical properties that are often not considered.

There are also many physical constraints; the material must be able to endure the weight of the tower, survive loading, and remain durable in a humid environment. Thermal cycling to temperatures of almost 200°C are necessary to release the CO_2 once captured, thus the material must also not burn or melt at these temperatures. To make matters more complicated, while some organics may not typically decompose at 200°C on their own, K_2CO_3 creates a strongly basic environment when wetted, and may induce base-catalyzed chemistry, reducing temperature of decomposition. Evidence for base-catalyzed decomposition will be further explored in Chapter 4. Lastly, when the material is wetted, it should not be susceptible to clumping, to avoid pressure drop.

3.3 Methods

3.3.1 Granulation Procedure

K_2CO_3-based sorbents made via wet-activated granulation method are presented and their properties compared. The particles were generated as follows: first, 500 g of dry materials were massed and mixed dry in a KitchenAid bowl-lift stand mixer with a flat beater for 5 minutes. Next, deionized water was added slowly over the course of another 5-10 minutes while mixing, typically around 20% of the dry mass. The wet-mixing period ended when

particle formation was significant, with an intent of forming particles of around 3 mm in diameter. This size range is of interest to minimize pressure drop in the packed bed reactor described in Chapter 2 and similar future designs. If only small agglomerates formed, typically more water was added (and more time was spent mixing) to increase cluster size. The particles were spread in a thin layer onto a tray and loaded into a counter-top convection oven. There, they were baked at 190°C with an internal fan for 2 hours. Once removed from the tray they were sieved. The saved and tested size range was 2.36-4.75 mm. For some formulations, the particles fused and had to be broken apart with a hammer. The particles had varying shape, especially if they had to be crushed. There was no way to normalize for shape differences across samples.

Figure 3.3 shows an example of particles formed from this process. The left panel shows wet particles still in the bowl of the stand mixer. On the right are the particles spread thin on a baking sheet after 2 hours in the convection oven. Wet granulation is a robust process; while the particles formed may not have regular size and shape distributions, coagulation through mixing and compaction works for most formulations (and worked for all formulations presented here).

3.3.2 Additive Selection and Formulations

Each formulation contains one (or more) of 10 additives: α and γ-Al_2O_3, CeO_2, $CaCO_3$, Na_2CO_3, $CaCl_2$, $MgCl_2$, 13X and clinoptilolite zeolite powder, and a Magnesium aluminum (Mg-Al) silicate. Most materials tested here are not laboratory grade, and for good reason. Economic viability necessitates that the material properties of additives be robust and not dependent on super high purities. If a material loses characteristic traits easily to small contaminations, then it is undesirable for process scale-up.

Anhydrous K_2CO_3 was purchased through Oakwood Chemical, with grains less than 44 microns. Of all the materials purchased we considered the K_2CO_3 source most important in impacting the final quality of the particles formed. Large K_2CO_3 crystals had been attempted previously and were found to not mix well, forming visibly heterogeneous particles. Additionally, hydrous grains must be dried prior to use to accurately determine the mass % composition. α and γ-Al_2O_3 were selected for testing as they appear promising in the literature when used via impregnation method, but less information is available regarding their use in other K_2CO_3 particle formation methods. The α-Al_2O_3 tested is a "rock polish," from Rock Shed Products, and range in grain sizes between 500 and 180 microns. The γ-Al_2O_3 tested is 99.9% purity with diameters around 20-nm purchased by SkySpring Nanomaterials. It was challenging to find lower grade γ-Al_2O_3, as the α phase is more common for polishing as it is courser. Two CeO_2 sources were used. One, noted "high grade" in Table 3.1, was purchased from Gold Label Detailing and is white. The other, noted "low grade" was purchased from Gordon Glass and is red, indicating substantial impurities from other earth metals like iron oxide.

$CaCO_3$ and Na_2CO_3 were considered alongside Al_2O_3 and CeO_2 as potential inert supports/fillers. They are notably different in that they are, like K_2CO_3, salts of carbonate. They are, however, significantly less deliquescent. The solubilities of K_2CO_3, Na_2CO_3 and $CaCO_3$ are 111, 30.7 and ~0g per 100g water at 25 °C, respectively.[30] It was hypothesized that $CaCO_3$ and Na_2CO_3 might provide strength through ionic bonding with the active material. $CaCO_3$ was purchased through Earthborn Elements and is food grade. Anhydrous Na_2CO_3 was reagent grade and purchased from Aldon. $CaCl_2$ and $MgCl_2$ were considered as potential desiccants as they are commonly used to absorb moisture in industrial and commercial settings, for example in road de-icing. $CaCl_2$ is generally considered more effective. Food grade $CaCl_2$ powder was purchased through Assencia, and food grade $MgCl_2$ was, like $CaCO_3$, purchased through Earthborn Elements. 13X and clinoptilolite were also explored, recognizing their potential to act as both a desiccant and a secondary support material. The 13X is crushed ADCOA beads, less than 180 microns. Clinoptilolite was from Stellar Chemical Corp, less than 400 microns grain size. Lastly, Mg-Al Silicate, "Van Gel B" was purchased from Vanderbilt Minerals.

Table 3.1: Formulation details of all sorbents

Ref	Formulation (mass %)	Water Added (% dry mass)	Bulk Density (g/mL)
A1	30 K_2CO_3 70 α-Al_2O_3, rock polish	24.6	1.14
A2	40 K_2CO_3 60 α-Al_2O_3, rock polish	22.9	0.72
A3	45 K_2CO_3 55 α-Al_2O_3, rock polish	22.7	0.67
A4	50 K_2CO_3 50 α-Al_2O_3, rock polish	23.8	0.66
A5	55 K_2CO_3 45 α-Al_2O_3, rock polish	24.4	0.66
A6	60 K_2CO_3 40 α-Al_2O_3, rock polish	24.9	0.66
A7	65 K_2CO_3 35 α-Al_2O_3, rock polish	26.3	0.64
B1	50 K_2CO_3 50 γ-Al_2O_3, 20 nm lab grade	99.5	0.42
B2	50 K_2CO_3 50 CeO_2, high grade	19.2	0.92
B3	50 K_2CO_3 50 CeO_2, low grade	23.4	0.79
B4	50 K_2CO_3 25 Al_2O_3, rock polish 25 CeO_2, high grade	21.9	0.64
B5	50 K_2CO_3 50 $CaCO_3$	20.9	0.90
B6	50 K_2CO_3 50 Na_2CO_3	20.8	0.71
B7	60 K_2CO_3 40 $CaCl_2$	34.3	0.62
B8	50 K_2CO_3 50 13X, size < 180 microns	25.8	0.75

Ref	Formulation	Water Added (% dry mass)	Bulk Density (g/mL)
C1	65 K_2CO_3; 15 $CaCl_2$ 20 Al_2O_3, rock polish	23.8	0.66
C2	50 K_2CO_3; 15 $MgCl_2$ 35 Al_2O_3, rock polish	20.6	0.75
C3	50 K_2CO_3; 15 $CaCO_3$ 35 Al_2O_3, rock polish	35.2	0.85
C4	50 K_2CO_3; 15 $CaCO_3$ 15 Clinoptilolite 20 Al_2O_3, rock polish	26.3	0.72
C5	50 K_2CO_3; 15 $CaCO_3$ 15 Mg-Al Silicate 20 Al_2O_3, rock polish	24.2	0.80
C6	50 K_2CO_3; 15 $CaCO_3$ 15 Zeolite 13X 20 Al_2O_3, rock polish	26.6	0.71
C7	70 K_2CO_3; 20 $CaCl_2$ 10 Al_2O_3, rock polish	21.4	0.67

Samples A1-A7 were generated with the intention of observing the impact of K_2CO_3% mass on total absorption capacity. As K_2CO_3 has poor pore formation, it was possible that capacity change would not be linear with K_2CO_3 mass added. Samples B1-B8 were manufactured to test the physical properties, capacity, and kinetics of binary mixtures with the additives of interest. Note that $MgCl_2$, Clinoptilolite, and Mg-Al silicate are not tested in the B series, however their properties will be compared to their analogues ($CaCl_2$ and 13X) in the C series. An attempt was made to have all the B series made with 50% K_2CO_3 to make comparing their respective capacities/kinetics simpler. B7 was made with 60% K_2CO_3 instead of 50% because a 50/50 mixture was hard to granulate. All the A and B series samples were run on the mini reactor. The B series was additionally humidity tested, and the granulation quality and relative durability noted. The C series forms trinary/quaternary mixtures of materials to test their synergy and was additionally cycled.

3.3.3 Testing Procedures

Three different stations were utilized to test the sorbent properties: a mini reactor (left panel of Figure 3.4), a humidification cell, and an auto-cycler (right panel of Figure 3.4). Before a sample was reacted, humidified or cycled it was first loaded into a 2cm diameter, 13cm long stainless-steel cylindrical cell. To prevent sample from falling out either side of the cell, a small ball of glass wool was placed on either end. In addition, to ease removal of sample from the cell after use, a thin Amazon Basics silicon baking mat was wrapped inside the wall of the cylinder. Approximately 20g of sample can then be loaded and was tapped repeatedly to minimize void fraction.

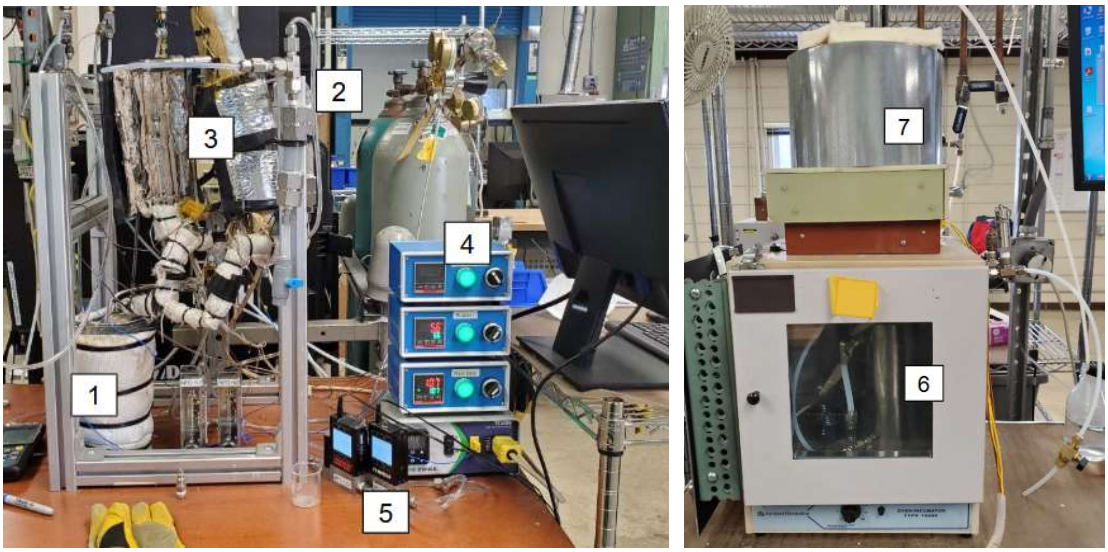

Figure 3.4 displays the mini reactor on the left panel and the auto cycler on the right. In the mini reactor the "flue" gas is injected by Omega mass flow controllers (5). The bubbler (1) is wrapped in fiberglass to help maintain temperature controlled via PID (4). The reactor (3) is also wrapped in fiberglass and controlled via PID (4). Unreacted water is removed via desiccant tube and drain valve (2). The auto cycler is also equipped with a bubbler (6) which is used during the absorption phase and bypassed during regeneration and cooling. The sorbent cell sits inside the "hat" (7) which controls the temperature.

The primary testing station utilized was the mini reactor (left panel of Figure 3.4), which consists of a bubbler, a cell mount (as well as gas connections), and a Hiden Analytical Quadrupole Mass Spectrometer (QMS) controlled by MASsoft 10. The bubbler, which is used in all three systems, is custom-made to hold over a liter of water which is temperature controlled via a Proportional–integral–derivative (PID) controller to 55°C.

During reaction, 150 ccm of 10% CO_2 in Argon (provided by Airgas) is injected into the bubbler via FMA-2606A Omega mass flow controller where the stream is humified to 15% absolute humidity. This temperature/absolute humidity was selected to have excess water in the "flue" stream so that the reaction is CO_2-limited. The humidified "flue" stream exits the bubbler and enters the sample cell, which itself is heated to 65°C via PID controller. The temperature increase from the bubbler to the cell also helps prevent condensation of water vapor. The reacted gas enters a desiccant tube (non-CO_2-absorbing) and drain valve (closed during reaction) to remove any unreacted water before it enters the QMS.

The humidification cell is essentially the mini reactor without a QMS attached; a 15% absolute humidity stream at 150 ccm through a sorbent cell held at 65°C. Since no reaction needs to occur, a more economical pure N_2 stream is used instead of a CO_2 in Argon mixture. The purpose of the humidity cell is to expose the samples to a prolonged humid environment. While during absorption the mini reactor does expose the material to moisture, a significant portion of that moisture is converted to $KHCO_3$, and when the reaction is complete the experiment terminates. As each material reacts for different lengths depending on their capacity and kinetics this means that some finish reacting significantly faster than others. The humidity cell provides a more standard comparison for how the material responds to moisture over a 6-hour period. Ideally, the material maintains its shape and structure though wetted. When materials begin to clump or K_2CO_3 begins to visibly dissolve the sorbent is considered inadequate.

Lastly the auto cycler (shown in the right panel of Figure 3.4) is self-explanatory; it is set up to perform many absorptions and desorptions in succession automatically. It is also like a mini reactor without a QMS attached. However, in addition to the absorption phase which utilizes 10% CO_2 (pre-humidification), it is also set up to regenerate with a 150 ccm N_2 stream at 180°C. The system currently has no way of detecting when absorption is complete, so the phase is set to 2 hours. The regeneration phase is 3 hours, with a cooldown period which typically takes about 3 hours (the cycler detects when the sorbent cell reaches 65°C). The regeneration phase is long enough that it essentially also acts as a drying phase. The presented sorbents are technically clusters (not covalently bonded as they are not calcined) thus after enough exposure to water and force they will eventually dissolve and

crumble. It is not necessary to have material that is completely insoluble, just resistant enough that it maintains shape and structure during the absorption phase. On the industrial scale, a drying phase can and should be implemented between absorption cycles to prevent leaching.

The capacity and second order rate calculation are essentially the same as was performed for the packed bed reactor, described in Chapter 2, Section 3.6, except that the %CO_2 is measured via QMS instead of CO_2 analyzer. In short, the CO_2 captured is determined via line 11, and the rate constant is calculated via line 12. In line 11, $N_{inj,t}$ is the total moles of CO_2 injected during a time t, and $N_{exit,t}$ is the exiting moles during that same time. Thus, the difference is the moles captured during that time. The total moles captured are the summation over the capture period. Line 12 shows that to calculate the rate constant requires the CO_2 and H_2O concentrations before ($[CO_2]_0$ and $[H_2O]_0$) and after ($[CO_2]_f$, and $[H_2O]_0$) the sorbent cell as well as the resonance time (τ). As the rate constant can be calculated at any point in the reaction, the first stable point of highest efficiency was selected for each sample. More details on these derivations are available in Chapter 2, Section 3.6. To calculate %CO_2 the QMS utilizes an internal standard, the CO_2:Ar ratio. Sampling is performed approximately every 20-25 seconds.

11. CO_2 captured = $\sum_0^f (N_{inj,t} - N_{exit,t})$

12. $$k = \ln\left(\frac{[CO_2]_0}{[H_2O]_0}\right) + \ln\left(\frac{[H_2O]_f}{[CO_2]_f}\right)([H_2O]_0 - [CO_2]_0)^{-1}\,\tau^{-1}$$

Replicates were not performed on most samples, making standard error hard to define. Based on a reference formulation (not listed here) replicated 5 times, we determined that the standard deviation in the capacities is approximately 10%. The 5 replicates were all performed on dry sample, were uncycled material, at the same temperature and humidity exposure. The standard deviation of the calculated rate constant tends to be a bit larger, on the order of 15%. We consider sample deviation error, but it should be noted that it is quite possible that some variation across samples is real, considering the irregularities in the particle shapes and sizes.

3.4 Results and Discussion

The calculated capacities, % K_2CO_3 reacted, as well as calculated rate constants are presented for the A, B and C series of sorbents. Capacity is listed two ways, mg CO_2 g^{-1} sorbent, and mg CO_2 mL^{-1} sorbent. When generating scalable sorbents both values should be considered. The mass dependent value is better for comparing the chemical efficiency of each formulation. However, ultimately reactors are designed with a finite volume and more dense materials are typically preferable (assuming the chemical activities are the same across densities) because they can fit more mass in the reactor. If a material has a low density but high mass-dependent capacity this results in a lower density-dependent capacity. Given that manufacturing process, like %water, mix time and mixing speed, does impact material density, some formulations may be further improved through optimization.

Table 3.2: Capacities and rate constants of A1-A7

Ref	K_2CO_3 : α-Al_2O_3	Cap (mg/g)[a]	Cap (mg/mL)[a]	% reacted[b]	k (m^3 mol^{-1} s^{-1})
A1	30 : 70	84	96	88	0.121
A2	40 : 60	135	97	105	0.070
A3	45 : 55	146	98	102	0.054
A4	50 : 50	167	110	104	0.046
A5	55 : 45	171	113	97	0.040
A6	60 : 40	195	129	103	0.040
A7	65 : 35	209	134	101	0.030

[a]Capacity is listed in mg CO_2 per g or mL sorbent (not K_2CO_3). mL sorbent is bulk density rather than individual particle density.
[b]The theoretical capacity of a pure K_2CO_3 sorbent is 319 mg CO_2 g^{-1} K_2CO_3.

In addition to the listed capacities, %reacted is also used a measure of K_2CO_3 availability. % reacted is the actual measured capacity divided by the mass-normalized theoretical capacity. For example, A1 has a mass normalized theoretical capacity of 95.7 mg g^{-1} sorbent (30% of 319 mg g K_2CO_3). It should be noted that some of our calculated %reacted are over 100%. We consider it unlikely that we observed significant physisorption or chemisorption from material other than K_2CO_3 (which would explain a real value over

100%). Instead, we recognize that our error is on the order of 10%, as described in section 3.3.3, and this likely means that about 100% of the K_2CO_3 present reacted.

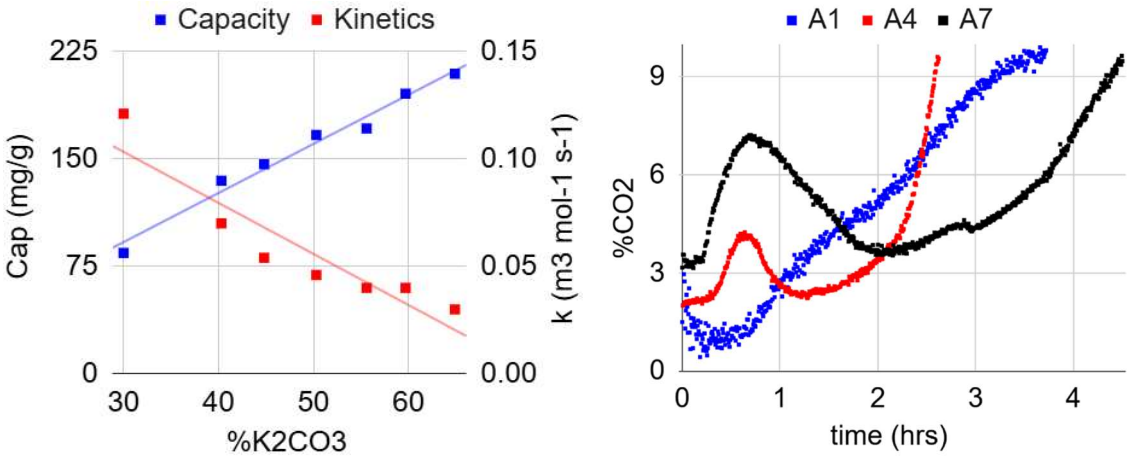

Figure 3.5 displays the capacity and kinetics for the A series on the left panel, and kinetic curves for A1, A4 and A7 on the right panel. Increases in K_2CO_3 shown on the x-axis of the left panel correspond to decreases in Al_2O_3, as they are binary mixtures. While capacity increases (linearly) with K_2CO_3, we simultaneously observe a clear decrease in rate of reactions. The kinetic curves (right panel) give some more insight into what may cause this kinetic decrease. As Al_2O_3 is removed, a hump grows in hinting again that the mechanism is more complex.

The calculated results for the A series are listed in Table 3.2, and the mass-dependent capacities and rate constants are plotted in left panel of Figure 3.5. The mass dependent capacities (mg CO_2 g^{-1} sorbent) increase nearly linearly as K_2CO_3 is added. The largest amount of K_2CO_3 tested was a 70:30 mixture as anything higher could not granulate and became slurries. Al_2O_3, even in low amounts, appears to provide sufficient surface area to make all the K_2CO_3 available for reaction, as indicated by the %reacted column of Table 3.2. In the K_2CO_3 range tested in the A series, the only sample that appears to have reactivity less than 100% is the lowest concentration sample, 30% K_2CO_3. Our expected error as described in Section 3.3 is expected to be around 10%. Assuming an error of 10%, 88 +/- 9% reactivity is reasonably high to suspect this sample is still in trend with the other formulations.

As the amount of Al_2O_3 decreases, so does the calculated rate (Table 3.2, Figure 3.5, left panel). By plotting the kinetic curves (Figure 3.5, right panel), it becomes clear that there is not just a uniform decrease in reaction rate. Instead, as Al_2O_3 decreases a hump appears, and grows larger as Al_2O_3 is further decreased. This hints at a more complex mechanism with a rate limiting step. Eventually, whatever process is causing the hump subsides, and the curve returns to its original lowest point. For example, in A4 the CO_2 curve begins at approximately 80% capture (2% CO_2 exiting) before a hump grows in, decreasing the capture efficiency to around 60% (4% CO_2 exiting) at 30 minutes. By an hour into capture, the A4 curve returns to approximately 80% capture.

This temporary rate decrease resembles the work of Luo *et al.* on pure K_2CO_3 samples. They found through XRD analysis and SEM imaging that slow transformation of $K_2CO_3 \cdot 1.5H_2O$ and $K_4H_2(CO_3)_3 \cdot 1.5H_2O$ to $KHCO_3$ caused an increase in surface occlusion. Once the surface transformed to $KHCO_3$, resistance appeared to decrease, allowing for further reactivity of K_2CO_3. Al_2O_3 appears to increase porosity such that these intermediate products do not block reactivity of unreacted K_2CO_3. Future works might also use SEM to image the surface of these samples after reaction to monitor occlusion and verify this hypothesis.

Table 3.3 lists the capacities and rate constants for the B series, which investigates mostly binary mixtures (excluding B4 which is trinary) of other additives. The metal oxides (B1-B4) unsurprisingly outperformed the other additives in terms of capacity and rate. However, activity differences were noted even across the metal oxide mixtures tested. The mass and density dependent capacities of these four samples are presented in Figure 3.7, alongside A4 which also had 50% K_2CO_3 and utilized α-Al_2O_3. Figure 3.7 shows that for the wet granulation method, our α-Al_2O_3 performs similarly to γ-Al_2O_3 and both CeO_2 grades when considering mass-dependent capacity. However, CeO_2 forms much denser material, making both the low and high grade CeO_2 sorbents more reactive per volume. The γ-Al_2O_3 formed the least dense material of all those tested, 0.42 gm/mL, resulting in a very low-density dependent capacity. We suspect that the density of the resultant sorbent is mostly due to the very fine grade of particles formed (20 nm), whereas all other additives were present in grain sizes on the order of 100+ microns.

Table 3.3: Capacities and rate constants of B1-B8

Ref	Formulation	Cap (mg/g)	Cap (mg/mL)	% reacted[b]	k ($m^3 mol^{-1} s^{-1}$)
B1	50:50 γ-Al_2O_3	150	63	94	0.057
B2	50:50 CeO_2, H grade	142	131	89	0.028
B3	50:50 CeO_2, L grade	158	125	99	0.06
B4	50:25:25 Al_2O_3, CeO_2	164	105	103	0.084
B5	50:50 $CaCO_3$	76	68	47	0.022
B6	50:50 Na_2CO_3	89	63	56	0.034
B7	60:40 $CaCl_2$	11	7	6	0.008
B8	50:50 13X	113	85	71	0.026

Figure 3.6 displays examples of unstable material after exposure to the humidification cell. The left shows what particle clumping looks like. The right shows disolved/deteriorated sorbent. Both samples are from the A series and have an appearance typical of sorbents which do not contain dessicant.

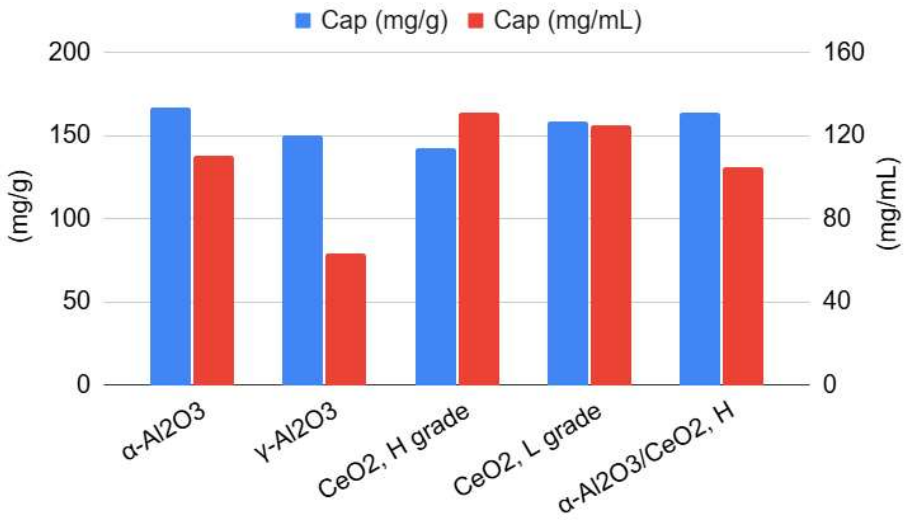

Figure 3.7 compares the mass dependent and volume dependent capacities of A4 (50/50 with α-Al_2O_3) to the other 50% K_2CO_3 metal oxide formulations, B1-B4. CeO_2 sorbents are very dense, resulting in high density-dependent capacities. Though γ-Al_2O_3 performs similarly in mass-dependent capacity to the other sorbents presented, it has a very low density, giving it a low density-dependent capacity. We hypothesize this is mostly due to the small grain size (20 nm).

The other additives tested in the B series, $CaCl_2$, $CaCO_3$, $NaCO_3$, and zeolite 13X, all displayed significantly lower mass-dependent and density-dependent capacities, as expected. More interesting is how these additives impacted other granule properties. The sample strength, shape, and response to humidity were observed. $CaCl_2$ did not granulate well, and clearly had a greatly adverse effect on capacity and kinetics (likely by inhibiting the formation of intermediate K_2CO_3-hydrates), but greatly increased the longevity when exposed to humidity, and even improved dry strength. $CaCO_3$ granulated well and provided the material compressive strength (when dry) and displayed moderate resistance to humidity. The ionic bonding networks formed between K_2CO_3 and $CaCl_2$ and $CaCO_3$ are likely responsible for their greater compressive strengths. The strength $CaCO_3$ provided is also intuitive as $CaCO_3$ is used in concrete for similar reasons. $NaCO_3$ observed similar capacity and kinetics to $CaCO_3$ and was decently strong (when dry). But, likely due to its much higher solubility, $NaCO_3$ granulated poorly and was not resistant to humidity. 13X granulated well, but did not have much compressive strength compared to formulations with $CaCl_2$ and $CaCO_3$. That said, 13X was able to lend substantial resistance to humidity without the huge capacity drop seen when $CaCl_2$ is used.

In summary, from series A we concluded that large quantities of K_2CO_3 (30% by mass is common in the literature) could be loaded to the sorbent, if sufficient porous support was present. While the A series did not survive a single absorption cycle or humidity test (see Figure 3.6), it did confirm that mass-dependent capacity does in fact increase linearly within our target K_2CO_3% range. We also note a substantial kinetic block (the hump in Figure 3.5) grows in at masses above 50%. From the B series we concluded that $CaCO_3$ benefits the dry strength of the material but could not act as the bulk support due to significant reduction in capacity. $CaCl_2$ and 13X provide humidity resistance which prevents K_2CO_3 from dissolving under the time scales we consider relevant for reaction in a tower. However, $CaCl_2$ appears to be so desiccating that in large amounts it outcompetes K_2CO_3 at bonding with water and deactivates the sorbent. It is possible that chemical desiccation as is observed with $CaCl_2$, and physical desiccation, as is 13X, have very different effects on K_2CO_3 activity. This should be investigated in future works.

We utilized these findings to propose potentially synergistic combinations of additives, which resulted in the C series. In series C, we also investigated the desiccating properties of $MgCl_2$ (C2), a $CaCl_2$ analogue, and Clinoptilolite and a Mg-Al silicate (C4 and C5), 13X analogues. As all the C series survived initial absorption and humidity testing, they were resultantly cycled. As $MgCl_2$ is known to not be as strong of a desiccant as $CaCl_2$, it was hypothesized that it might not have as strong of a deactivating effect on the sorbent. Simultaneously, we suspected it may not be able to provide as much humidity resistance, thus C1 and C2 were formulated to compare the effectiveness of $CaCl_2$ versus $MgCl_2$. C2 was prepared with 15% less K_2CO_3 in anticipation of these trends, then both were cycled. As is shown in Figure 3.8, C1 and C2 were each cycled 22 times. While C1 observed some loss of material strength during cycling, C2 suffered much more decomposition, indicated by a large portion of the surviving mass being dust (right panel, Figure 3.8). At the time this observation was made, there was not a procedure in place for quantitatively comparing survivability of the material. Future works might measure and compare the sample mass remaining in the original sieved size regime (2.36-4.75 mm) to the dust fraction. Similarly, future works might determine the mass lost by measuring the sorbent mass before and after cycling, as dissolved/leached K_2CO_3 was observed to occasionally coat the glass wool.

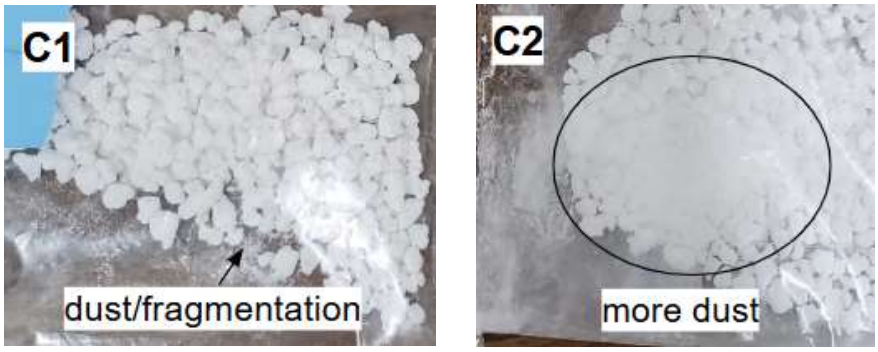

Figure 3.8 displays samples C1 and C2 after 22 cycles in the auto cycler. Despite being prepared with 15% less K_2CO_3, the $MgCl_2$ sorbent was much weaker, with much of the material crumbling into dust. It was concluded that for a $MgCl_2$ based sorbent to be as durable as those formed with $CaCl_2$ would require even more of the mass fraction to belong to $MgCl_2$ perhaps taking place of the porous support (Al_2O_3 here).

Table 3.4: Capacities and rate constants of C1-C7

Ref	Formulation	Cap (mg/g)	Cap (mg/mL)	% reacted[b]	k ($m^3mol^{-1}\ s^{-1}$)
C1	65 K_2CO_3; 15 $CaCl_2$ 20 Al_2O_3	118	78	57	0.024
C2	50 K_2CO_3; 15 $MgCl_2$ 35 Al_2O_3	76	57	48	0.048
C3	50 K_2CO_3; 15 $CaCO_3$ 35 Al_2O_3	139	118	88	0.031
C4	50 K_2CO_3; 15 $CaCO_3$ 15 Clinpt.; 20 Al_2O_3	90	65	57	0.053
C5	50 K_2CO_3; 15 $CaCO_3$ 15 Mg-Al Silicate 20 Al_2O_3	118	78	57	0.024
C6	50 K_2CO_3; 15 $CaCO_3$ 15 13X; 20 Al_2O_3	100	71	63	0.067
C7	70 K_2CO_3; 20 $CaCl_2$ 10 Al_2O_3	93 133[a]	62 89[a]	41 59[a]	0.034 0.074[a]

[a]In addition to first cycle absorption, C7 was also measured after 24 cycles

Similarly, C3-C6 were formulated to test the desiccating ability of 13X and its analogues. Again, one way in which these samples differ from those with $CaCl_2$ and $MgCl_2$ is these additives manage moisture through physisorption, instead of forming salt-hydrates. Since B8 (50/50 with 13X) was found to have less than desirable dry strength, $CaCO_3$ was also added. C3-C6 samples are presented after 33 cycles on the auto cycler (Figure 3.9). C3 contains just $CaCaO_3$ (15%) and Al_2O_3 (30%) as additives, C4, C5 and C6 has 15% Clinoptilolite, Mg-Al silicate or 13X added, respectively (Al_2O_3 is 20 instead of 35%). It is clear from visual inspection that C6 significantly outperformed the other materials when cycled. Surprisingly, C4 and C5 seemed to perform equally as poor as C3, which did not have any desiccant. By the dusty look of the material (apposed to materials which clump) and their poorer ability to granulate, it may be that the K_2CO_3 does not bind as strongly to these as 13X. It may also be as simple as 13X was more effective at controlling moisture. Unfortunately, without other characterization techniques it is challenging to assess why the 13X analogues did so poorly.

Figure 3.9 displays samples C3-C6 after 33 cycles on the auto cycler. C6, which contains 13X exited the cycler with minimal decomposition, clumping, or dust formation.

Lastly, C1 was taken a step further to form C7, which contained what we believe is the absolute maximum amount of K_2CO_3 that can be stabilized this way, 70%. Before testing, it was unclear whether the benefits (theoretical capacity) of having such a high amount of K_2CO_3 outweighed the large amount of $CaCl_2$ (deactivating) that would be needed to stabilize the material. When the material was removed from 24 cycles, it very much resembled C1 after 22 cycles. Despite having 5% more active material than C1, the increase in $CaCl_2$ resulted in a 15% drop in %reacted, thus the overall capacity was still less C1 (see Table 3.4). This insight may be important for future development; maximizing the amount of K_2CO_3 loaded alone may not be the best strategy for creating a sorbent with maximal capacity.

After cycling, C7 was reintroduced to the mini reactor for what would be its 25th cycle. The results were quite eye opening- the capacity and kinetics of the material both improved significantly (see Table 3.4). At first, this may not be intuitive, however it has been observed Beving *et al.* that repeated hydration cycling of raw K_2CO_3 resulted in microcracking, which stimulates surface area increase, and in the case of raw K_2CO_3 even particle expansion (loss of density).[31] These microcracks improved the reactivity such that the material no longer observed the "hump" (see Figure 3.10) characteristic of what we believe is surface occlusion by $K_2CO_3 \cdot 1.5H_2O$ and $K_4H_2(CO_3)_3 \cdot 1.5H_2O$.[14]

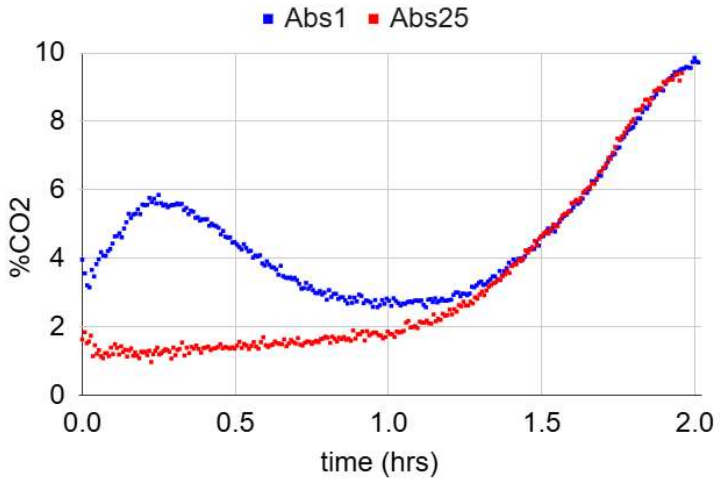

Figure 3.10 displays the kinetic profile for C7 during it's first absorption cycle against its 25th absorption cycle. The characteristic "hump" observed across most of the samples appears to have disappeared. We attribute this to microcracking.[31]

To further test how the $K_2CO_3 \cdot 1.5H_2O$ and $K_4H_2(CO_3)_3 \cdot 1.5H_2O$ intermediate products and bound water in general impact the reaction rate, some samples underwent mini reactor testing after hydration. Two B4 samples were exposed to 150 ccm of humidified N_2 for 35 minutes, and 90 minutes respectively (Figure 3.11). Unfortunately, the mass of water absorbed by the samples were not noted and should be monitored in future works.

It appears that a minimal amount of hydration achieved by the 35-minute exposure decreased the "hump" substantially, improving the overall capture rate while minimally impacting the capacity (164 and 158 mg CO_2 g^{-1} sorbent, dry and 35-min exposure respectively. However, 90-minute exposure appears to exceed this beneficial hydration period, in fact lowering both the kinetics and capacity significantly (122 mg CO_2 g^{-1} sorbent). The decrease in capacity due to excess hydration was also observed for the impregnated zeolite samples used in the packed bed reactor in Chapter 2. It is very likely that this is a property inherit of K_2CO_3 itself and not just the supporting material; as K_2CO_3 becomes excessively wet not only does it become unstable, the K_2CO_3 shifts from a primarily "dry" chemistry regime (lines 5-10) to a wet one (lines 1-4).

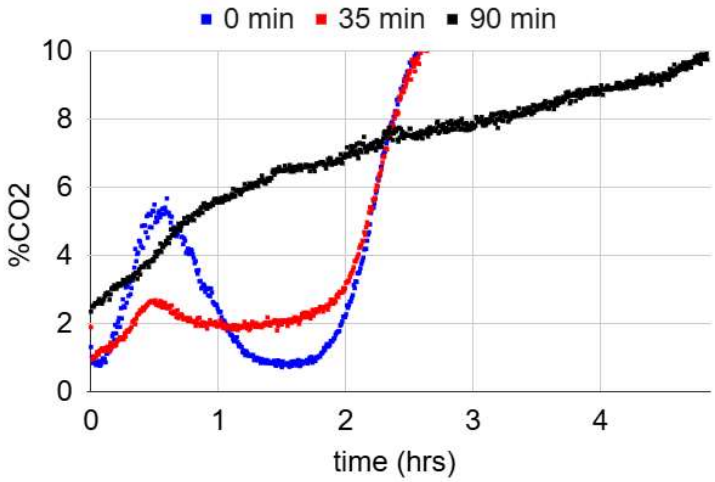

Figure 3.11 displays B4 mini reactor curves when reacted dry (0 min), lightly wetted (35 min) and heavily wetted (90 min). When dry, the material appears to experience occlusion around 30 minutes. After a 30-min hydration this occlusion period is greatly minimized, though the overall highest efficiency period (around 1.5 hours) is a bit lower than when the material was dry. In comparison to both of these, the 90-min hydrated sample was very slow, taking almost twice as long to reach breakthrough.

3.5 Conclusions

Three series of K_2CO_3-based wet granulated sorbents for carbon capture (A, B and C series) were manufactured and tested in a bench scale mini reactor. Positive activity in terms of capacity and kinetics were found for samples that contained Al_2O_3 or CeO_2, but they were not stable when exposed to humid flue gas on their own. $CaCO_3$ appears to increase dry strength though this should be further quantified, perhaps with a durometer. Desiccants like $CaCl_2$ and zeolite 13X help control in-particle moisture, resulting in sorbents which can maintain their structures of 20+ cycles when regenerated/dried with N_2. At larger mass loadings (50%+) of K_2CO_3 desirable to carbon capture, kinetic hindrances might occur due to the low porosity of K_2CO_3.

In this work we have observed that low amounts of pre-reaction hydration might give $K_2CO_3 \cdot 1.5H_2O$ and $K_4H_2(CO_3)_3 \cdot 1.5H_2O$ formation a head start to prevent significant surface build up and occlusion by these intermediate products. However, this may only benefit kinetics within a certain hydration range, which once breached appears to harm CO_2 diffusion, decreasing reaction rate. Lastly, K_2CO_3-based granulate sorbents appear to have the potential to improve in both capacity and kinetics when cycled due to microcracking.

3.6 Future Works

Further characterization of the particles in general might benefit this work by verifying observations, for example expectations of microcracking over cycling. Preferred methods for observing surface area and microstructure changes are BET and SEM respectively. Future works might also characterize other sorbent changes when cycled, for example compressive strength, mass loss or changes in particle density. Changes in particle density seem particularly important, as engineers might have to consider particle expansion over continued operation. Current literature on K_2CO_3-based sorbents focus heavily on reactivity and appear to neglect characterization of particle stability from a mechanical perspective. Any improvements in characterizing and quantifying sorbent mechanical stability would benefit this field.

Something that was only briefly touched up here is how grain size/source of additives used impact final sorbent quality. Future works might consider analyzing the properties of their additives more closely, like their grain size or contaminant sources (perhaps through ICP-MS). Based on the density of sorbent produced by 20-nm Al_2O_3 (B1), grain size of additives at the very least may impact final sorbent density and may perhaps even impact reactivity or stability.

Lastly, while these sorbents appear promising in their ability to be dry cycled (N_2-purged regeneration), their ability to survive steam regeneration, like the impregnated sorbents in Chapter 2, has not yet been verified. Should these materials struggle to maintain their structure when undergoing steam-regeneration, it may be beneficial to explore calcination of these materials to form covalent bonding networks between neighboring support grains.

3.7 Citations

(1) Park, S.-B.; Shim, C.-S.; Lee, H.; Lee, K.-H. Solubilities of Carbon Dioxide in the Aqueous Potassium Carbonate and Potassium Carbonate poly(Ethylene Glycol) Solutions. *Fluid Phase Equilibria* **1997**, *134* (1), 141–149. https://doi.org/10.1016/S0378-3812(97)00052-6.

(2) Rochelle, G. T. Amine Scrubbing for CO2 Capture. *Science* **2009**, *325* (5948), 1652–1654. https://doi.org/10.1126/science.1176731.

(3) Eide-Haugmo, I.; Brakstad, O. G.; Hoff, K. A.; Sørheim, K. R.; da Silva, E. F.; Svendsen, H. F. Environmental Impact of Amines. *Energy Procedia* **2009**, *1* (1), 1297–1304. https://doi.org/10.1016/j.egypro.2009.01.170.

(4) Dutcher, B.; Fan, M.; Russell, A. G. Amine-Based CO2 Capture Technology Development from the Beginning of 2013—A Review. *ACS Appl. Mater. Interfaces* **2015**, *7* (4), 2137–2148. https://doi.org/10.1021/am507465f.

(5) Pérez-Salado Kamps, Á.; Meyer, E.; Rumpf, B.; Maurer, G. Solubility of CO2 in Aqueous Solutions of KCl and in Aqueous Solutions of K2CO3. *J. Chem. Eng. Data* **2007**, *52* (3), 817–832. https://doi.org/10.1021/je060430q.

(6) Liu, N.; Zhao, X.; Wang, Y.; Fei, W. Electrolytic Regeneration of Decarbonising Potassium Carbonate Solution. *Chinese Journal of Chemical Engineering* **2010**, *18* (4), 538–543. https://doi.org/10.1016/S1004-9541(10)60256-X.

(7) Savage, D. W.; Sartori, G.; Astarita, G. Amines as Rate Promoters for Carbon Dioxide Hydrolysis. *Faraday Discuss. Chem. Soc.* **1984**, *77* (0), 17–31. https://doi.org/10.1039/DC9847700017.

(8) Harjac, S. J.; Atrens, A.; Moss, C. J.; Linton, V. Influence of Solution Chemistry and Surface Condition on the Critical Inhibitor Concentration for Solutions Typical of Hot Potassium Carbonate CO2 Removal Plant. *J Mater Sci* **2007**, *42* (18), 7762–7771. https://doi.org/10.1007/s10853-007-1613-y.

(9) Boonprasop, S.; Chalermsinsuwan, B.; Piumsomboon, P. Effect of the Operating Parameters on the CO2 Capture Capacity of Potassium Carbonate Supported on Gamma Alumina (K2CO3/γ-Al2O3) Using Conventional Heat Regeneration. *Journal of the Taiwan Institute of Chemical Engineers* **2017**, *78*, 282–289. https://doi.org/10.1016/j.jtice.2017.06.016.

(10) Meis, N. N. A. H.; Frey, A. M.; Bitter, J. H.; de Jong, K. P. Carbon Nanofiber-Supported K2CO3 as an Efficient Low-Temperature Regenerable CO2 Sorbent for Post-Combustion Capture. *Ind. Eng. Chem. Res.* **2013**, *52* (36), 12812–12818. https://doi.org/10.1021/ie4017072.

(11) Hirano, S.; Shigemoto, N.; Yamada, S.; Hayashi, H. Cyclic Fixed-Bed Operations over K2CO3-on-Carbon for the Recovery of Carbon Dioxide under Moist

Conditions. *Bulletin of the Chemical Society of Japan* **1995**, *68* (3), 1030–1035. https://doi.org/10.1246/bcsj.68.1030.

(12) Hayashi, H.; Taniuchi, J.; Furuyashiki, N.; Sugiyama, S.; Hirano, S.; Shigemoto, N.; Nonaka, T. Efficient Recovery of Carbon Dioxide from Flue Gases of Coal-Fired Power Plants by Cyclic Fixed-Bed Operations over K2CO3-on-Carbon. *Ind. Eng. Chem. Res.* **1998**, *37* (1), 185–191. https://doi.org/10.1021/ie9704455.

(13) Zhao, C.; Chen, X.; Zhao, C.; Liu, Y. Carbonation and Hydration Characteristics of Dry Potassium-Based Sorbents for CO2 Capture. *Energy Fuels* **2009**, *23* (3), 1766–1769. https://doi.org/10.1021/ef800889m.

(14) Luo, H.; Chioyama, H.; Thürmer, S.; Ohba, T.; Kanoh, H. Kinetics and Structural Changes in CO2 Capture of K2CO3 under a Moist Condition. *Energy Fuels* **2015**, *29* (7), 4472–4478. https://doi.org/10.1021/acs.energyfuels.5b00578.

(15) Qin, C.; Yin, J.; Ran, J.; Zhang, L.; Feng, B. Effect of Support Material on the Performance of K2CO3-Based Pellets for Cyclic CO2 Capture. *Applied Energy* **2014**, *136*, 280–288. https://doi.org/10.1016/j.apenergy.2014.09.043.

(16) Lee, S. C.; Kwon, Y. M.; Jung, S. Y.; Lee, J. B.; Ryu, C. K.; Kim, J. C. Excellent Thermal Stability of Potassium-Based Sorbent Using ZrO2 for Post Combustion CO2 Capture. *Fuel* **2014**, *115*, 97–100. https://doi.org/10.1016/j.fuel.2013.07.007

(17) Rodríguez-Mosqueda, R.; Bramer, E. A.; Roestenberg, T.; Brem, G. Parametrical Study on CO2 Capture from Ambient Air Using Hydrated K2CO3 Supported on an Activated Carbon Honeycomb. *Ind. Eng. Chem. Res.* **2018**, *57* (10), 3628–3638. https://doi.org/10.1021/acs.iecr.8b00566.

(18) *Bulk Buy China Wholesale White Powder Zro2 Nanometer Zirconium Dioxide Price Industrial Grade Ceramic 99.5-99.99 $4000 from Linbing International Trading Hebei Co.,Ltd | Globalsources.com*. Global Sources. https://www.globalsources.com/Industrial-chemical/zirconium-dioxide-1217274849p.htm (accessed 2024-11-29).

(19) *Zirconium Dioxide（Zr(Hf)O2≥99.5%） price today | Historical Zirconium Dioxide（Zr(Hf)O2≥99.5%） Price Charts | SMM Metal Market*. https://www.metal.com/Other-Minor-Metals/202302020006 (accessed 2024-11-29).

(20) Gao, Y.; Zhao, C.; Huang, P.; Zeng, P.; Yang, Y.; Guo, Y.; Sun, J. Enhanced K2CO3 Utilization Efficiency of K2CO3/Al2O3 Adsorbents Using a Large-Scale Production Spray Agglomeration Synthesis. *Chemical Engineering Journal* **2024**, *485*, 149728. https://doi.org/10.1016/j.cej.2024.149728.

(21) Jo, S. B.; Lee, S. C.; Chae, H. J.; Cho, M. S.; Lee, J. B.; Baek, J.-I.; Kim, J. C. Regenerable Potassium-Based Alumina Sorbents Prepared by CO2 Thermal Treatment for Post-Combustion Carbon Dioxide Capture. *Korean J. Chem. Eng.* **2016**, *33* (11), 3207–3215. https://doi.org/10.1007/s11814-016-0162-y.

(22) Yi, C.-K.; Jo, S.-H.; Seo, Y.; Lee, J.-B.; Ryu, C.-K. Continuous Operation of the Potassium-Based Dry Sorbent CO2 Capture Process with Two Fluidized-Bed Reactors. *International Journal of Greenhouse Gas Control* **2007**, *1* (1), 31–36. https://doi.org/10.1016/S1750-5836(07)00014-X.

(23) Quang, D. V.; Dindi, A.; Rayer, A. V.; Hadri, N. E.; Abdulkadir, A.; Abu-Zahra, M. R. M. Impregnation of Amines Onto Porous Precipitated Silica for CO2 Capture. *Energy Procedia* **2014**, *63*, 2122–2128. https://doi.org/10.1016/j.egypro.2014.11.229.

(24) Buys, S.; Oakley, V. *Conservation and Restoration of Ceramics*; Routledge: London, 2014. https://doi.org/10.4324/9780080502892.

(25) Vadaga, A. K.; Gudla, S. S.; Nareboina, G. S. K.; Gubbala, H.; Golla, B. Comprehensive Review on Modern Techniques of Granulation in Pharmaceutical Solid Dosage Forms. *Intelligent Pharmacy* **2024**, *2* (5), 609–629. https://doi.org/10.1016/j.ipha.2024.05.006.

(26) Shanmugam, S. Granulation Techniques and Technologies: Recent Progresses. *Bioimpacts* **2015**, *5* (1), 55–63. https://doi.org/10.15171/bi.2015.04.

(27) Muley, S.; Nandgude, T.; Poddar, S. Extrusion–Spheronization a Promising Pelletization Technique: In-Depth Review. *Asian Journal of Pharmaceutical Sciences* **2016**, *11* (6), 684–699. https://doi.org/10.1016/j.ajps.2016.08.001.

(28) *Potassium Carbonate Prices, News, Monitor, Analysis & Demand*. https://www.chemanalyst.com/Pricing-data/potassium-carbonate-1164 (accessed 2024-11-27).

(29) *Titanium Dioxide Prices, Monitor, Market Analysis & Demand*. https://www.chemanalyst.com/Pricing-data/titanium-dioxide-52 (accessed 2024-11-27).

(30) PubChem. *Potassium Carbonate*. https://pubchem.ncbi.nlm.nih.gov/compound/11430 (accessed 2024-11-30).

(31) Beving, M. A. J. M.; Frijns, A. J. H.; Rindt, C. C. M.; Smeulders, D. M. J. Effect of Cycle-Induced Crack Formation on the Hydration Behaviour of K2CO3 Particles: Experiments and Modelling. *Thermochimica Acta* **2020**, *692*, 178752. https://doi.org/10.1016/j.tca.2020.178752.

[[This chapter is temporarily embargoed]